THE UNIVERSITY OF OKLAHOMA

GRADUATE COLLEGE

LIFETIMES OF EXCITED ELECTRONIC STATES OF CHEMICALLY ACTIVE GASES

A DISSERTATION

SUBMITTED TO THE GRADUATE FACULTY

in partial fulfillment of the requirements for the

degree of

DOCTOR OF PHILOSOPHY

BY

GARY EARL COPELAND

Norman, Oklahoma

1970

LIFETIMES OF EXCITED ELECTRONIC STATES OF CHEMICALLY

ACTIVE GASES

APPROVED BY

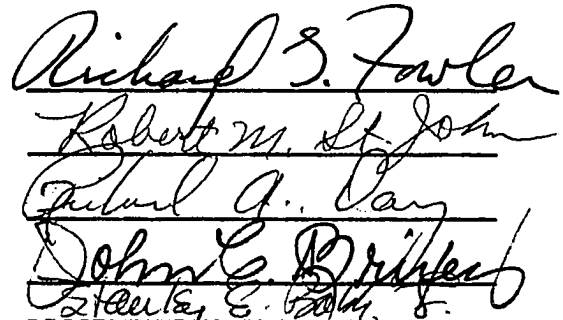

DISSERTATION COMMITTEE

ACKNOWLEDGEMENT

I wish to express my gratitude to my parents for unending faith in my ability to complete this project. Their steadfast support of my goals has enabled me to accomplish this work. I wish to thank Dr. R. G. Fowler for his advice and encouragement through the many years of graduate school. His faith in my ability to attain a proficience in physics always served as a great incentive for excellence. His uncanny ability to secure research funds when nearly all other avenues for support were closed has enabled me to complete this work.

Drs. T. M. Holzberlein, R. M. St. John, S.J.B. Corrigan, A. W. Johnson, R. Anderson and S. E. Babb, Jr., supplied just the proper amount of pressure, assistance and inspiration to prompt a deep respect for the methods and techniques of experimental physics. The invaluable assistance in mechanical design problems given to the author by Mr. Gene Scott are acknowledged. The excellent vacuum technology and skill as a glassblower of Mr. Ron Stermer in construction of the apparatus are acknowledged.

My coworkers in the atomic and molecular physics group have devoted a great amount of time and work in the construction, testing, and data analysis of this experiment. Special thanks are given to R. T. Thompson for his fantastic ability to overcome a difficult data analysis problem. In a great measure the successful completion of this program is due to his efforts. The daily discussions of mutual experimental problems between the author, R. Mickish, and R. Schaefer have produced

unique solutions. Special thanks are given to Carl Bush for his graphical data analysis and computer assistance and to Dale Bradshaw for his assistance in establishment of time standards.

DEDICATION

This dissertation is dedicated to the memory of two friends, excellent physicists and coworkers.

Owen Lee Robinson

and

Geoffrey Russell

TABLE OF CONTENTS

TABLE OF CONTENTS (Continued)

LIST OF TABLES

LIST OF FIGURES

LIST OF FIGURES (Continued)

GLOSSARY

PMT - Photomultiplier Tube

TDG - Timing and Delay Generator

MFG - Master Firing Generator

PFG - Pulse Forming Generator

CRG - Crowbar Generator

THC - Time-to-Height Converter

PTD - Photomultiplier Timing Discriminator

MCA - Multichannel Analyzer

ADC - Analog Digital Converter

DHM - Data Handling Module

PHA - Pulse Height Analysis

MS - Multiscaling Mode

PART I

CHAPTER I

INTRODUCTION

Even before the development of the spectroscope man had wondered at the cause of the many beautiful spectral lines revealed to his eyes by the natural spectroscopy of the rainbow. This amazement continues today, several centuries later. Only in the last seventy years has man been able to explain their existence and predict still others he can not see with his eyes. The development of quantum mechanics in the 1920's was in great part due to man's inability to explain spectra.

Isotopes (deuterium, tritium) whose existence were never previously suspected, first showed their presence in spectra. The intensity alterations in various spectral bands indicated molecules which chemists knew could not exist. The intensity modulation in other bands enable man to measure the temperature of the stars, the planets and comets. The appearance of certain lines and not of others enables man to probe the very core of matter, the nucleus. The composition of the stars and of the planetary atmospheres can now be determined by examination of spectra. The wonders of life saving drugs can be unraveled by their absorption, emission, infrared and Raman spectra. The very structure of molecules may be determined by examination of their spectra.

Man now attempts to safeguard himself from nuclear catastrophy by monitoring the $N_2^+(1-)$ (3914 Å) band of his home planet's atmosphere since it is excited when upper atmospheric nuclear blasts are set off. The development of lasers, many which utilize molecular transitions, may one day provide unlimited communication facilities. All life is composed of molecules. Life, as we know it, depends upon the oxygen molecules for its existence.

This dissertation is an attempt to increase mans knowledge of the universe by a detailed experimental examination of two diatomic molecules, oxygen and nitric oxide. The techniques utilized[1] may be applied to still other atomic and molecular species as well. The primary goal of this research is to measure the mean time excited states of these species exists. Typically this time is of the order of one to one hundred billionths of a second. This time scale is of such short duration, that it's very difficult for man to comprehend its brevity. Roughly a nanosecond is the time it takes light travelling 186,000 miles each second to travel one foot, i.e., the length of this page.

Part I of this dissertation is a detailed description of the quantum mechanical background necessary to describe diatomic molecules. A description of transition probability is developed. The experimental apparatus is described in Part II together with the method of measurement adopted, i.e., the delayed coincidence method. Part III describes the type of data and how it is analyzed to yield lifetimes of excited states. In Part IV the results of the detailed examinations are reported and discussed.

CHAPTER II

MODEL OF DIATOMIC MOLECULES

We shall assume for our model of a diatomic molecule, that first put forth by Born and Oppenheimer[2]. In this model the total eignfunction of the molecule is represented by a product of three functions, i.e., the electronic, vibrational, and rotational eigenfunctions. When such an eigenfunction is substituted into the exact Schroedinger equation for a diatomic molecule, it is seen that the equation separates into three ordinary differential equations, if, and only if, one neglects variations of the first and second derivatives of the electronic eigenfunctions with respect to the internuclear distance[3]. This is equivalent to writing the Schroedinger equation $H\Psi = E\Psi$ for the molecule and leaving out of the Hamiltonian all terms in which electronic, vibrational, and rotational motions interact with one another.

Thus we proceed with our first approximation to the total wave function of the undisturbed diatomic molecule, in which we write[4]

$$\Psi_{nv,m} = \frac{1}{r}\Psi(n|\vec{r}_m,R)\phi(v|R)\chi(Jm|\Theta\phi) \qquad (1)$$

where

$\Psi(n|\vec{r}_m,R)$ = electronic wave function

$\Phi(v|R)$ = vibrational wave function

$\chi(Jm|\Theta\Phi)$ = rotational wave function

and the quantum numbers are

n = electronic

v = vibrational state

J = rotational state

M = projection of J on internuclear axis

$\vec{r}_m$ is the radius vector of the mth electron from the center of mass of the molecule. $|\vec{R}|$ is the internuclear distance and Θ and Φ are angles which fix the internuclear axis with respect to our axis at the center of mass.

The total energy of the molecule neglecting spin and magnetic interactions consists of the potential and kinetic energies of the electrons and the nuclei. It is clear that the electronic energy will depend upon the internuclear distance R. The small mass of electrons when compared to the nuclear mass makes it clear that the electrons move much more rapidly than the nuclei, thus the electronic energy depends upon the position of the nuclei. In order to move the nuclei one must do work against their Coulombic repulsion and supply the energy necessary to change the electronic energy as well. Thus the sum of the electronic energy and the Coulombic potential of the nuclei acts as the potential energy under whose influence the nuclei carry out their vibrations. Therefore, we see why the electronic and vibrational eigenfunctions depend explicitly on the internuclear distance R.

In all but one realistic case it is found that it is impossible to solve in closed analytic form for the total eignfunctions of a diatomic molecule[5]. It is necessary to seek ways in which these wavefunctions may be found from empirical data, i.e., the spectroscopic constants for each state. We will dwell on these techniques later in this dissertation.

The electronic states in a molecule are classified according to the Hund's[6] coupling cases. The quantum number usually used are $(\Lambda,\Sigma,\Omega,J)$. Λ is the projection on the internuclear axis of the total electric orbital angular momentum and takes the values 0,1,2,...L; producing Σ,Π,Δ,Φ states which are doubly degenerate (expect for Σ states). The component M_s of the resultant spin vector S on the internuclear axis is called Σ and takes values S, S-1, ...,-S. The total electronic angular momentum about the internuclear axis is denoted by Ω and is given by

$$\Omega = |\Lambda + \Sigma| \quad .$$

Other quantum numbers of interest are the rotational quantum numbers (J,K) which are used in various coupling schemes.

Most electronic states can be classified as belonging to Hund's coupling case a, intermediate between Hund's coupling a and b, and/or belonging to Hund's case b. The mutual interaction of vibrational and electronic motions is taken into account if the vibrational levels are chosen to fit the potential curve of the electronic state. The influence of rotational and electronic motions on each other vary strongly

and the relative strength of their coupling determines which of the Hund's coupling cases is used for description of that state.

In Hund's case (a) it is assumed that the interaction of nuclear rotation with the total electronic motion is very weak and the electronic motion itself is coupled very strongly to the internuclear axis. The electronic angular momentum $\vec{\Omega}$ is well defined and with the angular momentum $\vec{N}$ of nulcear rotation forms the resultant $\vec{J}$. The coupling is similar to that of a symmetric top. $\vec{J}$ is constant in magnitude and direction and $\vec{\Omega}$ and $\vec{N}$ rotate about $\vec{J}$ (nutation). $\vec{L}$ and $\vec{J}$ precess about internuclear axis very much faster than the nutation frequency. Since Ω is a component of $\vec{J}$, it follows that

$$J = \Omega, \Omega+1, \Omega+2, \ldots$$

and levels with $J < \Omega$ do not occur.

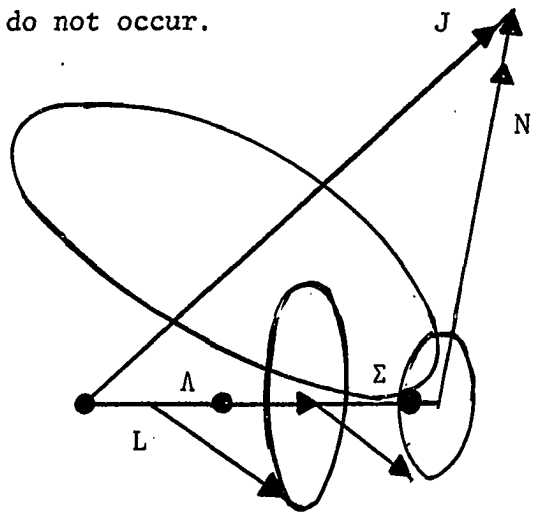

Hund's Coupling, Case (a)

In Hund's case (a) when $\Lambda = 0$ and $S \neq 0$, $\vec{S}$ is not coupled to the internuclear axis at all. Thus $\vec{\Omega}$ is not defined. In cases where $\vec{S}$ is only weakly coupled to the internuclear axis we use Hunds coupling

case (b) even if $\Lambda \neq 0$. In this case $\vec{\Lambda}$ and $\vec{N}$ form a resultant which is called $\vec{K}$, which can have the interger values

$$K = \Lambda, \Lambda+1, \Lambda+2, \ldots .$$

$\vec{K}$ is the total angular momentum apart from spin. The momenta $\vec{K}$ and $\vec{S}$ form the resultant $\vec{J}$, the total angular momentum including spin. The possible values of J for a given K are

$$J = (K+S), (K+S-1) \ldots |K-S| .$$

Thus each level with given K has 2S+1 components.

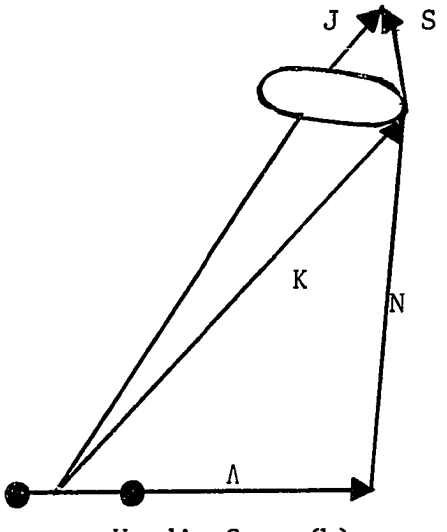

Hund's Case (b)

The potential energy diagram[7] for the two molecules NO and O_2^+ are shown in Figs. (1) and (2). The electronic states are labeled according to international notation (Herzberg)[8]. Inside the potential wells are shown the vibrational levels which are observed in both emission and absorption (electronic spectra). The rotational levels are not shown since they would be on much too small scale.

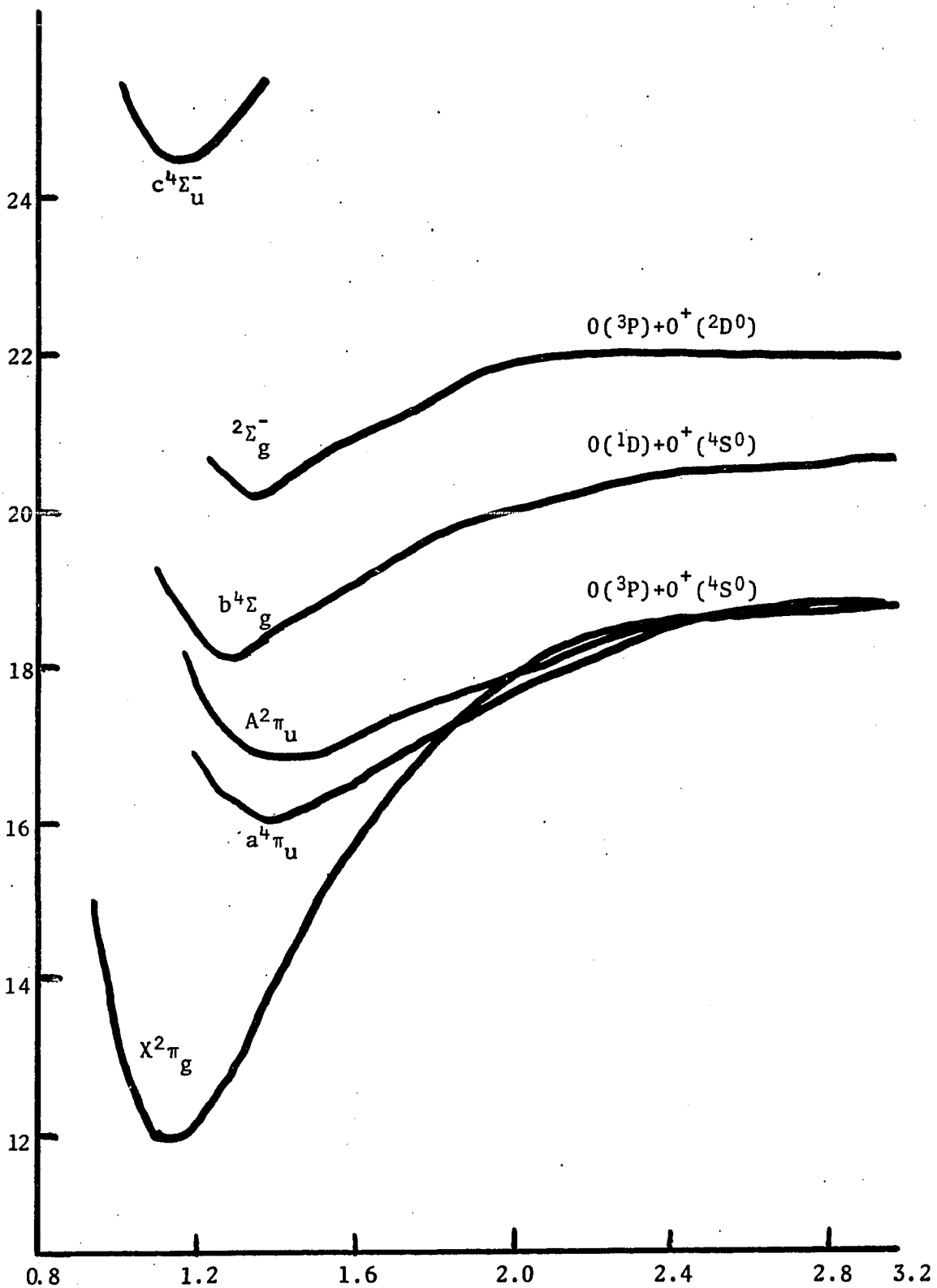

Figure 1. O_2^+ Energy Level Diagram.

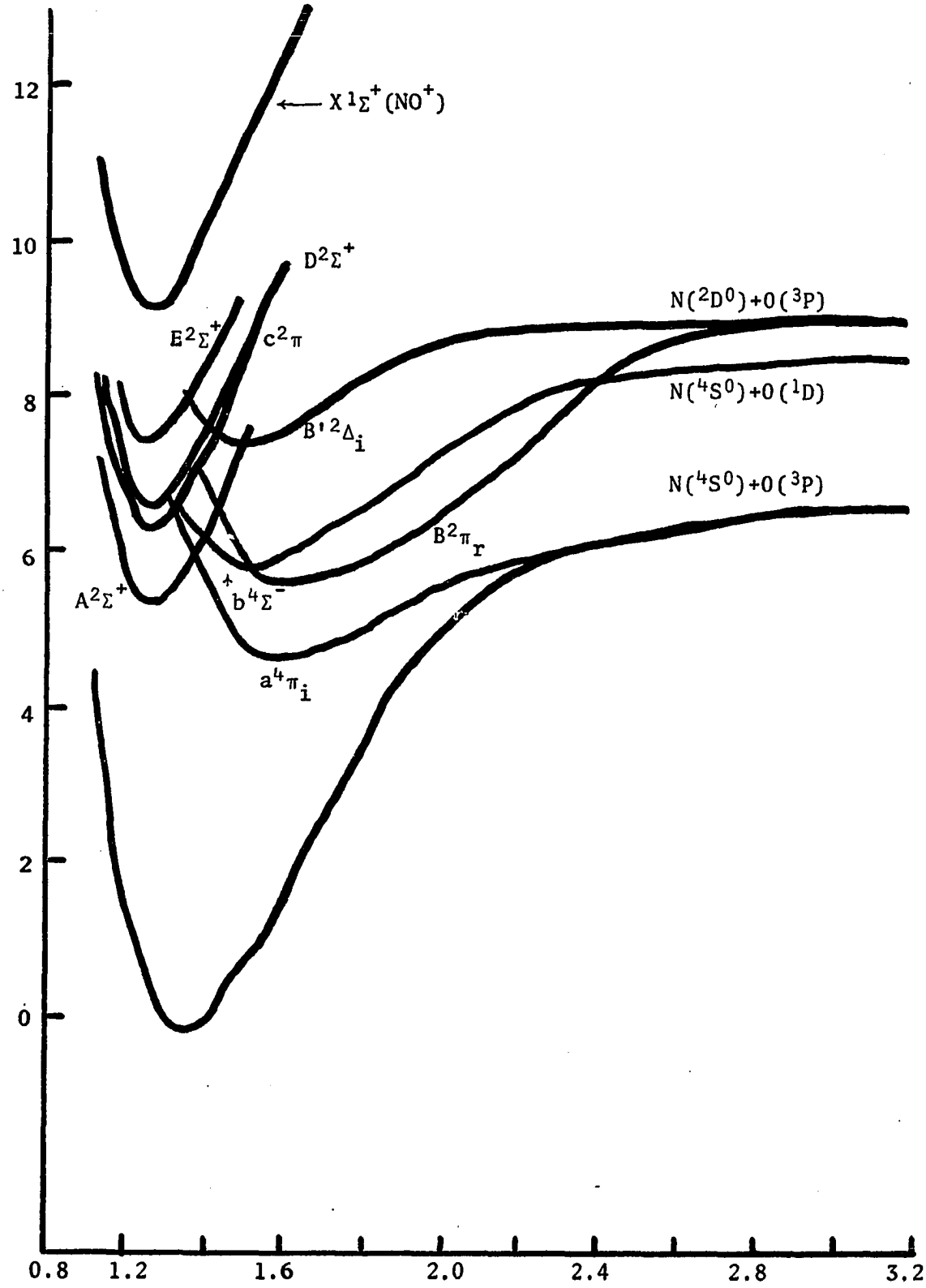

Figure 2. NO Energy Level Diagram.

Using notation introduced previously, we have the wave function of an excited state (n', v', J', m') as

$$\Psi_{n'v'J'm'} = \frac{1}{r} \Psi(n'|\vec{r}_m,R)\Phi(v'|R)\chi(J'm'|\Theta\Phi)$$

and in the same manner for lower state (n''v''J''m'')

$$\Psi_{n''v''J''m''} = \frac{1}{r} \Psi(n''|\vec{r}_m,R)\Phi(v''|R)\chi(J''m''|\Theta\Phi) \quad .$$

CHAPTER III

QUANTUM-MECHANICAL TRANSITION PROBABILITIES

The probability of a transition between a state characterized by (n'v'J'm') and a lower energy state (n''v''J''m'') is proporational to the square of the matrix element of the electric dipole moment (the transition moment)

$$R = \int \Psi'^* \vec{M} \Psi'' d\tau \quad .$$

Where $\vec{M} = \sum_{i=1}^{n} e \vec{r}_i$ and has components of $\Sigma e_i x_i$, $\Sigma e_i y_i$, $\Sigma e_i z_i$. The dipole moment $\vec{M}$ can be written as the sum of two parts $\vec{M}_e$ (depending upon the electrons) and $\vec{M}_n$ (depending upon the nuclei)

$$\vec{M} = \vec{M}_e + \vec{M}_n \quad .$$

Then

$$\vec{R} = \int \Psi'^* (\vec{M}_e + \vec{M}_n) \Psi'' d\tau \quad .$$

Using the product functions for the wave functions, as obtained from the Born Oppenheimer separation, we have

$$\vec{R} = \int \Psi^*(n' | \vec{r}_m, R) \Phi^*(v' | R) \chi^*(J'm' | \Theta\Phi) \\ *(\vec{M}_e + \vec{M}_n) \Psi(n'' | \vec{r}_m, R) \Phi(v'' | R) \chi(J''m'' | \Theta\Phi) d\tau$$

We now calculate the Z component of the transition moment.

$$R_Z = \int \psi'^{*}_{n'} \frac{1}{r} \Phi^{*}_{v'} \psi^{*}_{J''n'} M_Z \psi_{n''} \frac{1}{r} \Phi_{\sigma''} \chi_{J''m''} d\tau \quad .$$

But $M_Z = M \cos\Theta$, $d\tau = d\tau_e r^2 \sin\Theta \, d\Theta \, d\Phi \, dr$ where $d\tau_e$ is volume element of configuration space of the electrons, then we have ($\Phi^{*}_{v'} = \Phi_{v'}$)

$$R_Z = \int \psi^{*}_{n'} \Phi_{v'} M \psi_{n''} \Phi(v'') d\tau_e$$

$$* r^2 \frac{1}{r} \frac{1}{r} dr \int \sin\Theta \cos\Theta \chi^{*}_{J'n'} \chi_{J''n''} d\Theta d\Phi \quad .$$

The second for the two integrals is constant for a given J', J" combination. Moreover the first integral is independent of J in this approximation. We may conclude that one may neglect the rotation of the molecule entirely for calculations of the electronic transition moment.

Now proceeding with the calculation of $\vec{R}$, we find

$$\vec{R} = \int \vec{M}_e \psi^{*}_{n'} \Phi(v') \psi_{n''} \Phi(v'') d\tau + \int \vec{M}_n \psi'^{*}_{n'} \Phi_{v'} \Phi_{v''} \psi_{n''} d\tau \quad .$$

But $\vec{M}_n$ does not depend upon the coordinates of the electrons, so the second integral is

$$\int \vec{M}_n \Phi_{v'} \Phi_{v''} d\tau_n \int \psi^{*}_{n'} \psi_{n''} d\tau_e \quad .$$

Since we are dealing with different electronic states (n',n"), the electronic eigenfunctions are orthogonal, and thus $\int \psi^{*}_{n'} \psi_{n''} d\tau_e = 0$. Thus

$$\vec{R} = \int \Phi_{v'} \Phi_{v''} d\tau \int \vec{M}_e \psi^{*}_{n'} \psi_{n''} d\tau_e$$

or

$$\vec{R} = \int \Phi(v'|R)\Phi(v''|R)d\tau \int \Psi^*(n'|\vec{r}_m,R)\vec{M}_e^*\Psi(n''|\vec{r}_m,R)d\tau_e \quad .$$

The second integral is called the electronic transition moment and its square is proportional to the electronic transition probability. The first integral squared is called the Frank-Condon factor $q_{v'v''}$. The product of the two integrals squared is called the relative vibrational transition probability $p_{v'v''}$

$$p_{v'v''} = \left|\int \Phi(v')\Phi(v'')d\tau \int \Psi^*(n')\vec{M}_e\Psi(n')d\tau_e\right|^2 \quad .$$

Thus

$$\vec{R}^2 = p_{v'v''} = q_{v'v''}R_e^2(r) \quad .$$

Where $R_e(r)$, the electric transition moment is assumed to be independent of r. The quantum mechanical statement of the Frank-Condon principal rests upon the fact that $R_e(r)$ is independent of the radial parameter r and that the relative transition probabilities are essentially determined by the $q_{v'v''}$. In many cases the assumption of independence of R_e from r is not valid. R. W. Nicholls, W. R. Jarmain[9] and P. A. Fraser[10] have found by numerical evaluation of the following integrals

$$\langle v'|1|v''\rangle, \quad \langle v'|r|v''\rangle, \quad \langle v'|r^2|v''\rangle, \quad \langle v'|r^{-1}|v''\rangle$$

that very closely

$$\frac{\langle v'|r^2|v''\rangle}{\langle v'|r|v''\rangle} = \frac{\langle v'|r|v''\rangle}{\langle v'|v''\rangle} = \frac{\langle v'|v''\rangle}{\langle v'|\frac{1}{r}|v''\rangle} \quad .$$

The middle integral is just an expression for the r-coordinate of a centroid. The r centroid is defined as

$$\bar{r}_{v'v''} = \frac{\int \Phi(v') r \Phi(v'') dr}{\int \Phi(v') \Phi(v'')} .$$

Using this definition of the r centroid, it is found that when the electric transition moment $R_e(r)$ is evaluated at $r = \bar{r}_{v'v''}$ for each v', v'' it is then insensitive to radial variations. Then the dipole matrix element can be written as

$$R^2 = p_{v'v''} = q_{vv''} R_e^2(\bar{r}_{v'v''}) .$$

It must be stressed that there is no theoretical basis for this procedure. In addition there is no theoretical means by which R_e^2 can be related to $\bar{r}_{v'v''}$.

Calculations of the Franck-Condon factors have been carried out for over fifty band systems[11]. Basically the $q_{v'v''}$ is the square of the integral of the overlap of the vibrational wavefunctions in the different electric states. Nearly all calculations of $q_{v'v''}$ use the Morse potential function

$$V(r\text{-}re) = De(1-e^{-\beta(r-re)})^2$$

where $\beta = (\frac{2\pi^2 c\mu}{De\ h})^{\frac{1}{2}}$. ω_e, as a basic potential since it produces analytic wave functions. Thus $q_{v'v''}$ can be easily calculated once the spectroscopic constants for the state are known.

A more recent method utilizes a calculational technique divised by Rydberg[12], Klein[13] and Rees[14] and is thus termed the RKR method.

Following Klein and R. J. Spindler[15], we can define an action function S(u,k)

$$S(u,k) = \frac{1}{\sqrt{2\mu\pi}} \int_0^I (u-E)^{\frac{1}{2}} dI \ .$$

We desire to know r_{max} and r_{min} from the equation

$$r_{min}^{max} = [\frac{f}{g} + f^2] \mp f$$

where f and g are found from

$$f = (\frac{\partial s}{\partial u})_k ; \qquad g = -(\frac{\partial s}{\partial k})_u$$

where $I = h(v+\frac{1}{2})$, $K = \frac{\hbar^2}{8\pi\mu} J(J+1)$ and μ is reduced mass.

One changes variables (I,K) into the <u>continuous</u> vibrational and rotational quantum numbers v, J and defines a function Φ such that

$$\Phi(U,J) = \int_{-\frac{1}{2}}^{v'} [U-E(v,J)]dv$$

where v' is the value of v where E(v,J) = U, E(v,J) is defined as

$$E(v,J) = G(v) + [B_v J(J+1) - D_v J^2(J+1)^2 + H_v J^3(J+1)^3] \ .$$

Where G(v), V_v, D_v, H_v are directly determined from measured energy levels. No reference is made to the reported spectroscopic constants since once the potential is found, they may be calculated.

Then the parameters f and g are found to be given by (N_o is Avagrado's number)

$$f = \frac{10^3}{\pi} \sqrt{\frac{b\ N_o}{2\mu_A c}} \left(\frac{\partial \phi}{\partial u}\right)_{\substack{n = \mu_o \\ J = J_o}}$$

$$g = -\frac{8\pi x 10^{-8}}{2J_o + 1}\sqrt{\frac{\mu_o c}{2h N_o}}\left(\frac{\partial\phi}{\partial J}\right)_{\substack{J = J_o \\ u = u_o}} .$$

Since f and g determine the classical turning points of vibration, the potential curve is known. The wave functions $\Phi v'$, $\Phi v''$ are found by numerical integration of the radial Schroedinger equation and the Franck-Condon factors are obtained via overlap integrals.

Franck-Condon factors determined by Morse functions and RKR methods seem to agree for states nearly at the minimum of potential wells which are not widely separated in radial position. As v' (or v'') is increased to the point where the energy approaches the dissociation limit, the two methods diverge from one another. Evidence indicates that RKR method can be applied to high vibrational quantum numbers with confidence[16].

CHAPTER IV

VIBRATIONAL BANDS

The Einstein transition probability A of two states n' and n'' (in molecular physics a single prime indicates the upper level) which are $d_{n'}$ and $d_{n''}$ fold degenerate is

$$A_{n'n''} = \frac{64\pi^4\nu^3}{3h\ c^3} \sum_{i,K} \frac{|R_{n_i'n_K''}|^2}{d_{n'}}$$

where i and K are substates, ν in the frequency in sec^{-1} and $|R_{n'_i n''_K}|^2$ the transition momement of the states n_i' and n_K''. The basic law leading to this equation is that the total transition probability is the sum of all transition probabilities of the non-degenerated substances averaged over the initial substates, i.e.,

$$A_{n'n''} = \frac{1}{dn'} \sum_{i,K} A_{n_i'n_K''}$$

When discussing an electronic vibrational transition of a molecule, the rotational transitions may be disregarded under the assumption that the rotation does not interact with the vibrational - electronic motions. The electronic-vibrational transition is then independent of the initial rotational state of the molecule, and symbolically one may

write

$$A^{v'v''}_{n'n''} = A^{v'}_{n'J'n''} \qquad \text{for each } J'' \ .$$

We consider the molecular transition n'v'→n''v''. The (2S+1) electronic spin multiplies of the electronic state n' is treated as a (2S+1) fold degeneracy, since the energy differences of the resulting spin substates Σ' is small usually. A second degeneracy is Λ type doubling for states with $\Lambda \neq 0$, the resulting substates are denoted by P for parity. The vibrational states of a diatomic molecule are non-degenerate so, $d_v = 1$. Thus we see the total statistical weight for n' is[17]

$$d_{n'v'} = (2-\delta_{o,\Lambda'})(2S+1) \ .$$

The Einstein spontaneous transition probability A for the transition (n'v'→n''v'') is

$$A^{v'v''}_{n'n''} = \frac{64\pi^4\nu^3}{3h\ c^3} \frac{\sum_{p'p''} \sum_{\Sigma'\Sigma''} |R^{v'v''}_{n'\Sigma'n''\Sigma''p''}|^2}{(2-\delta_{0,\Lambda'})(2S'+1)} \ ,$$

and the corresponding absorption oscillator strength is

$$f_{v'v''} = \frac{m_e\ c^3}{8\pi^2\nu^2e^2} \frac{d_{n'v'}}{d_{n''v''}} A^{v'v''}_{n'n''}$$

$$f_{v'v''} = \frac{8\pi^2 m_e c}{3h\ e^2\lambda} \frac{\Sigma |R_e{}^{v'v''}|^2}{(2-\delta_{0,\Lambda''})(2S''+1)}$$

where $\Sigma|R_e^{v'v''}|^2$ is a short handed notation for the detailed sum above.

The lifetime of the state n'v' is given by the reciprocal sum of the transition probabilities from that state

$$\tau_{n'v'} = \frac{1}{\sum_{n'',v''} A_{n'n''}^{v'v''}}$$

or

$$\frac{1}{\tau_{n'v'}} = \frac{64\pi^4}{3h\ c^3 n''v''} \sum \frac{\nu^{+3}(n'v',n''v'')\ p'p''\ \Sigma'\Sigma''|R_{n'\Sigma'n''\Sigma''p''}^{v'v''}|^2}{(2-\delta_{0,\Lambda'})(2S'+1)}\Bigg\}^{-1}$$

Rotational Lines

A rotational transition n'v'Σ'J'→n''v''Σ''J'' may consist of two Λ-doubling components which are never resolved in this experiment. Treating this doublet as a whole we see that each rotational level has 2J+1 coincident levels characterized by their magnetic quantum numbers m(m=-J,...-J+1,...+J). The total degeneracy of the nvΣJ level is $(2-\delta_{0,\Lambda})(2J+1)$. Thus the Einstein A coefficient for the transition n'v'Σ'J'→n''v''Σ''J'' is

$$A_{n'v'\Sigma'J'}^{n''v''\Sigma''J''} = \frac{64\pi^4\nu^3}{3h\ c^3} \frac{p'p''\ m'm''|R_{n'\Sigma'p'm'n''\Sigma''p''m''}^{v'v''}|^2}{(2-\delta_{0,\Lambda})(2J'+1)} .$$

Hönl and London[18] have shown that if the total wave function of a molecule is separated into a radial and an angular part, it is possible to write the transition moment as a product function.

That is

$$\sum_{p'p''} \sum_{m'm''} |R^{v'v''}_{n'\Sigma'm'n''\Sigma''p''m''}|^2 \equiv R_{rad} S_J$$

and thus

$$A_{J'J''} = \frac{64\pi^3 \nu^3}{3h\ c^3} \frac{R_{rad} S_J}{(2-\delta_{0,\Lambda'})(2S'+1)} \quad .$$

The factor S_J is called the Honl-London factor , or the rotational line strength and has been calculated for most transitions by Schadee[19], Tatum[20] and Kovács[21]. It obeys a sum rule such that their sum for all transitions from the levels with equal J' is equal to the number of initial sublevels,

$$\sum_{\Sigma'\Sigma''} \sum_{J''} S_J = (2S+1)(2J'+1) \quad .$$

The value for the radial factor is determined by the same sum rule.

$$A^{v'v''}_{n'n''} = \frac{\sum_{\Sigma'\Sigma''} \sum_{J'} A_{J'J''}}{2S' + 1}$$

$$= \frac{64\pi^4 \nu^3}{3h\ c^3} \frac{R_{rad} \sum_{\Sigma'\Sigma''} \sum_{J''} S'_J}{(2-\delta_{0,\Lambda'})(2S'+1)(2J'+1)} \quad .$$

Using the sum rule, we have by comparing two forms of $A^{v'v''}_{n'n''}$,

$$R_{rad} = \frac{\sum_{p'p''} \sum_{\Sigma'\Sigma''} |R^{v'v''}_{n'\Sigma'p'n''\Sigma''p''}|^2}{(2S' + 1)} \quad .$$

PART II

EXPERIMENTAL APPARATUS

CHAPTER I

VACUUM SYSTEM

The vacuum system utilized evolved during the course of the experiment. Basically it consisted of a fore pump, mercury diffusion pump, several traps, a gas purification system, gas reserviors, and several types of pressure measuring devices. It was necessary to maintain a base pressure less than 10^{-6} Torr in order to insure a minimum of contamination of the gases to be studied.

In Fig. 3 a general block diagram of the vacuum system is found. The system contained no Apiezon W "Black Wax" or epoxy seales for maintenance of its vacuum. Each subsystem of the vacuum system is described in detail below.

The fore pump was a CENCO-WELCH DUO-SEAL Model 1402 capable of pumping 100 liters per minute and with base pressure of 10^{-4} Torr. The pumping fluid was Cenco Hyvac. The fore pump was connected to the main vacuum system by means of tygon tubing.

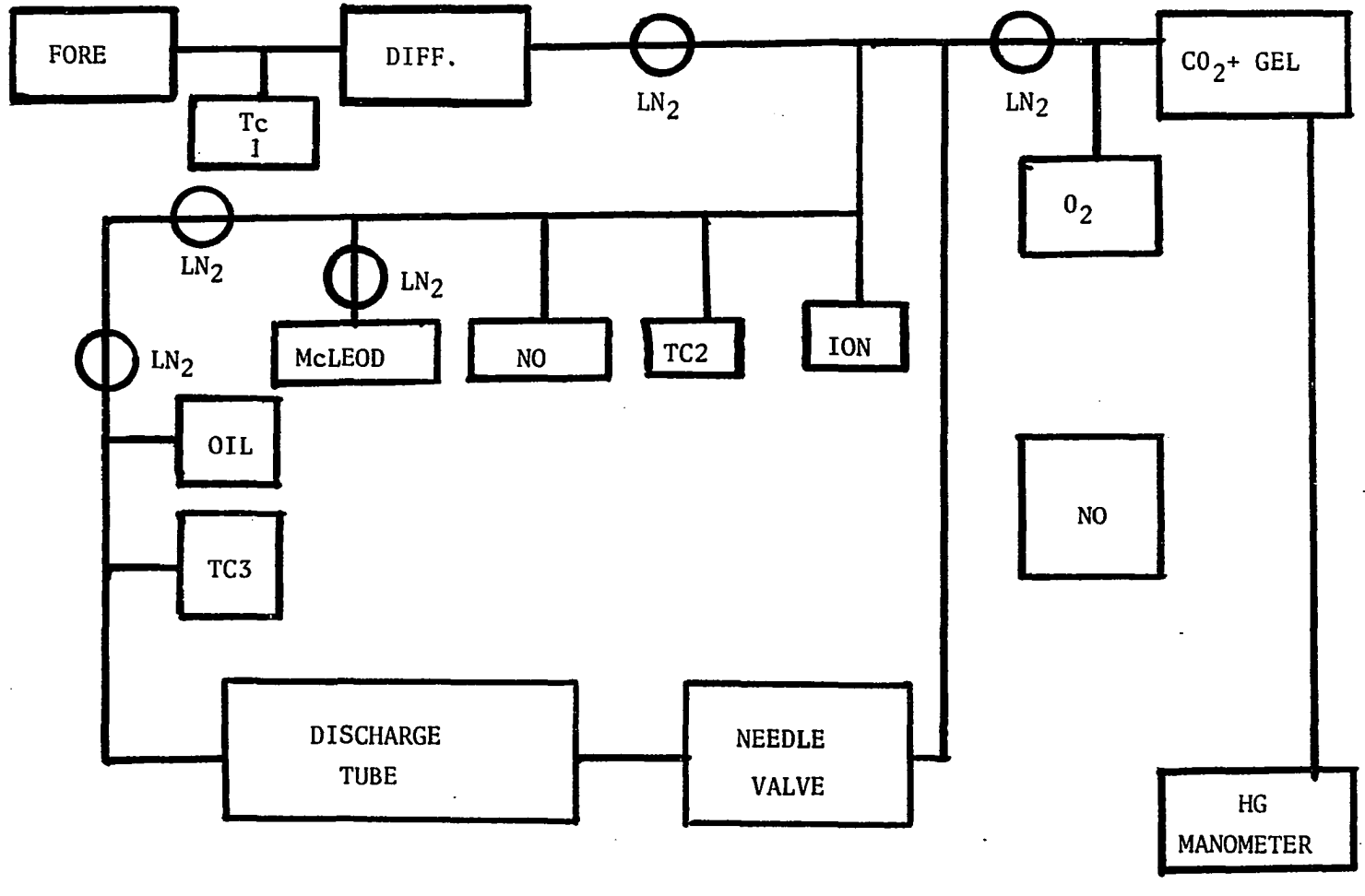

Figure 3. Block Diagram of Vacuum System.

The glass ware of the entire vacuum system was made from Corning number 7740 pyrex tubing. All stopcocks were of high vacuum quality having pumpable bores. The stopcock grease used throughout was Apiezon N which has a base pressure at 20° C of $1x10^{-8}$ Torr.

The diffusion pump was a water cooled Eck and Krebs, two-stage mercury diffusion pump. It was followed by a liquid nitrogen cold trap in order to trap all back streaming mercury. It was preceded by a spherical dead volume of approximately 1000 cm^3 which served as a vapor trap for oils from the fore pump.

The pressure in the vacuum system was monitored by three thermocouple gauges, one oil manometer, one mercury McLeod gauge, one ionization gauge and one mercury manometer. The three thermocouple gauges and the ion gauge were commercial units manufactured by Consolidated Vacuum Corporation. They were controlled by a CVC type GIC-110B gauge pack. The thermocouples were CVC type GTC-004 and had a maximum pressure reading of two (2) Torr and a minimum of 10^{-3} Torr. These thermocouple gauges were silver soldered to a kovar to pyrex seal which was attached to the vacuum system. The ion gauge (CVC type GIC-017) was an inverted Bayard Alpert gauge. Its maximum pressure reading was $1x10^{-3}$ Torr and its minimum was $1x10^{-10}$ Torr. It was attached to the system by a nonex-to-pyrex seal.

The thermocouples were calibrated by comparison with an oil manometer. This manometer utilized Octoil S as its working fluid since Octoil S has an extremely low vapor pressure and a low value of the ratio of its density to that of mercury. At 20° C 14.85 millimeters of oil deflection equals one Torr. Care was taken to thoroughly out gas the silicon oil.

The mercury McLeod gauge had its useful range, using the standard quadratic McLeod formulae, of 4.6×10^{-2} Torr to 1×10^{-5} Torr. This gauge was fitted with a special cold trap which had equal input and output dynamic flow impedances. In addition, when the gauge was used, the mercury cutoff portion of the gauge was cooled to 0° C in order to reduce the Gaede effect[22].

Quite early in the experiment it was found that commercial Nitric oxide (NO) was only 95 per cent pure. Thus a gas purification system was built for the NO according to the suggestions of Hughes[23]. This system is composed of the Matheson commercial NO container which is connected to a stainless steel needle valve. The needle valve is silver soldered to a kovar to pyrex seal which in turn is connected to the pyrex system. The nitric oxide is first admitted to a trap filled with 6-16 mesh Indicating Silica Gel. (Fisher number S-155). This trap is maintained at -78.5° C by a dry ice (CO_2) and acetone bath. Pressure in this system is measured by a standard U-tube mercury manometer and is always kept below atmospheric pressure. Several minutes after the nitric oxide is introduced into the silica gel trap, the gel changes color from its normal blue to a deep gray. The nitric oxide is then released into a second trap which is maintained at 77° K by liquid nitrogen. Although the NO now solidifies, it still has a vapor pressure of 100 μHg. The trap is then opened to the diffusion pump and the residual gases are pumped away. When this vacuum distillation is completed the diffusion pump line is closed and the liquid nitrogen is removed from the trap. The trap then serves as the nitric oxide reservoir. It is connected via a 1 cm diameter pyrex tube to a pyrex to

a pyrex to kovar seal which is silver soldered to a stainless steel needle valve. The needle valve connects to a 0.020" I.D. stainless steel tube which is inserted via an "O" ring pressure seal to the back end of the discharge tube.

The research grade oxygen used in the experiment was obtained in one liter pyrex flasks from Airco Corporation and was attached to the system via two dosing high vacuum stopcocks. Soft iron "breakers" covered with pyrex envelope were used in all three one-liter reservior flasks.

The general procedure before each data run was to pump the entire system to 1 x 10^{-3} Torr using only the fore pump. Next the diffusion pump was activated after the cold traps were in place. The entire system was thoroughly outgased by heating tapes and natural gas flames until the base pressure was less than 1 x 10^{-6} Torr. Next the thermocouple gauges were calibrated and zeroed against the oil manometer. Finally the flow system was set into operation. The flow system worked so well that a pressure of 30 μHg would be maintained with the discharge tube in operation for several hours at a time without resupplying the nitric oxide reservoir.

CHAPTER II

COLD CATHODE DISCHARGE TUBE

The heart of the entire experiment is the discharge tube. Its design changed several times during the initial phase of the experimental work. The specifications for the excitation source were (1) excitation of atoms and molecules without using a heated cathode, (2) possibility of flow system, (3) use in vacuum UV experiments, if possible, (4) quick electronic excitation shutoff (i.e. less than 10 nanoseconds fall time for excitation pulse). All four of the criteria of performance have been achieved.

The excitation tube is basically a modified Geiger-Meuller Tube, but is used in an entirely different mode of operation. The discharge tube has a 6" long hollow cylinder as its cathode. The cathode has an I.D. of 2" and is constructed from standard stock aluminum. The anode is a stainless steel cylinder which fits coaxially into the cathode. It has a 4 mm diameter and is somewhat longer than the cathode assembly.

The anode is insulated electrically from the cathode by two boron nitride spacers. These spacers located at the back of the discharge cavity are fitted with viton "O" rings in order to insure pressure seals. The anode fits through the middle of the boron nitride spacers and has an "O" ring seal maintaining its position as well as

the pressure integrity. The outside back end of the tube is fitted with machine treads which fit the inside of a male UHF connector. This maintains the coaxial arrangement of the system and thus produces minimum stray inductance and capacitance.

The other end of the discharge tube is connected by a slip "O" ring arrangement to the vacuum system. This viewing end is equipped with a quartz window seal to a 2" diameter quartz pump chamber. The pump steam consists of a vycor to pyrex graded seal and is 1/4" diameter. If necessary the viewing end could be left open or fitted with lithium fluoride window for use on a vacuum ultraviolet spectrograph.

A later model of the discharge tube was equipped with a flow system for the NOγ studies. The back of the discharge tube was pierced with a hole and a 0.020" I.D. stainless steel pipe was inserted as the source of the gas. This arrangement is fitted with an "O" ring seal which is easily assembled.

A cross sectional view of the discharge tube is shown in Fig. 4. Note the arrangement of the coaxial insulation spacers and pressure seals. A picture of the discharge tube assembled is seen in Fig. 5 and in Fig. 6 the tube is shown in its various components.

COLD CATHODE DISCHARGE TUBE (Not to scale)

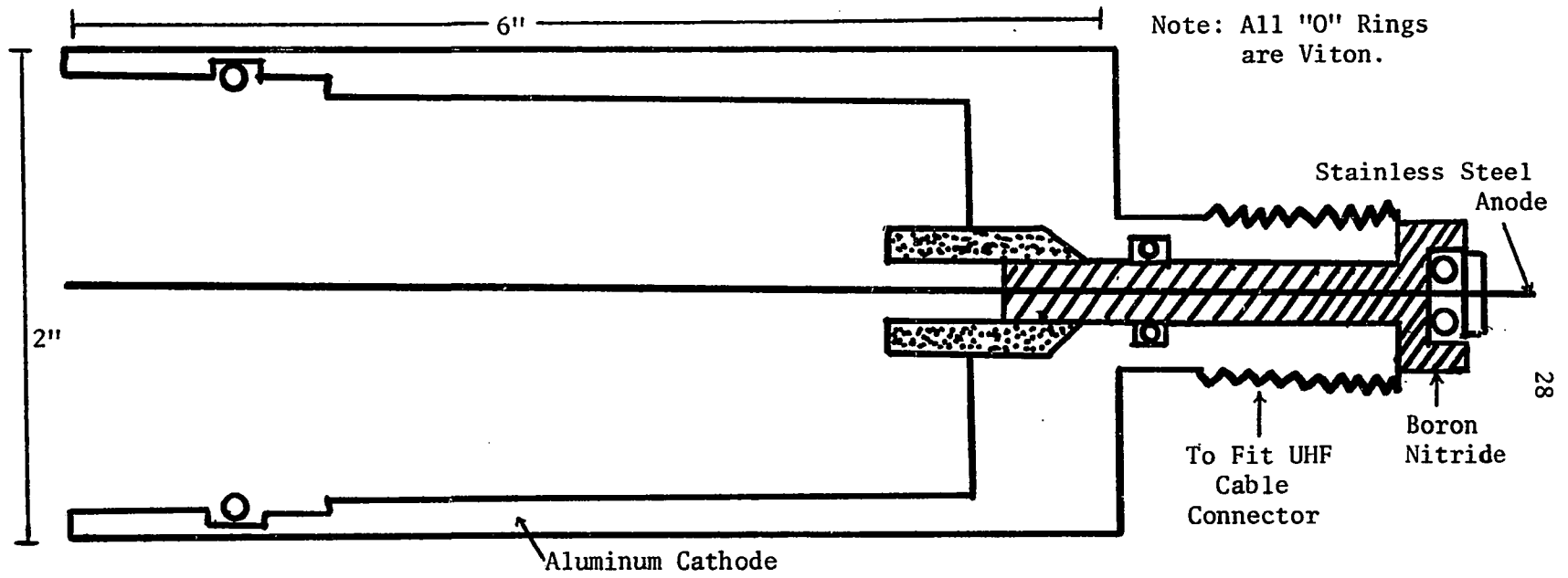

Figure 4. COLD CATHODE Discharge Tube Cross Sectional View.

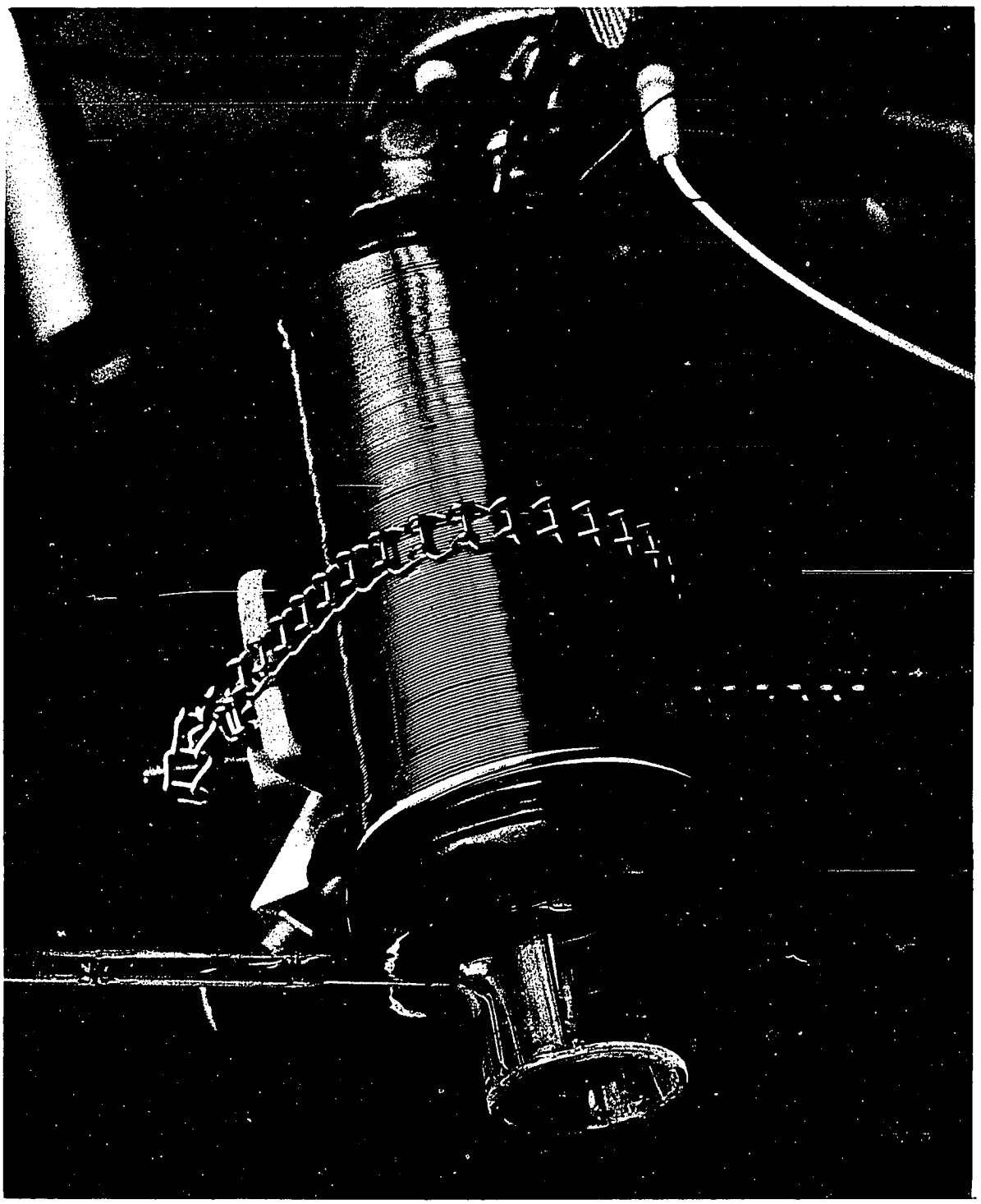

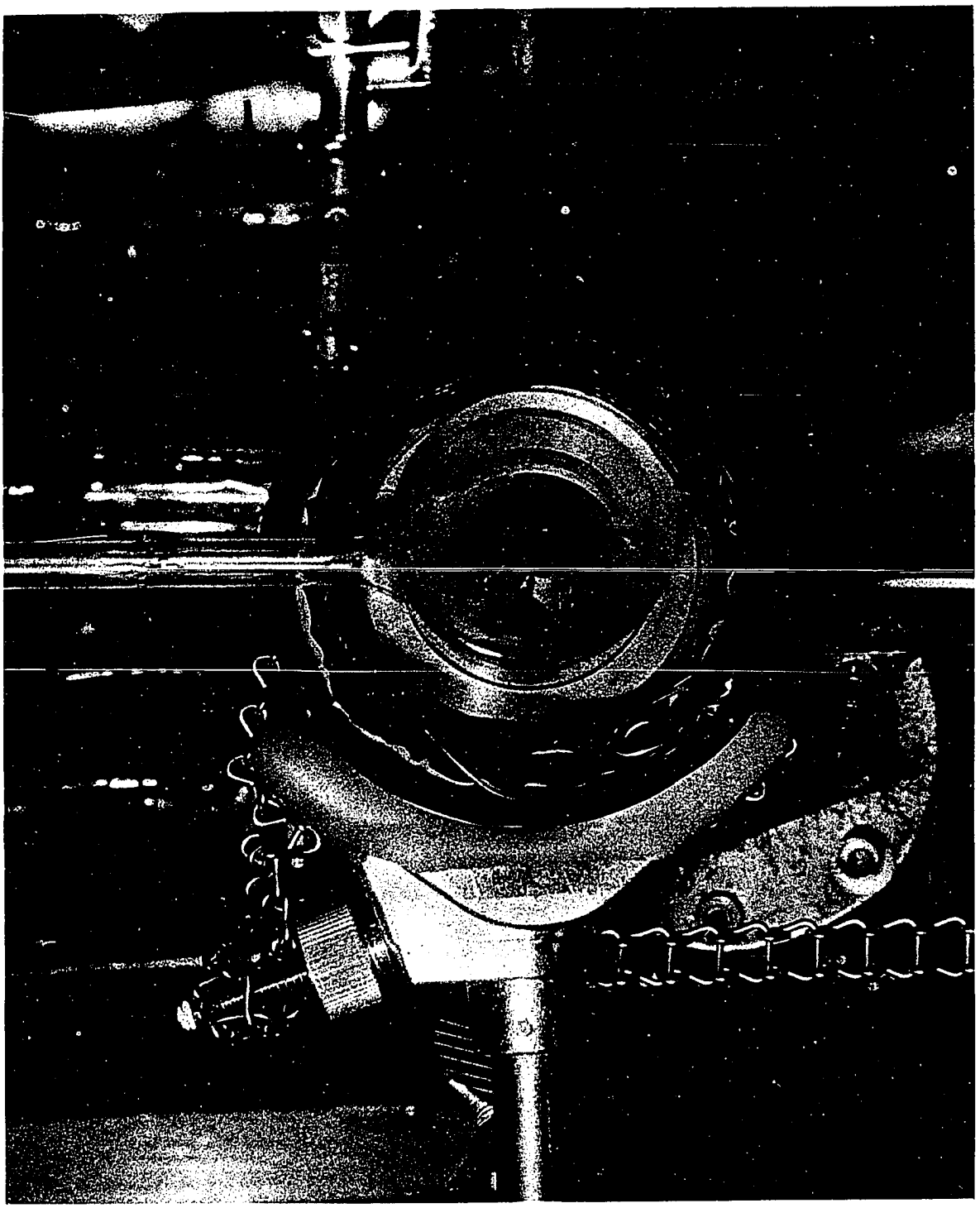

CHAPTER III

MAGNETIC FIELD SYSTEM

Due to the fact that the electrical breakdown taking place at the onset of the discharge is governed by Paschen's Law, the breakdown potential is a strong function of pd, where p is pressure in Torr and d is distance between anode and cathode. This discharge tube has a fixed d of 2 cm. Paschen's Law states the breakdown voltage has a minimum value and rises steeply as pd decreases and slowly as pd increases. The exact analytic form for Paschen's Law is extremely complicated in the coaxial cylinder geometry since the electric field between anode and cathode cylinders is not constant but dependent upon the radial coordinate.

It was found that at 0_2 pressures of less than 90 μHg, the discharge was very difficult to turn on since the breakdown voltage was exceeding 3 kilovolts. The excitation pulse system could deliver 3KV pulses but only at 60 Hz, which is too low a repetition rate to be useful in photon counting work.

Thus a method had to be found to decrease the breakdown voltage of the discharge tube. Since Vb = f(pd) only, we have to change the product pd. Moreover, we want to be able to operate at low values of p. This implies that d must be changed and thus a large tube and long shut off times. This is an unacceptable solution.

Another way to lower Vb was found. As is well known a charged particle will, when enjected into a magnetic field, rotate about the magnetic field lines in a circular path. The path diameter and angular frequencies are determined by the field strength. Thus if a magnetic field was created in the discharge cavity perpendicular to the electric field, the electrons collision frequency would increase. The "effective" pressure is increased and the breakdown voltage is dramatically decreased. This effect was first noticed by Valle[24] and later Somerville[25] worked out the details.

The cold cathode discharge tube was placed inside a solenoid-magnetic field. The field was created by a coil 15 cm long and 5 cm diameter wound on the outside of the discharge tube. The field inside the solenoidal cavity is given by

$$H = (106.4)(I) \text{ gauss}$$

where I is measured in amperes. The field was measured with a commercial Hall probe and at I = 1.61 amps, H theoretical was 176 gauss while H measured was 172 gauss. During most of the data runs the field coil current was kept between 1.35 and 1.45 amps.

The current source for the magnetic field was a 48 volt DC power supply manufactured by Western Electric. The current was monitored by 170 Hickock Laboratory ammeter. The circuit for the magnetic field coils is shown in Fig. 7.

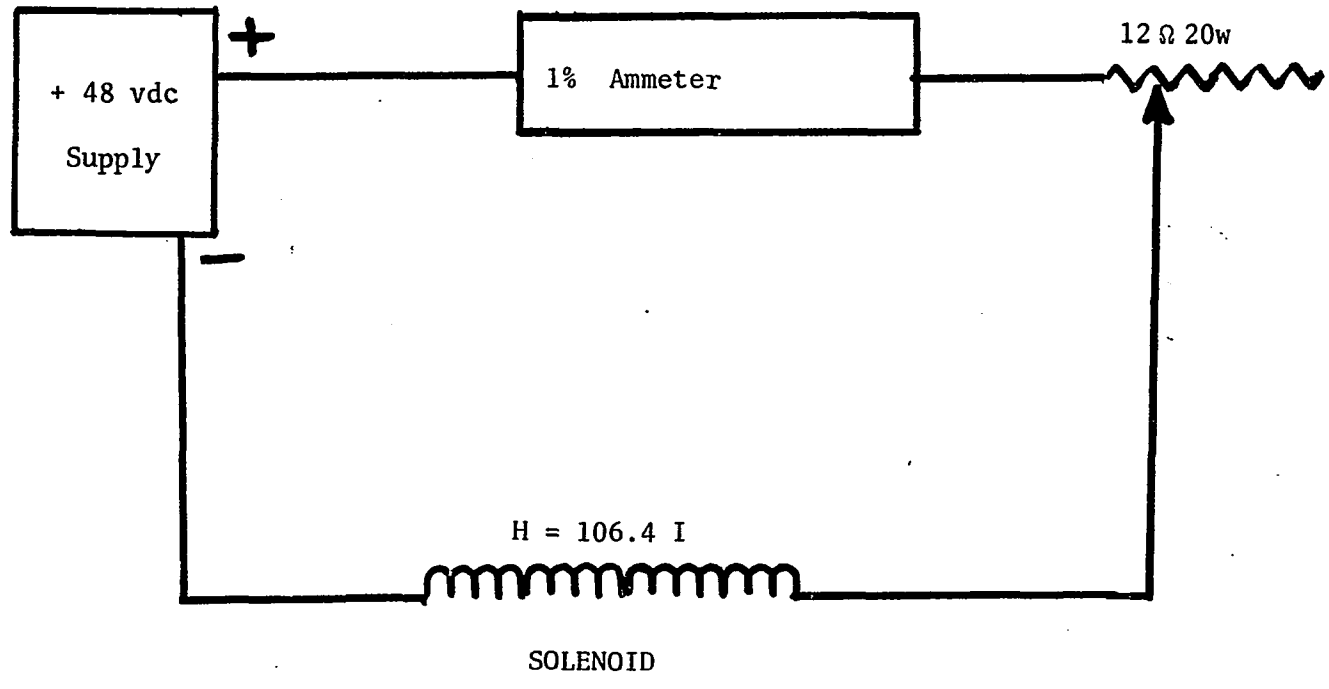

Figure 7. Magnetic Field Coil Circuit.

CHAPTER IV

OPTICAL SYSTEM

The basic optical system is shown in block form in Fig. 8. It is seen to consist of the discharge tube with quartz window, a f/4 3" diameter quartz lens, a ½ meter (16 Å/mm) Jarrell Ash monochromator and the RCA 8575 photon counting photomultiplier tube. When transitions were measured in the visible (λ 4000 Å) wavelength range, a Corning glass filter #3-73 was inserted into the beam path in front of the entrance slit of the monochromator. For transitions whose wavelength was less than 3500 Å a plastic scintillator Pilot B, ¼" thick and 2" in diameter, was placed ½" in front of the photomultiplier cathode in order to convert the ultraviolet photons to visible ones for detection.

The measurements as shown in Fig. 9 were made on the NOγ system which lies in the wavelength region 2000 Å to 3000 Å. In this case the lens was located midway between discharge tube and the entrance slit and was 35 cm from entrance slit. This separation of 70 cm of the discharge tube from the monochromator was necessary since the 100 gauss field inside the discharge tube was found to affect the PMT performance at closer distances.

The measurements performed on the $O_2^+(1-)$ system were done with a different optical arrangement. Since this system is entirely in the

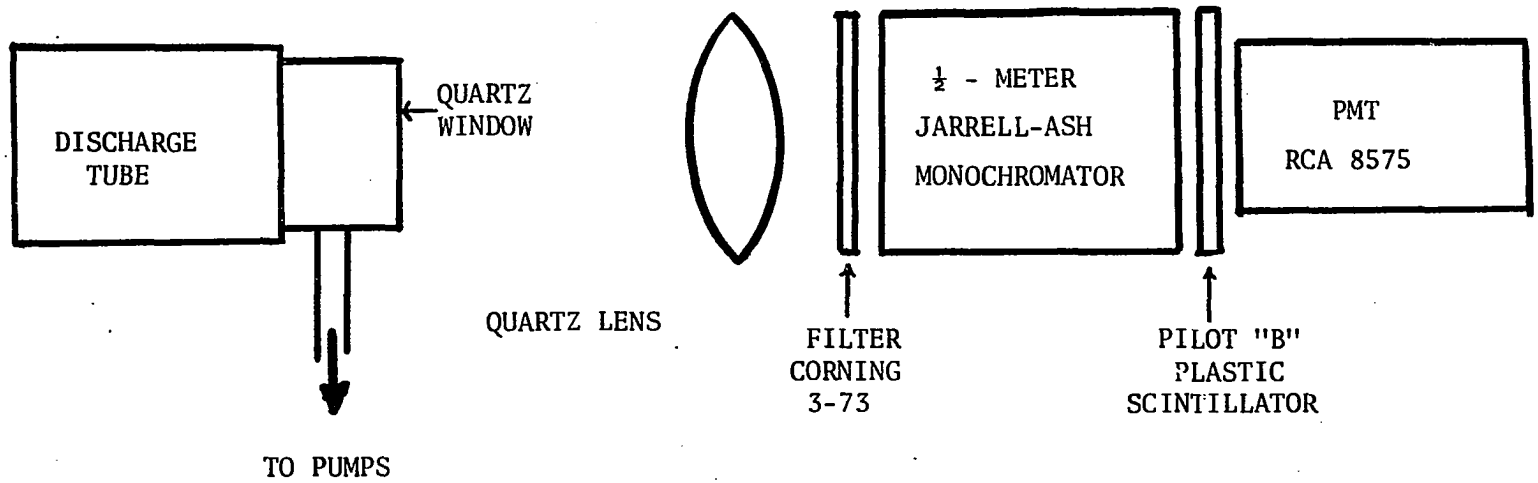

Figure 8. Block Diagram of Optical System.

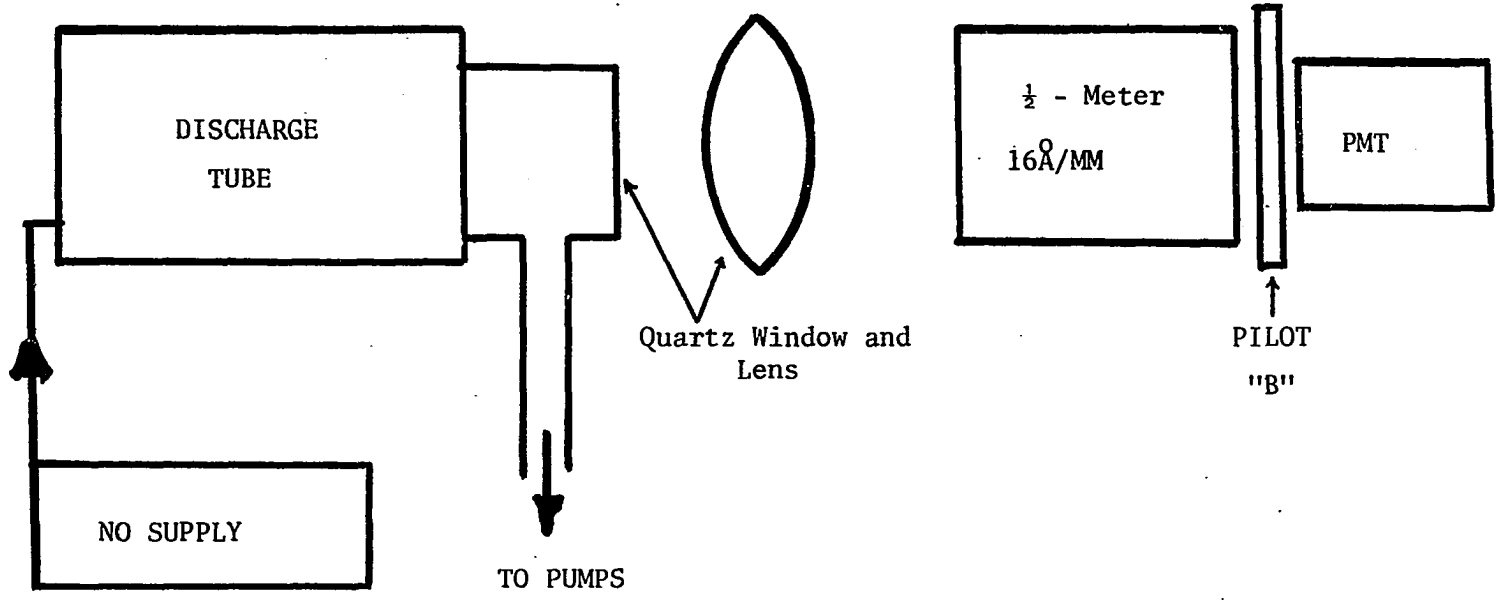

Figure 9. Optical System for NO Measurements.

visible the Corning filter was used as a guard against scattered light in the monochromator. In addition the discharge was viewed through two lens and three 90° silvered prisms. This arrangement is shown in Fig. 10. The total path length was 1.5 meters. Lens one was a compound lens 2.3 inch diameter and effective focal length of 18 inches manufactured by Bausch and Lomb. Lens 2 was the quartz lens described previously. P1, P2, P3 were fully silvered 90° reflecting glass prisms with entrance faces 1.65 in. x 1.65 in. The plastic scintillator was used in this series of experiments when spectra were taken from 2000 to 6000 Å, but was not used when lifetimes were measured in the $0_2^+(1-)$ system.

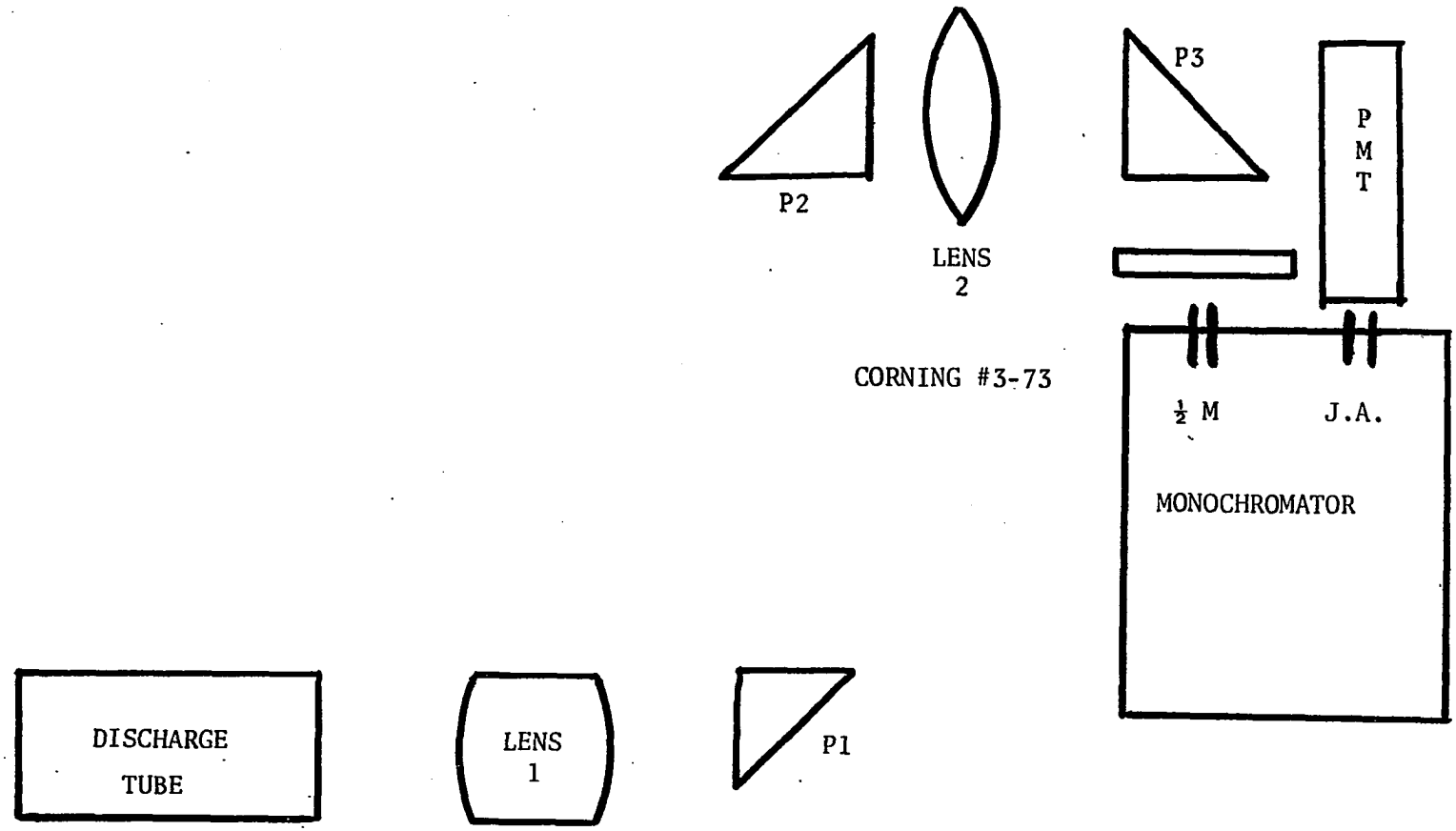

Figure 10. Optical System for O_2^+ Measurements.

CHAPTER V

EXCITATION PULSE AND TIMING SYSTEMS

The general purpose of these subsystems of the experiment was to supply a square wave potential of some 2 kilovolts of variable duration (100 nanoseconds to 20μ seconds) at variable repetition frequencies (60 to 1000 HZ). The general technique used was to charge a capacitor C and then discharge it through a resistance R (partially the resistance of the discharge tube). This produces an exponentially decaying voltage of time constant equal to RC seconds. After this potential was applied to the discharge tube, a 2D21 argon filled miniature thyratron placed in parallel with it, was turned on to "crow bar" the discharge. In this manner the square wave of up to 2 kilovolts, 400 nanosecond duration, 1 KHZ repetition rate, and three nanosecond fall time was produced.

We shall now trace out the evolution of this system. A block diagram is shown in Fig. 11 and contains all essential elements of the system. Figure 12 gives the circuit diagram for the +54 vdc and +27 vdc power supplies which are used to power the TIMING and DELAY GENERATOR These supplies are full wave bridge rectified and have Zener Diode stabilization. After long run periods (exceeding 8 hours) insufficient heat is dissipated by heat sink of 2N104 and the transformer and the output voltage decreases. This problem can be eliminated by placing the power supply in a blast of cool air.

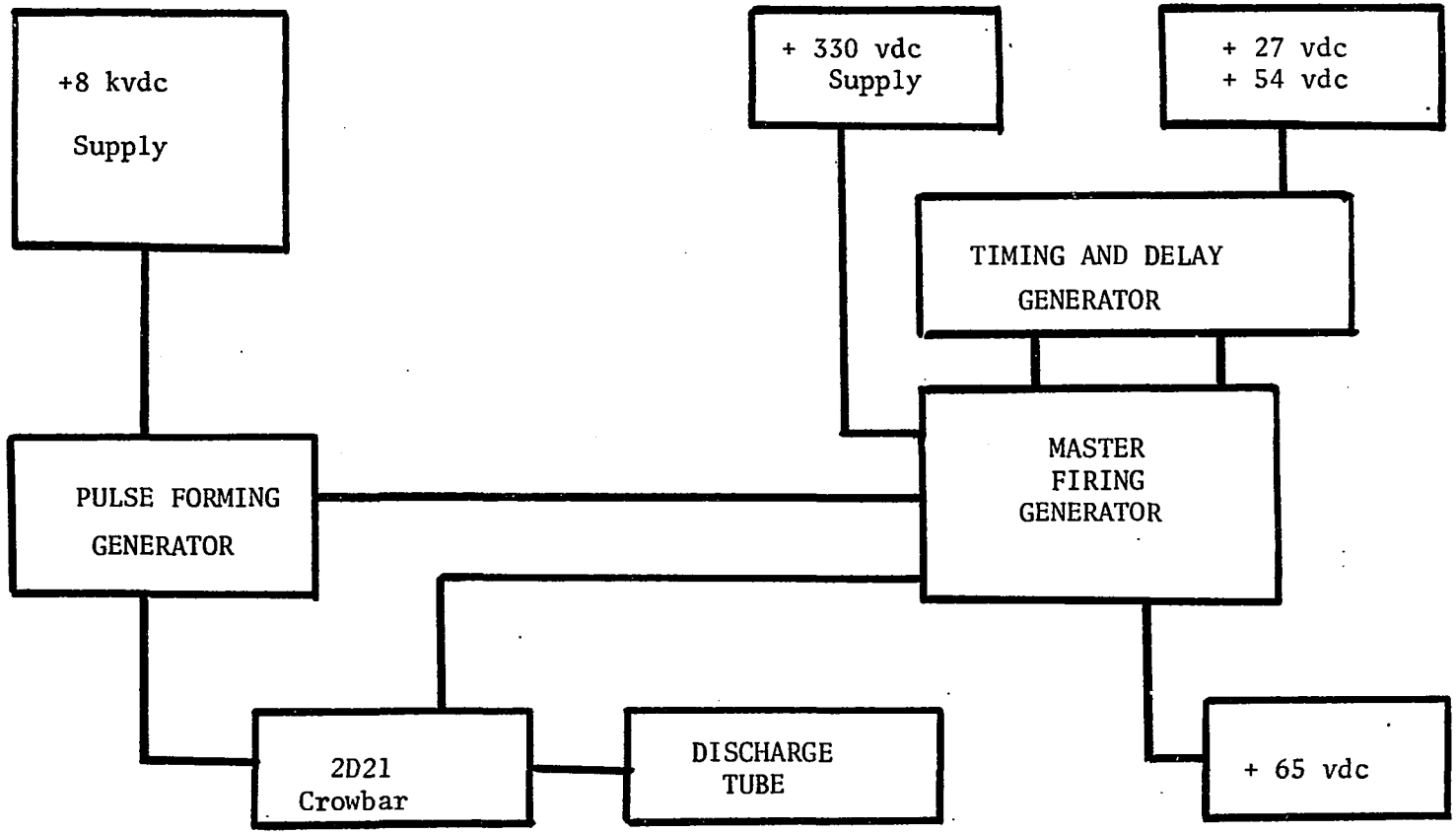

Figure 11. Block Diagram of Excitation System.

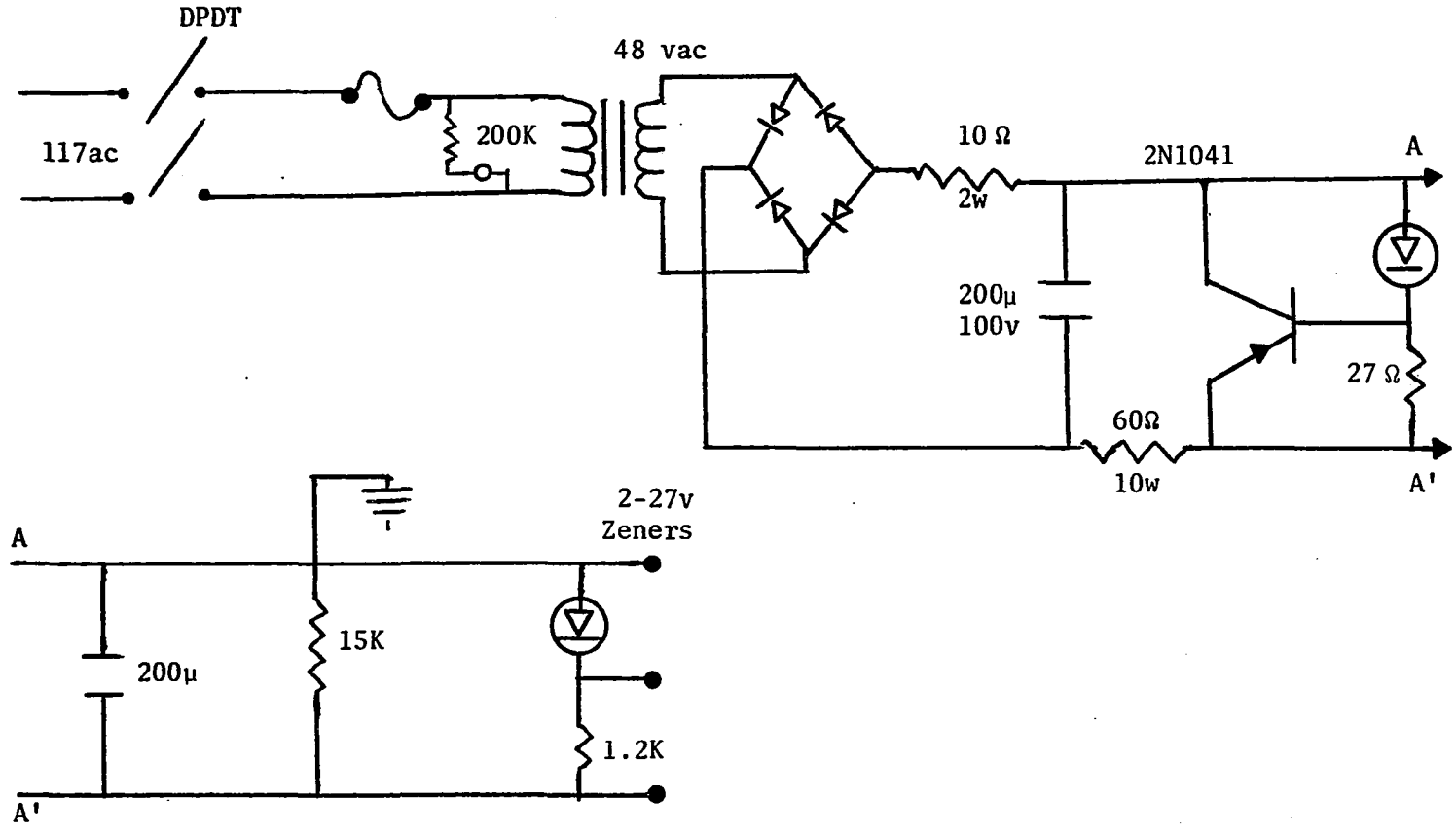

Figure 12. Circuit Diagram for +54 and +27 V dc Supplies.

Figure 13 gives the details of the TIMING and DELAY GENERATOR. This circuit uses three power supplies +27 vdc, +54 dc and +65 vdc. It is essentially a variable tunnel diode oscillator and time delay clock. This oscillator is connected to two identical pulse forming networks whose duty is to supply a fast rising (τ rise <300 nsec) high voltage and energy pulse to the grids of two 2D21 thyratrons. Each of the pulse forming networks contains a dual flip flop (multivibrator) with variable reset and delay times. These multibrations are followed by inverting and pulse shopping networks. The entire TIMING AND DELAY GENERATOR is built on two chassis. The outputs of the first chassis are negative going spikes 20 volts high and one microsecond long. These are fed via 50Ω shielded coaxial cable to the 2D21 MASTER FIRING CIRCUIT chassis where they are inverted and sharpened by the 2N3440 RCA high voltage switches.

The circuit for the 2D21 MASTER FIRING GENERATOR is shown in Fig. 14. The chassis is supplies with +310 vdc, -310 vdc +65 vdc, and 6.3 vac by a well regulated commercial power supply built by U. S. Science Corporation and obtained through the Oklahoma State Agency for Surplus Property. The master firing generator consists of two 2D21 thyratrons which have negative bias on their grids. Each thyratron is fired by the Timing and Delay Generator by a voltage pulse 65 volts high, 10μ seconds long, and rise time less than 200 ns. These 2D21 thyratron switches then close and discharge small capacitors charged to 310 volts through a 50Ω cathode load resistor. The first output of these devices are sent to the pulse forming generators while the second output is time delayed is sent via 50Ω coaxial cable to the 2D21 crowbar.

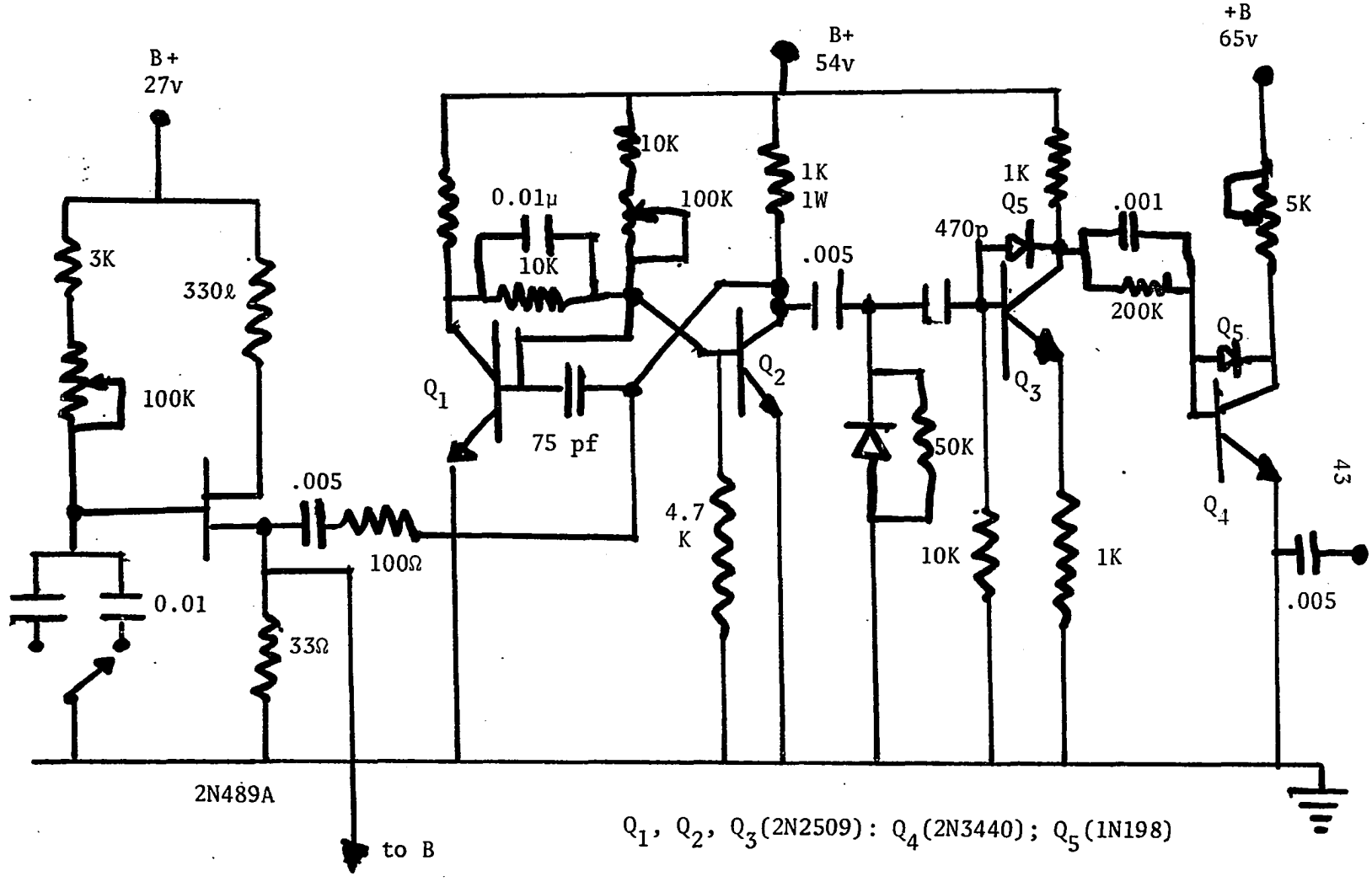

Figure 13A. Circuit Diagram for Timing and Delay Generator (TDG).

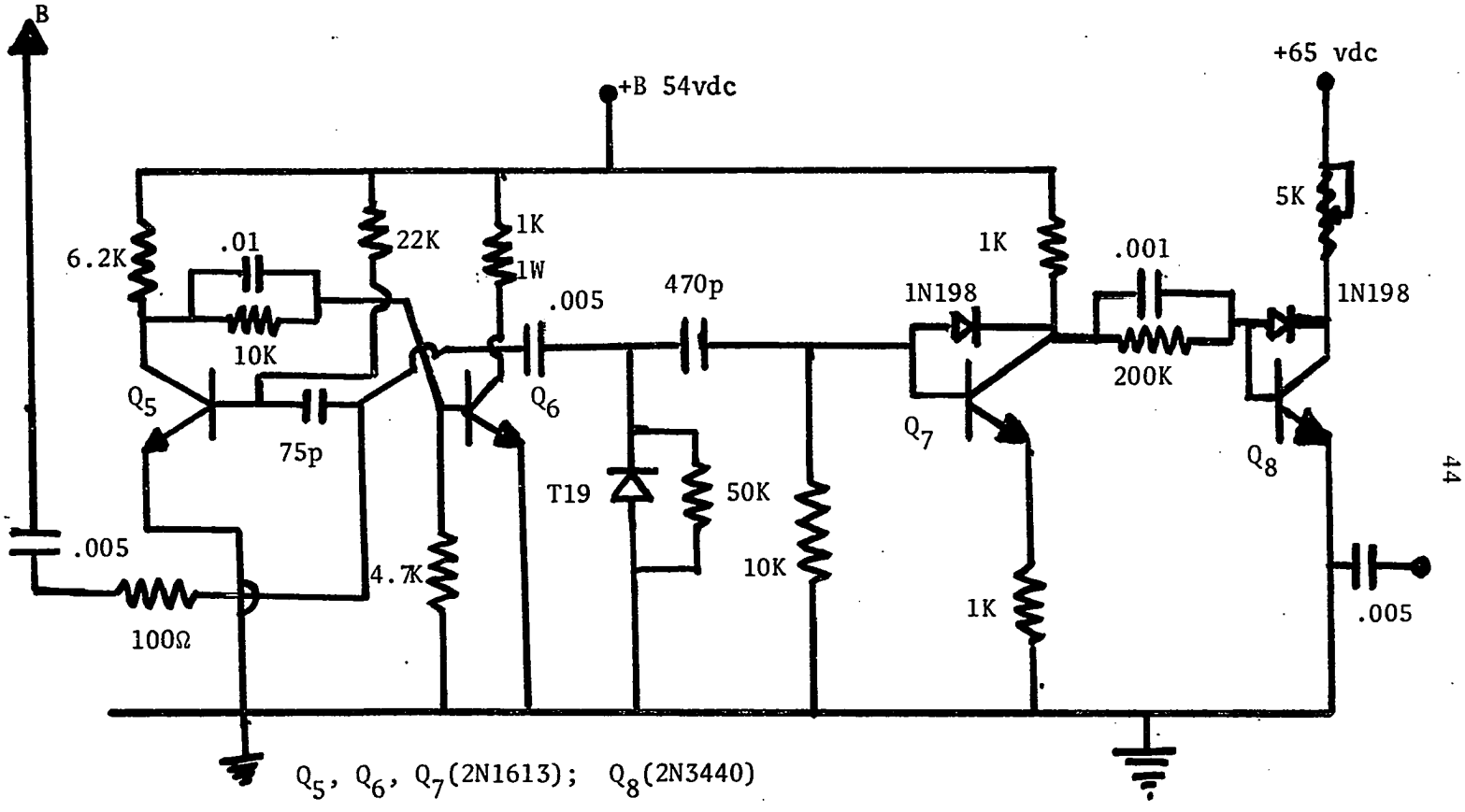

Figure 13B. Circuit Diagram for Timing and Delay Generator (TDG)

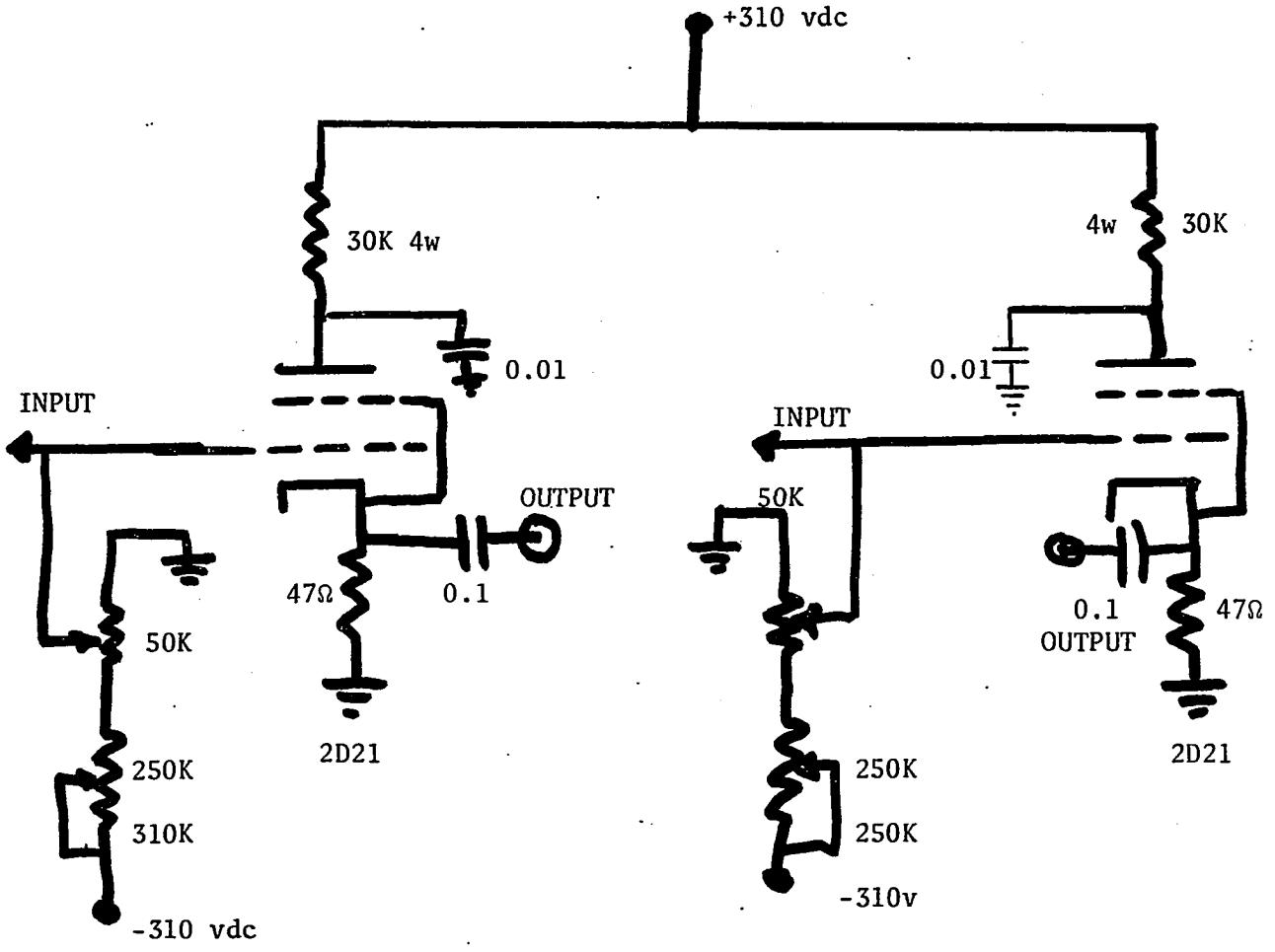

Figure 14. Circuit Diagram for Master Firing Generator (MGF).

The PULSE FORMING GENERATOR is shown in Fig. 15. It consits of a high voltage, high current hydrogen triode thyratron type 6130/3C45 which is used to discharge a capacitor through the discharge tube. The chassis contains heater and isolation transformers for the 3C45, in addition the 3C45, a 10 kV .001 μf oil capacitor, a cathode resistance (multiple resistors of 10 watts each), coupling capacitors to the 3C45 grid, and input connectors for high voltages.

The high voltage supply for the excitation pulse is supplied by a very high current and high voltage supply. It contains a power line transformer which will deliver 5 amps at 7700 volts, (35kV A). The alternating current is fed via high current and voltage cables to another chassis where it is converted to direct current by a bridge rectifier circuit. The arm of the bridge consists of three silicon diodes which are rated at 4000 volts peak inverse and one amp forward current. Each of the three diodes in the arm is placed in parallel with a 5 watt 1 megohm resistor, and a 0.005 μf disc ceramic capacitor in order to provide a bleeder string to ground and to reduce spike amplitudes on the silicon diodes. The diode bridge charges a 14 μfd 50 kV peak oil filled capacitor which is provided with an automatic bleeder in addition to a voltage monitor. Output of this power supply is fed directly to the plate capacitor of the PULSE FORMING GENERATOR via UHF coaxial cable. The circuit diagram for this high voltage supply is shown in Fig. 16.

The excitation pulse to the discharge tube was shut off, i.e., crowbarred, by turning on another discharge in parallel to the cold-cathode discharge tube. A special circuit was mounted directly to the cold cathode discharge tube using UHF connectors. The output pulse

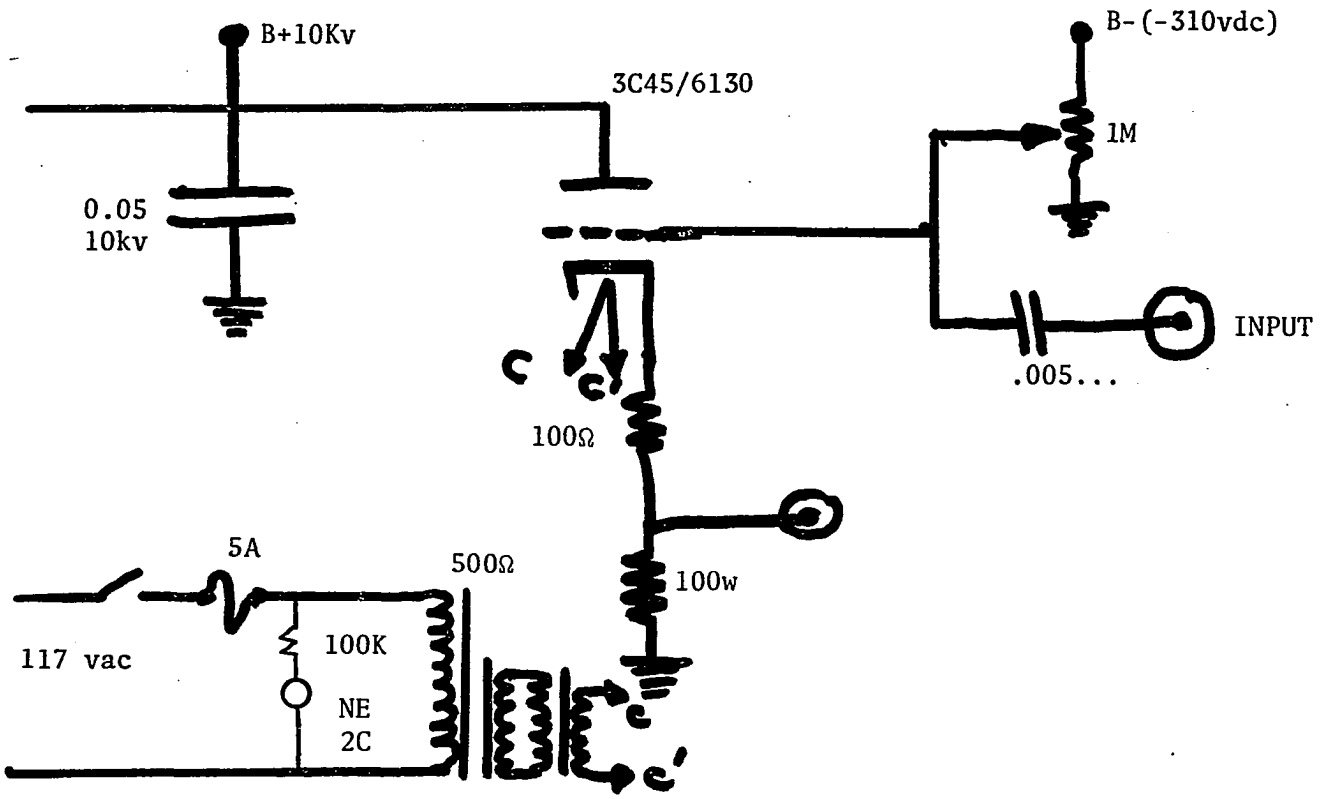

Figure 15. Circuit Diagram for Pulse Forming Generator (PGF).

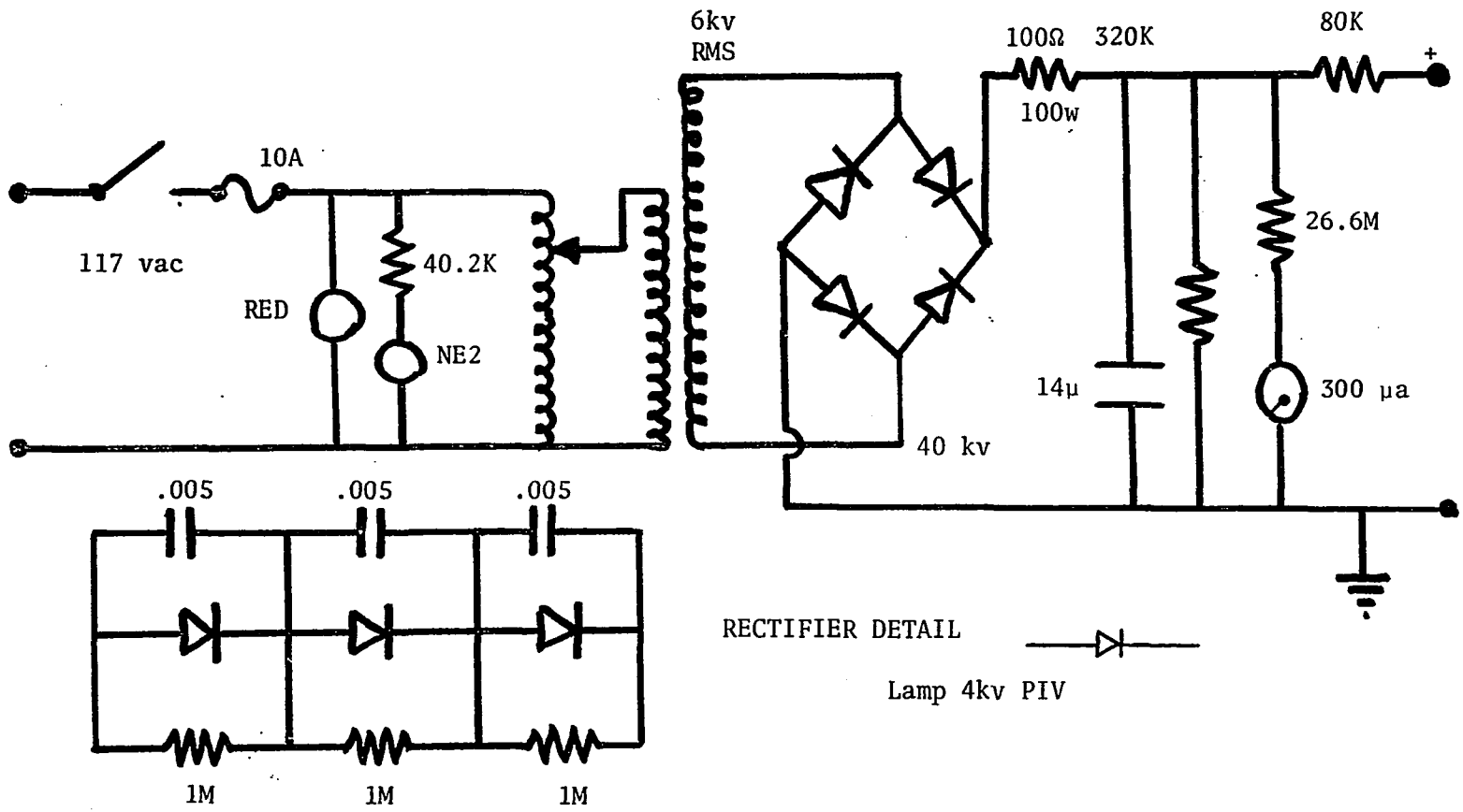

Figure 16. Circuit Diagram for High Voltage Supply

from the PULSE FORMING GENERATOR was conducted to cold cathode tube anode by way of UHF (50Ω) cable. This voltage pulse was applied to the anode of the cold cathode tube where, after a certain statistical lag time, a discharge was struck. After the discharge had been on for less than one microsecond, a signal was sent to the CROWBAR GENERATOR from the MASTER FIRING GENERATOR which turned on the 2D21 in parallel to the cold cathode tube. This effectively shunted out the discharge tube and produced an applied wave form of the desired shape. Great care was taken in the design and construction of the GROWBAR GENERATOR in order to insure the shortest possible lead length and thus minimize stray inductance and capacitance. Figure 17 shows the circuit diagram of the GROWBAR GENERATOR. Other features of the CROWBAR GENERATOR include an output (the START OUTPUT) to the Ortec time-to-height converter. This signal must be 5 nanosecond wide, -250 mvV deep and must be syncronized with the disruption of the discharge. This is generated by tapping some of the excitation pulse from the anode of the 2D21 via an 11 megohm carbon resistor chain. This effectively differentiates that signal and produces a positive pulse (which does not effect the time-to-height converter) followed by a negative going pulse (START) which activates the clock.

Figure 18 shows the excitation voltage as applied to the anode of the discharge tube. This figure was taken utilizing a type 555 Tektronix Oscilloscope, a type L plug in amplifier, and a 100 x probe. The frequency response is limited to about 50 mHZ for this system; thus, the apparent rise time is that of the measuring system. The time base is 500 ns/cm and vertical deflection is 200 v/cm.

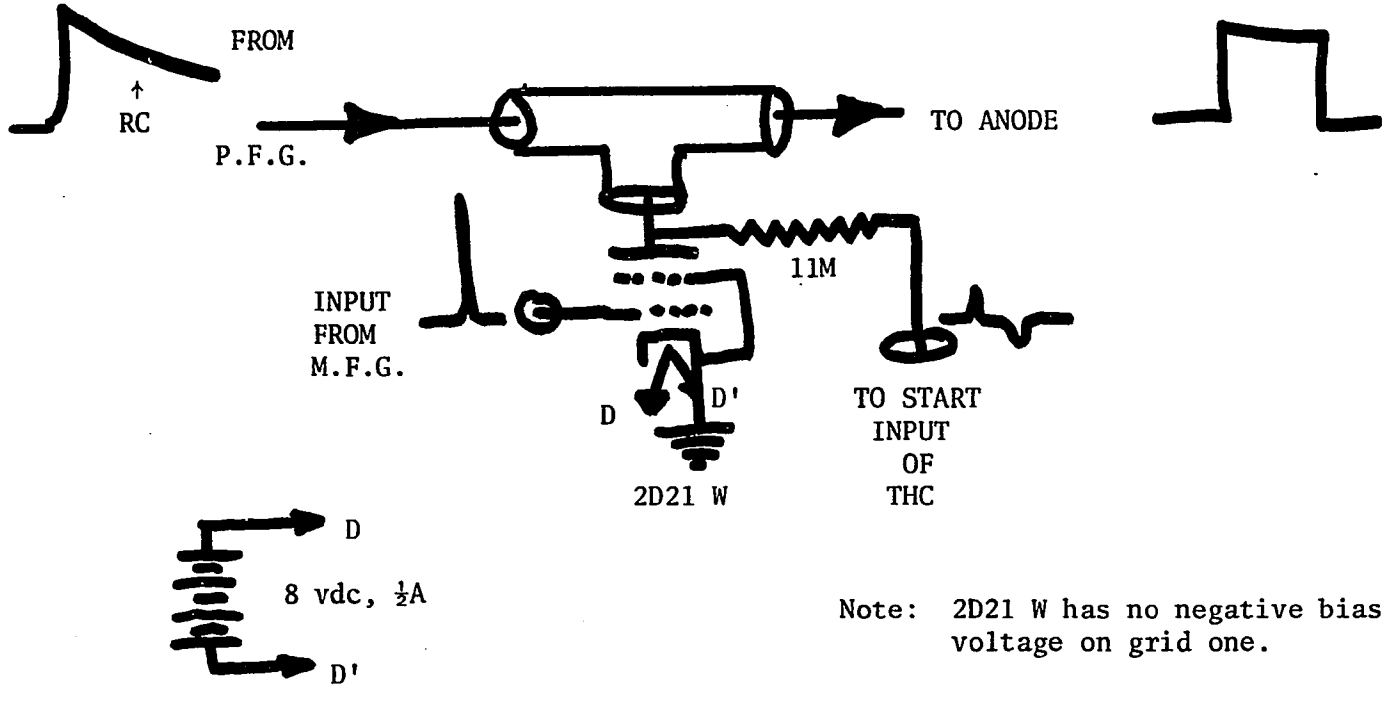

Figure 17. Circuit Diagram for Crowbar Generator.

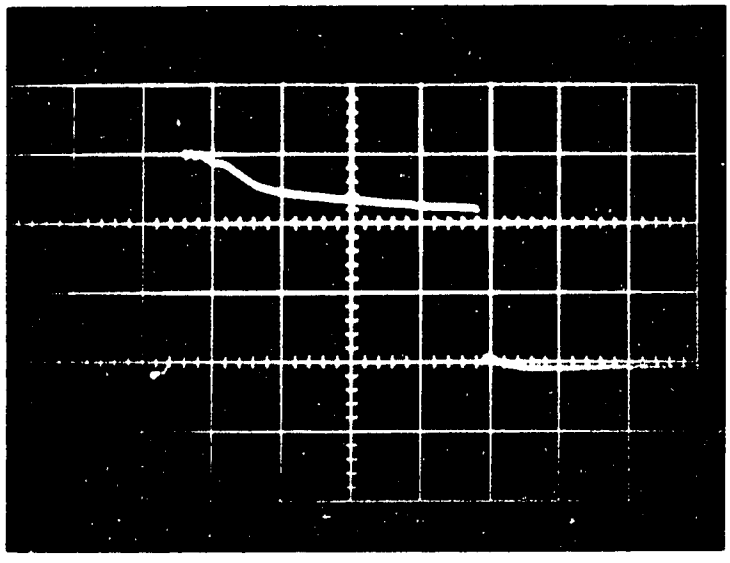

EXCITATION VOLTAGE

200 v/cm and 500 ns/cm.

100x probe type 555

Type L Preamplifier

Figure 18. Photograph of Excitation Voltage Waveform.

Figure 19 shows the shut off of the excitation voltage as photographed from a Tektronix type 454 150 mHz Oscilloscope. The time base is set at 5 nanoseconds / cm and the vertical diffection is 100 volts/cm. The apparent full time is that of the discharge tube and is less than 5 ns.

Figure 20 shows the START pulse which is the differentiated form of the excitation pulse terminated in 50Ω. Vertical deflection is 100 mV/cm and time base is 5 ns/cm. The photograph is of display on Tektronix type 454 150 mHz oscilloscope.

Figure 21 shows the output of the Ortec tube base which serves as the STOP pulse to the Ortec Time to Pulse Height converter. The photograph is taken from display on type 454 oscilloscope and time base is 5 ns/cm and vertical deflection is 100 mV/cm.

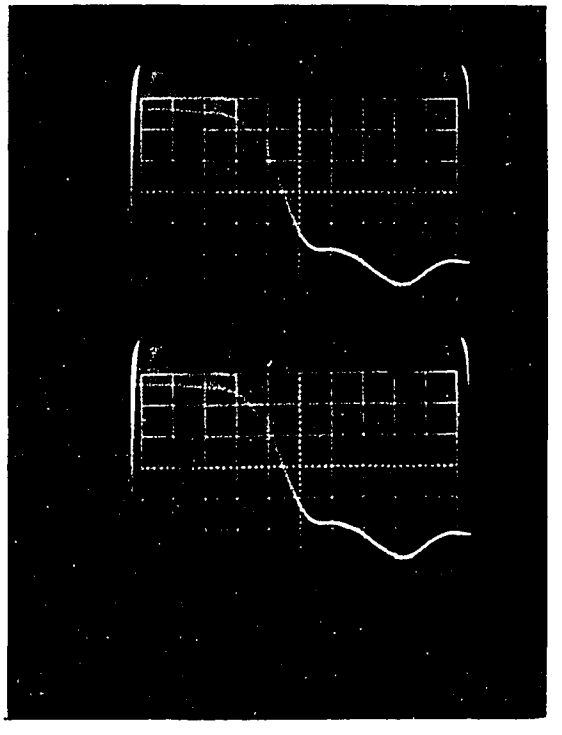

VOLTAGE CROWBAR

100 v/cm; 5 ns/div

100x probe type 454

Zero Voltage At Plus One Division

Figure 19. Photograph of Falltime of Excitation Waveform.

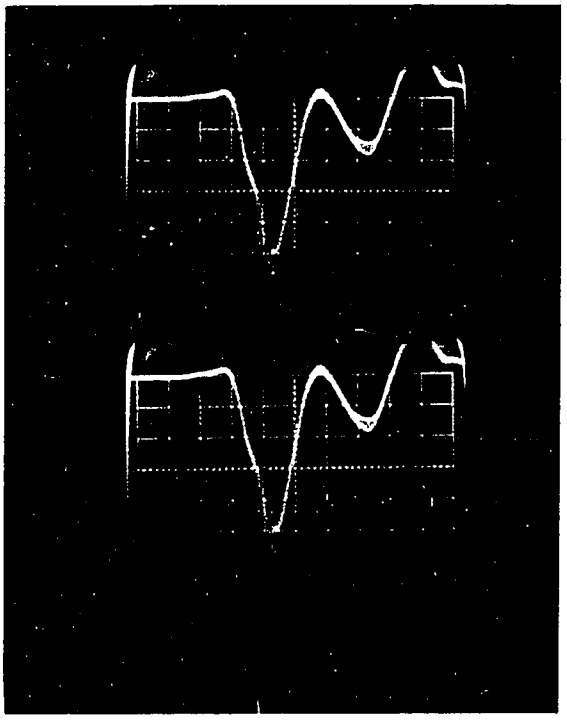

Figure 20. Photograph of START Pulse.

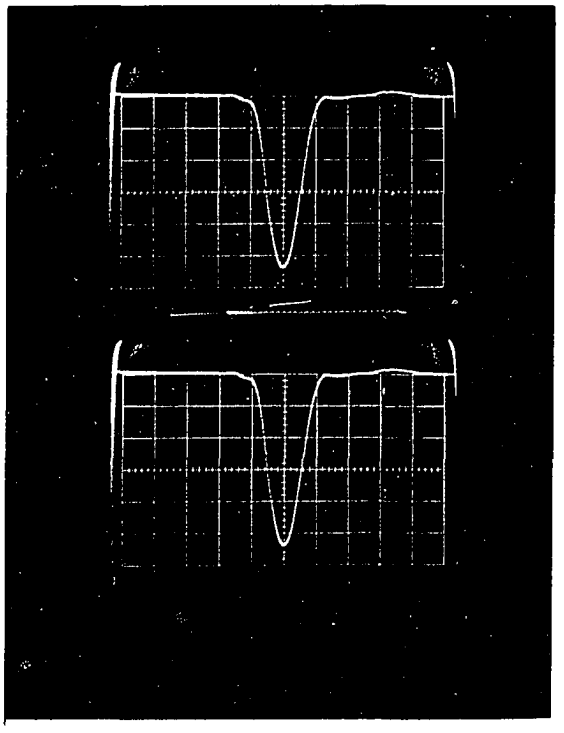

Figure 21. Photograph of STOP Pulse.

CHAPTER VI

DELAYED COINCIDENCE SYSTEM

The photon counting system is designed to build up in a ferrite core memory a signal which represents accurately the intensity of a given spectral line as a function of time after a desired point in time. This is done by sampling many hundreds of thousands of events which are repetitive and reproducible. An event is defined as the sequence of turning on a discharge, turning off the discharge, sensing a START signal and detecting a STOP signal. The act of turning on and off the discharge is handled by the excitation pulse system which has been previously described. The apparatus which detects the START, and the STOP signals and then performs pulse height analysis is called the delayed coincidence-lifetime apparatus.

A general block diagram of the entire detection apparatus is shown in Fig. 22. The exact sequence of events which take place in this apparatus will now be described.

We shall assume, that during the first microsecond after the discharge has been shut off, only one photon of proper wavelength will reach the photomultiplier cathode and produce a photon pulse at the output. This is not a necessary restriction but it simplifies somewhat the explanation of the delayed coincidence technique.

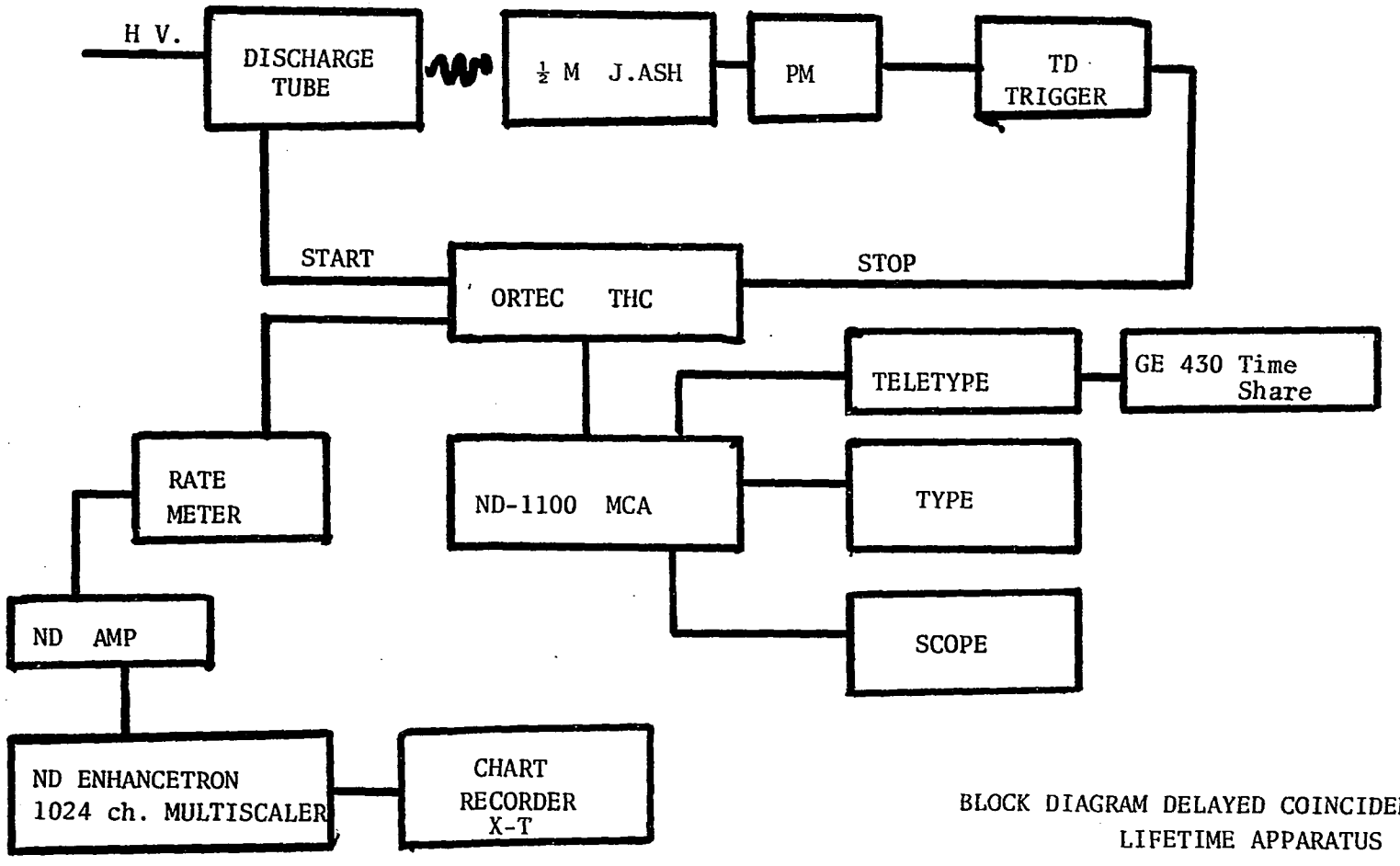

Figure 22. Block Diagram of Detection Apparatus.

At the termination of the discharge a signal is sent via 50Ω coaxial cable to the START input of the ORTEC Model 437 Time-to-Pulse Height Converter (THC). Upon reception of the proper START signal a clock in the THC is started. The first photon, which strikes the photocathode of the RCA 8575 photomultiplier after the START signal is received at the THC, produces, at the output of the ORTEC Model 264 Photomultiplier Timing Discriminator and Preamplifier (PTD), a negative going pulse of at least 250 mV and 5 ns rise time. This pulse is called the STOP pulse. The STOP pulse stops the clock contained in the THC. The THC changes this time delay into a voltage pulse. The shorter the time delay the lower the voltage pulse from the THC. The THC is operated in the anticoincidence mode and no gate is applied to its timing circuits. It processes signals only if a START pulse precedes the STOP pulse, thus any background photons which do occur during the first microsecond after the START pulse may be counted as signal. All other photon pulses (STOP signals) are rejected by the THC. This produces very large signal to noise ratios, typically 10^5:1. The output pulse of the THC is a bipolar positive portion leading variable amplitude pulse, which has a source impedance of 1 ohm.

The output of the THC is fed into a Nuclear Data 1100 multichannel analyzer (MCA) - which is operated in the pulse height analysis (PHA) mode. The THC signal is an analog signal which is first sent to the 1024 channel, Analog Digital Converter (ADC) operating in the 256 channel mode. In the ADC the analog signal is changed into a digital signal for processing in the data handling module (DHM). Maximum data acquisition rate for the ADC is four mega-hertz.

The digital information from the ADC is sent directly to the DHM which is operated in PHA mode. The DHM consists of a hard wired computer which sorts the information as to magnitude and assigns all pulses which fall within given tolerence to single channels of the memory module. The memory module contains 256 channels each of which has a count capacity of 10^6-1. For every event (START and STOP), one count is placed in one of the 255 data channels. Within which channel number an event is registered, depends linearly upon the voltage height of the bipolar THC output signal and thus directly upon time after discharge termination. The probability a photon hitting the PMT after the discharge is terminated depends exponentially upon time according to the lifetime of the excited state. After many hundreds of thousands of events the memory of the MCA will have stored the intensity of the spectral line as a function of time after discharge is shut off.

The information contained in the memory when doing a PHA experiment is portrayed live on an auxillary oscilloscope and is available in numeric form at either an IBM selectric typewriter or at a 33 ASR teletype in hard copy and punched paper tape.

The effective count rate in events/sec converted by THC is presented to an observer by a Nuclear Chicago Rate Meter. This information is obtained from the THC as a bipolar signal and is converted by a tunnel diode amplifier[26] into uniform positive pulses for acceptance by the rate meter. The rate meter provides a visual meter scale reading of count rate as well as an audio signal. In addition, an output of the rate meter is provided to a Nuclear Data Enhancetron for multiscaling experiments.

CHAPTER VII

TIMING CALIBRATION PROCEDURE

In order to use the information supplied by the delayed coincidence method, it is necessary to know the linearily of the time base of the THC. This leads to its calibration. This information can easily be obtained once a set of accurately known time delays standards are available. The procedure for calibration of the THC is nearly the same as used in collection of data for lifetimes. A start pulse is generated and fed into the START input of the THC. At the same time a portion of the pulse is sent through a known time delay and into the STOP input. The output of the THC will be a series of bipolar pulses of the same magnitude. By changing the values of the known times delays, one is able to construct the calibration of the time base.

If we are given m time delays, the output of the memory will contain only K nonzero channels ($m \geq K$). The count rate stored in these K channels is not useful data, but the channel number is important. Let c be the channel numbers. If t is the real time then, we find

$$t = a + bc$$

where $\underline{a}$ is the intercept on the time axis and $\underline{b}$ is the number of time increments per channel number. Usually $\underline{b}$ is measured in nanoseconds/channel. In general $\underline{a}$ will be nonzero which is due to time delays in

cables and settings on upper and lower discrimination circuits in the ADC. Thus of m cables used for calibration, only the m-k largest values of time delays are recorded. A linear least squares analysis of the data (t_k, c_k) will yield values of a and b.

CALIBRATION OF TIME DELAY CABLES

A series of seven different lengths of 50Ω RG 58/U calbe has been made into the time standard for this experiment. RG 58/U has chosen since it was a commonly available high frequency 50Ω BNC compatible cable. RG 58/U has a loss of .614 decibels/100 feet at 100 MHZ.

The essence of the calibration scheme lies in the ability to obtain electrical lengths of cables to better than one per cent for time delays longer than 80 nanoseconds. A sinusoidal signal of frequency ω is sent through an impedance matched cable in which it suffers a time delay t_d. If the signals observed as it enters the cable and after it leaves the cable are algebraically added, one has

$$V_{out} = A_1 \text{ Sin } \omega t + A_2 \sin(\omega t + t_d) \ .$$

If by varying the gain of null detectors working on each of the signals, the amplitudes of the two sinusoidal waves are made equal, then

$$V_{out} = 2A \sin \omega(t + \frac{t_d}{2}) \cos \frac{\omega t_d}{2}$$

clearly this expression implies nulls occurring when

$$\omega t_d = (2n-1)\pi \ ,$$

or

$$\omega = (\frac{2n-1}{t_d})\pi \ .$$

If nulls are recorded as the frequency is changed, then the time delay, t_d is obtained as

$$t_d = \frac{1}{f_2 - f_1} = \frac{1}{\Delta f} \quad .$$

A given length of coaxial cable RG 58/U was terminated at both ends by its characteristic impedance of 50 ohms. A constant amplitude harmonic free sinusoidal signal was introduced at one end of the cable using a Tektronix model 190B constant amplitude signal generator. The frequencies used were between 1 MHZ and 50 MHZ. The frequency of the electrical signal was measured using a Hewlett-Packard model 524D frequency counter interfaced with a Hewlett-Packard 525A frequency converter. This counter combination is useful to 100 MHZ and has a time base stability of one part in 10^8 per week! Frequencies could be measured to one part in 10^6 regularly without appreciable error. The time calibration of the counter was checked with the NBS time station WWV. The null detectors used in the experiment was a Tektronix type 454 oscilloscope. Its upper 3db point occurs at 150 MHZ. The signals were applied as shown in Fig. 23. The reference signal was applied to channel 2 and the delayed signal to channel 1. The gain on channel 1 was changed until both signals were of the same deflection as viewed on the oscilloscope. This method compensates for the signal attenuation in the delay cable. Channels 1 and 2 were algebraically added and the frequency changed until an absolute null was reached. The frequency was measured and the procedure repeated until the frequency reached 50 MHZ.

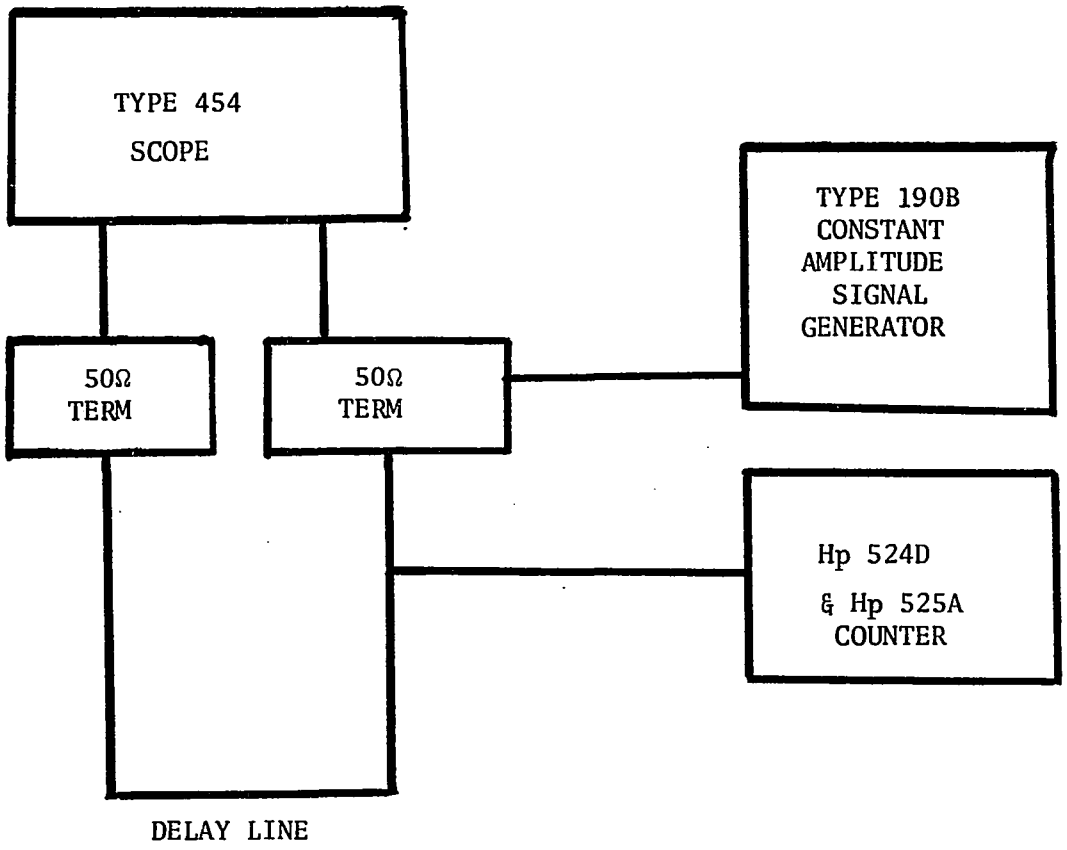

Figure 23. Block Diagram of Time Delay Calibration Apparatus.

Long cables were measured first since they produce the greatest number of nulls in the frequency range (1 to 50 MHZ). Short cable time delays were found by measurement of various combinations of cables. Largest percentage errors are thus on short time delays.

The final results and standard deviations are shown in Table 1.

Table 1. Time Standards

CABLE NUMBER	TIME DELAY NS	STANDARD DEV NS
1	101.4	0.50
2	88.09	0.90
3	44.0	0.2
4	28.0	0.3
5	378.5	2.2
6	183.2	1.6
7	88.7	0.77

CHAPTER VIII

SPECTROHISTOGRAM SYSTEM

In order to measure lifetimes of states which have transitions in that portion of the spectrum that can be detected by photomultipliers, it is necessary to have knowledge of the spectrum of the source. One must make certain that band systems and atomic spectral lines are free from impurity spectra and that the spectral calibration of the monochromator is known. Thus a detailed spectrogram must be obtained of the discharge.

It is important that a spectrum is obtained under the same conditions that a lifetime is measured. A method for taking a time-resolved spectrum was developed. A time resolved spectrum as defined here is the spectrum that is observed only during a certain time increment in which the source is on or just after the source is turned off. Thus the spectra which is recorded is biased time wise with respect to the relative intensity of the various transitions. This is due to the fact that if the time increment were set at 100 nanoseconds only those photons which are admitted to the counting system during the 100 nanoseconds are recorded. Moreover only the first photon in the time increment is counted. This implies that short lived states will be recorded as more intense lines and long lived states as relatively weaker lines. Even

though in real time using an integrating spectral detector (photographic plate), the relative intensity of the lines may be reversed.

The apparatus that perform this spectral analysis has been mentioned briefly above. The photon counting system is set to operate exactly as in the lifetime measuring mode. However, the output of the THC is sent to a device which performs a multiscaling experiment. The grating in the monochromator is driven by a dc timing motor in a linear manner, such that the wavelength appearing at the output slit of the monochromator changes linearly with time.

Since the MCA currently in use has only 256 channels and in its multiscaling mode the maximum dwell time per channel is only 800 milliseconds, only a very limited portion of the spectrum can be recorded and then only with poor definition. This problem is solved by tapping out of the rate meter a pulse signal which can be used as an input to a larger multiscaler.

A Nuclear Data Inc., 1024 channel Enhancetron, Model ND-800, is used in the pulse counting multiscaling mode (MS). The input pulse has a fixed amplitude between +3 and +10 volts and has a duration of 27μ seconds. Since the repetition rate of the source is less than one per 30.52 microseconds, all pulses sent to the MS are recorded. This instrument has 1024 channels each of which will hold 8192 positive counts. The dwell time of the MS is variable, and varies from 0.032 to 2048 seconds in factors of two. Usually data is collected using a dwell time of 512 seconds/1024 channels.

The output spectrum can be portrayed on an auxillary X-Y oscilloscope and photographed. A typical photograph is shown in Fig. 24. However, this mode of output is not useful for detailed analysis.

NO 170μ Pressure

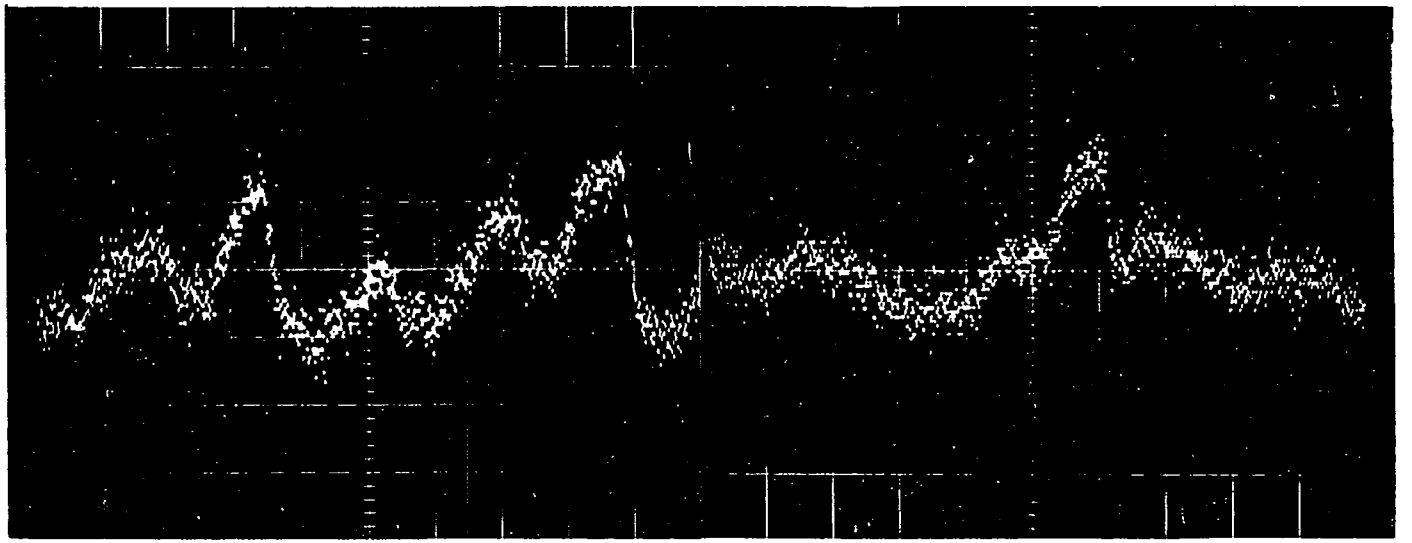

Figure 24. Photograph of Spectrohistogram.

An alternate and useful output mode is to plot out the contents of the memory and thereby obtain a hard copy of the spectrum. The method chosen for this output utilizes a Bausch & Lomb model V. O. M. 7 Laboratory Recorder. This output is called a spectrohistogram. The output from the Enhancetron has a base line from 0 to 0.3 volts positive and consists of pulses whose height is directly proportional to the number of counts in each channel. The pulses are separated in time. This is not an excellent signal for use with a recorder since recorders do not have high frequency response and usually do not have a current offset built into them.

A circuit which is shown in Fig. 25 was built for use with the recorder available. The recorder was generally operated as a current meter at the 100μ ampere scale. Chart speed was set at 5 in/min and the Enhancetron time base was set at 256 seconds. After nulling the recorder with the Enhancetron in the STOP 2 mode, with the vertical deflection output connected to the recorder, the readout sequence was begun. The response time of the recorder although less than ½ second was quick enough to produce a very readible chart of much higher fidelity than oscilloscope display. An example of the output spectrohistogram can be seen in Fig. 26.

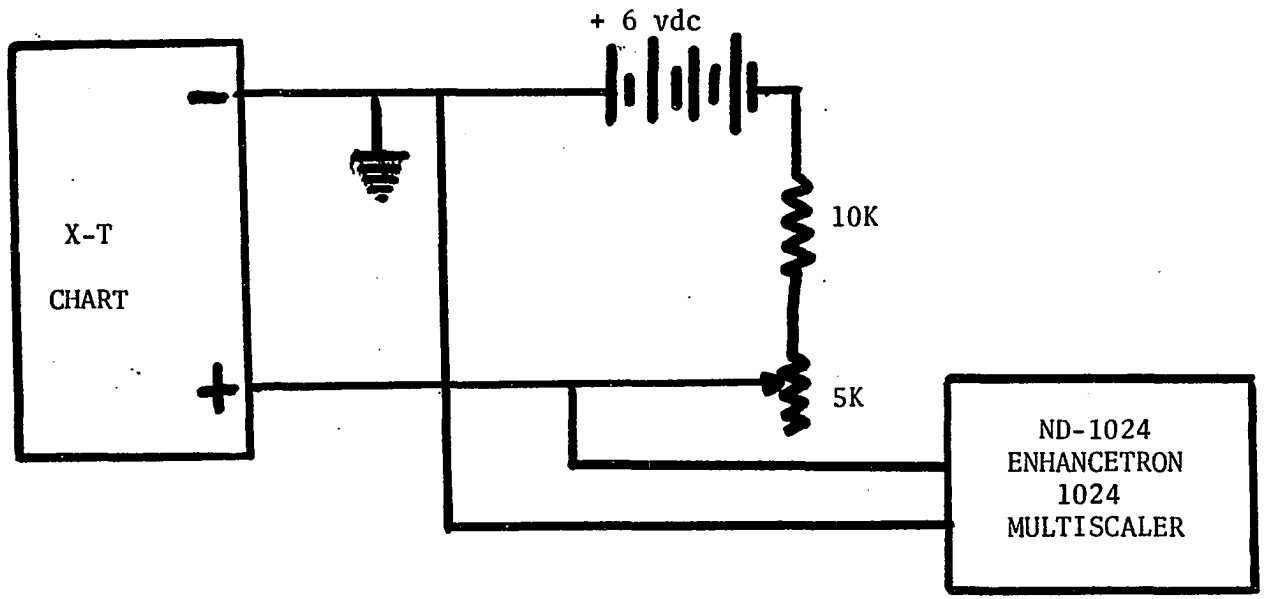

Figure 25. Circuit Diagram for Spectrohistogram Apparatus.

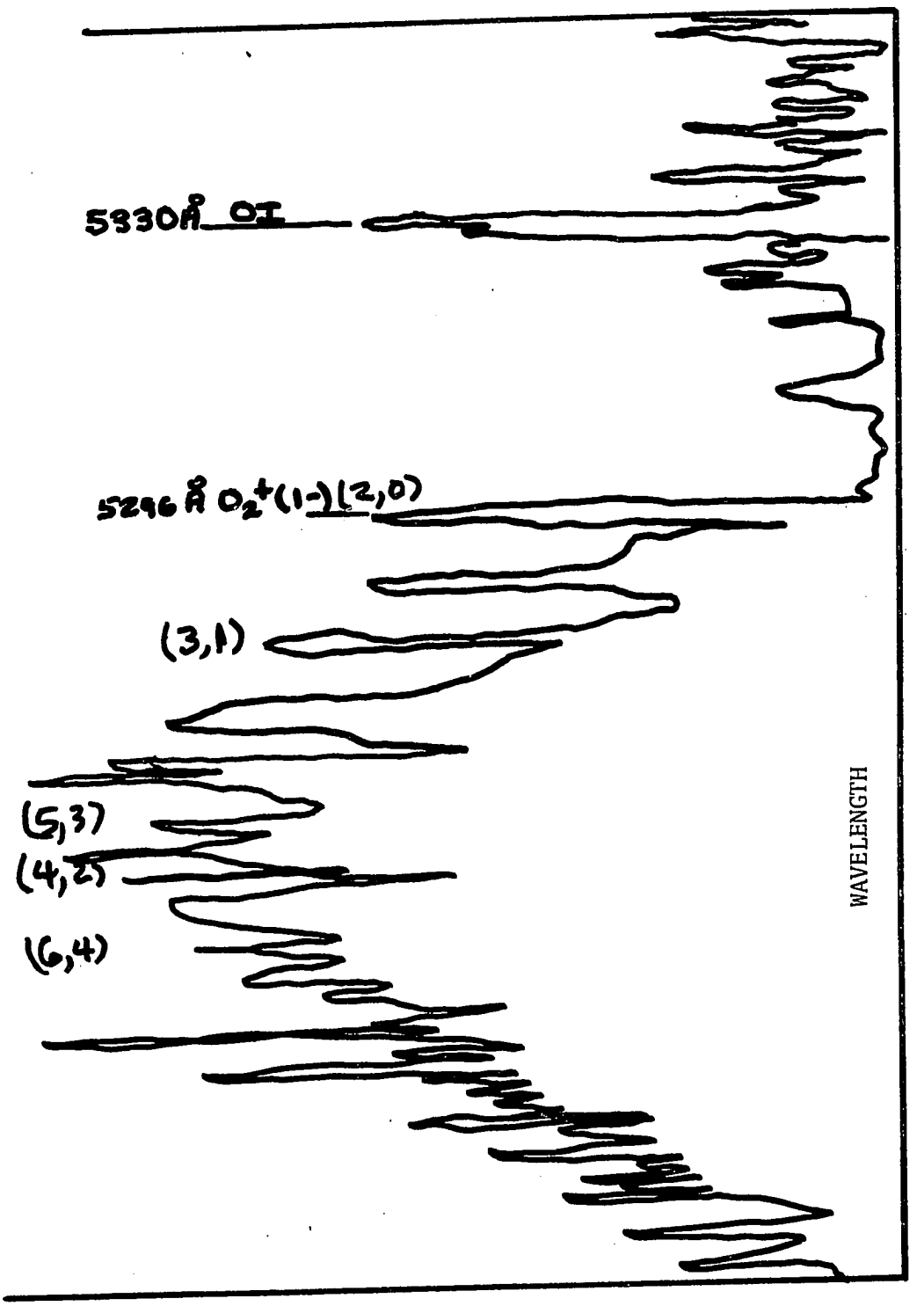

Figure 26. Example Output Spectrohistogram.

PART III

DATA ANALYSIS

CHAPTER I

INTRODUCTION

In a low pressure discharge there are many processes which affect the time rate of change of the population of a given state in a molecule or atom. The production processes include direct electron excitation from all lower states to the state of concern, cascade into the given state from higher excited states, and direct population by collisions with excited species (Penning transfer of excitation). The de-excitation process include spontaneous emission, stimulated emission and collisions of various types which transfer excitation from the state of concern. As is well known these processes depend upon parameters such as electron current and energy, gas density and temperature, flow rate, recombination coefficients, diffusion coefficients, various electron excitation cross sections, radiation field density, Einstein coefficients of spontaneous and stimulated emission, and Einstein coefficients of absorption.

Let us now restrict our view to the problem of analysis of data obtained in a delayed coincidence lifetime experiment. We have as output from the multichannel analyzer 256 data points which represents in channel one the total time the experiment was run and in each of the remaining 255 channels the intensity of the decaying state as a function of time.

In general the data should conform to the following analytic expression. Let A be the coefficient of the shortest lifetime B, C be the coefficient of the next shortest lifetime D, and K the background count. Then letting y be the number of counts/channel, we have

$$y = Ae^{-t/B} + Ce^{-t/D} + K \ .$$

We have assumed that the only other process active after t = 0, besides spontaneous emission, is the cascading which gives rise to the term $Ce^{-t/D}$ and the back ground count K. There is not any reason to consider only one cascade contribution to the state's population. When the shortest lifetime is less than about 20 per cent of the total time increment used for collection of data, many times three exponentials are observed. In these cases one can write

$$Y = Ae^{-t/B} + Ce^{-t/D} + Ee^{-t/F} + K \ .$$

Of course, the contents of the MCA memory contains noise as well as signal so the algebraic form assumed above is not entirely correct. In addition if collisional depopulating mechanisms are present then there will be terms to include which are proportional to the collision

frequency, i.e., pressure. If resonance trapping of the photons takes place the effective lifetimes of states are lengthened and the algebraic form must include terms to change the lifetimes accordingly.

The exact precedure one uses in the analysis of data has had an interesting history as to techniques and precision. Exactly how one can treat the data depends upon the relative ratios of the parameters, A, B, C, D, K. Several methods exist which can be used to unravel these parameters. Their relative accuracies vary widely and depend upon the ratios of A, B, C, D, K. We shall now discuss in detail the several data analysis methods.

CHAPTER II

THREE AND FOUR LEVEL TRANSITIONS

Three Level Case

Let us derive for two cases the expressions which data may be interpreted in terms of atomic parameters. We first deal with a three level problem and later with a four level problem.

We start with a situation in which there is a ground state g, first excited state j and one higher level i. We wish to derive an expression relating the intensity of the spectral line as a function of time during and after termination of the discharge. We assume that the only populating processes are direct electron excitation from ground state and cascade from higher states. While the discharge is on, the time rate of change of the concentration of the states i and j is given by

$$\dot{N}j = Ng\frac{I}{e} Qj + NiAij - NjAj$$

$$\dot{N}i = Ng\frac{I}{e} Qi - NiAi \ .$$

Where (Qi,Qj) are excitation cross sections, Aij is spontaneous transition probability for transition $i \rightarrow j$, Ai, Aj are transition probabilities for transition from i to all lower states and j to all lower states.

As time goes on the concentration of states i and j tend toward saturation values N_j^{Δ} and N_i^{Δ}. At equilibrium

$$N_j(t) = N_j^{\Delta}[1-e^{-Ajt}-Fe^{-Ait}]$$

where

$$F = + \frac{Q_i A_j A_{ij}}{A_i (A_j - A_i)\left[Q_j + \frac{Q_i A_{ij}}{A_i}\right]} .$$

For t=0 the current is shut off and the time rate of change of concentration in i and j is given by

$$\dot{N}_j = N_i A_{ij} - N_j A_j$$

$$N_i = - N_i A_i .$$

Integration of these two equations yields

$$N_i = N_i^{\Delta} e^{-A_i t}$$

$$N_j = (N_j^{\Delta} - \frac{N_i A_{ij}}{A_j - A_i}) e^{-A_j t} + N_i^{\Delta} \frac{A_{ij}}{A_j - A_i} e^{-A_i t} .$$

The intensity of a spectrum line λ jg is given by

$$I_{jg} = N_j \, h\nu_{jg} \, A_{jg}$$

where ν_{jg} is frequency of transition.

We may now solve for I_{jg} in terms of atomic parameters for time after termination of the discharge once N_j^Δ and N_i^Δ are determined. N_j^Δ and N_i^Δ are found by setting $\dot{N}_j = \dot{N}_i = 0$. Then

$$N_i^\Delta = N_g \frac{I}{e} \tau_i Q_i$$

$$N_j^\Delta = N_g \frac{I}{e} \tau_j (Q_j + Q_i \tau_i A_{ij})$$

where N_g is gas density, I is current, e is electronic charge and τ_i, τ_j are lifetimes of states i, j. Then I_{jg} is obtained as

$$I_{jg} = A_{jg} h\nu_{jg} \left\{ \left(N_j^\Delta - \frac{N_i^\Delta A_{ij}}{A_j - A_i}\right) e^{-A_j t} + \frac{N_i^\Delta A_{ij} e^{-A_i t}}{A_j - A_i} \right\} .$$

Substitution of N_i and N_j yields

$$I_{jg} = Ae^{-t/B} + Ce^{-t/D} ,$$

where

$$A = A_{jg} h\nu_{jg} \left(N_g \frac{I}{e}\right) \left\{ B(Q_j + Q_i D A_{ij}) - A_{ij} \frac{DB}{D-B} DQ_i \right\}$$

$$B = 1/A_j = \tau_j$$

$$C = A_{jg} h\nu_{jg} A_{ij} \left(\frac{DB}{D-B}\right) N_g \frac{I}{e} DQ_i$$

$$D = \frac{1}{A_i} = \tau_i .$$

When lifetime measurements are performed we obtain the values of (A,B, C,D). B and D are lifetimes, but A and C contain information as to cross sections. The ratio A/C is important and is given by

$$\frac{A}{C} + 1 = \left(\frac{D-B}{D^2}\right) \frac{Q_j + DA_{ij}Q_i}{A_{ij}Q_i} .$$

The experiment measures everything except Q_j and $A_{ij}Q_i$, and if one of these is known, say $A_{ij}Q_i$, then Q_j may be determined. This technique can be used to find Q_j when λ_{jg} lies in the vacuum ultraviolet. This is of particular importance since it provides absolute spectral intensity calibration in the vacuum ultraviolet.

Four Level Case

Now let us look at a four level atom or molecule. The states are labeled the same except the upper level is now h. The rate

_____ h
_____ i
_____ j
_____ g

equations for time before discharge is terminated are

$$\dot{N}_h = N_g \frac{I}{e} Q_h - N_h A_h$$

$$\dot{N}_i = N_g \frac{I}{e} Q_i + N_h A_{hi} - N_i A_i$$

$$\dot{N}_j = N_g \frac{I}{e} Q_j + N_h A_{hj} + N_i A_{ij} - N_i A_j .$$

Once again when the states are saturated they have the populations N_j^{Δ}, N_i^{Δ}, N_h^{Δ}. For time after termination the rate equations are those above with current (I) set to zero.

First we shall look at λ_{ij} since it will have a two exponential decay, one due to spontaneous transitions and the other (long) is due to cascades from level h. The solutions of the equations for time after termination are below.

$$N_h = N_h^{\Delta} e^{-A_h t}$$

$$N_i = N_h^{\Delta} \frac{A_{hi}}{A_i - A_h} e^{-A_h t} + (N_i^{\Delta} - \frac{N_h^{\Delta} A_{hi}}{A_i - A_h}) e^{-A_i t}$$

$$N_j = N_h^{\Delta}(A_{h_j} - \frac{A_{ij}A_{hi}}{A_i - A_h}) \frac{e^{-A_h t}}{A_j - A_h} + (\frac{A_{ij}}{A_j - A_h})(N_i^{\Delta} - N_h^{\Delta} \frac{A_{hi}}{A_i - A_h}) e^{-A_i t}$$

$$+ \{N_j^{\Delta} - \frac{N_h^{\Delta}}{A_j - A_h}(A_{h_j} - \frac{A_{ij}A_{hi}}{A_i - A_h}) - \frac{A_{ij}}{A_j - A_i}(N_i^{\Delta} - N_h^{\Delta} \frac{A_{hi}}{A_i - A_h})\}$$

$$* e^{-A_j t} .$$

Looking at λ_{ij}, we find

$$I_{ig} = Ae^{-t/B} + Ce^{-t/D}$$

where

$$A = (N_g \frac{I}{e} h\nu_{ij}) \; A_{ij}A_{hi}Q_h(\frac{BD^2}{D-B})$$

$$B = \tau_i; \qquad D = \tau_h$$

$$C = (N_g \frac{I}{e} h\nu_{ij})A_{ij}B(Q_i - \frac{DB}{D-B} A_{hi}Q_h)$$

and

$$\frac{A}{C} = \frac{D}{B} \frac{DB}{D-B} (\frac{A_{hi}Q_h}{Q_i - \frac{DB}{D-B} A_{hi}Q_h}) .$$

The same remarks apply here as in the case of the three level case.

If we monitor the transition $I_{jg} = h\nu_{jg} N_j$, we obtain three exponential decays. The first is the spontaneous decay. The second and third are due to cascades into j from i and h. The algebraic form is now much more complicated.

$$I_{jg} = Ae^{-t/B} + Ce^{-t/D} + Ee^{-t/F} .$$

A, C. E are coefficients containing cross section information and (B,D, F) are lifetimes of j, i, h states. A, C, E are given by

$$A = BQ_j - \frac{B^2D}{D-B} A_{ij}Q_i - FB^2Q_h\left(\frac{A_{hj}}{(F-B)} + \frac{A_{ij}A_{hi}FD}{(F-B)(D-B)} + A_{hi}A_{ij}\frac{D}{D-B}\right)$$

$$C = \frac{BD^2}{D-B} A_{ij}\left[Q_i - A_{hi}Q_h \frac{DF}{(F-D)}\right]$$

$$E = \frac{BF^2}{(F-B)} Q_h\left[A_{hj} - A_{ij}A_{hi} \frac{DF}{(F-D)}\right] .$$

It is unlikely A/C, A/E, C/E, etc together with values of DFB contain enough information to be useful for cross section determination. This is particularly true if the lifetimes of the excited states are nearly equal since in that event large uncertain coefficients would appear in the above results.

CHAPTER III

GRAPHICAL METHOD

We shall assume for purpose of discussion that the data contains only two exponentials for analysis. Let the data be plotted on semilogarithmic scale where number of counts/channel is the dependent variable and channel number is the independent variable. The channel numbers may be transferred to real time by a simple least squares fitting procedure.

Let us assume the data can be represented by

$$Y = Ae^{-t/B} + Ce^{-t/D} .$$

Where Y is the number of counts/channel, B and D lifetimes and A, C are related to excitation cross sections.

If $B << D$ and if at times long compared to the short lifetime, one can assume the linear "tail" data is purely due to the cascade component. A straight line is now fitted through the tail data by visual inspection. If one subtracts the values of the straight line fit to the long lived cascade component point by point from the real data, then one has left only the short lived component which should be a linear curve.

This procedure works well only under certain restrictions. Firstly, the technique cannot deal with a constant back ground count. It cannot estimate or even suggest the existence of such information.

Thus errors are made in the analysis of the short and long lived components. Extra information is needed to obtain the background counting rate K.

A second and basic defect of the graphical procedure involves the approximation of fitting a straight line to the tail points. The short lifetime is always present and thus should be dealt with even though its amplitude is small for large times.

The third defect defines the ability of the method to work at all and depends upon ratios of the parameters A:C and B:D. If, for instance, $10 < (A/C) < 1$, then the amplitude of the short lived component is clearly larger than the cascade component. But this condition is not sufficient for the graphical subtraction technique to work. In addition we must have $B \ll D$. That is, the lifetimes of the two components must be significantly different in order for the technique to be useful. In reality this latter restriction is of more importance for use of the method.

These two ratios (A/C) and (B/D) determine the applicability of the method. Very little can be said in general about the precision of the lifetimes (B,D) determined by graphical methods unless the two ratios are first determined. Experience has told us to say that for (A/C) = 1 separation can be obtained, if $D \simeq 5B$. This result depends upon a small noise background, for if the data contained a third long lived component, it, together with noise, may be counted as a constant background, which may at long times exceed the second components amplitude. Thus the "background" would seriously alter the lifetime of the cascade component.

Figure 27 shows real data as collected and plotted in semi-logithrmic manner. A straight line has been fitted through the cascade component and point by point subtraction has yielded the short component. No attempt has been made to average data points to reduce the noise on the information. In fact data averaging improperly treated, could seriously alter the short lived components.

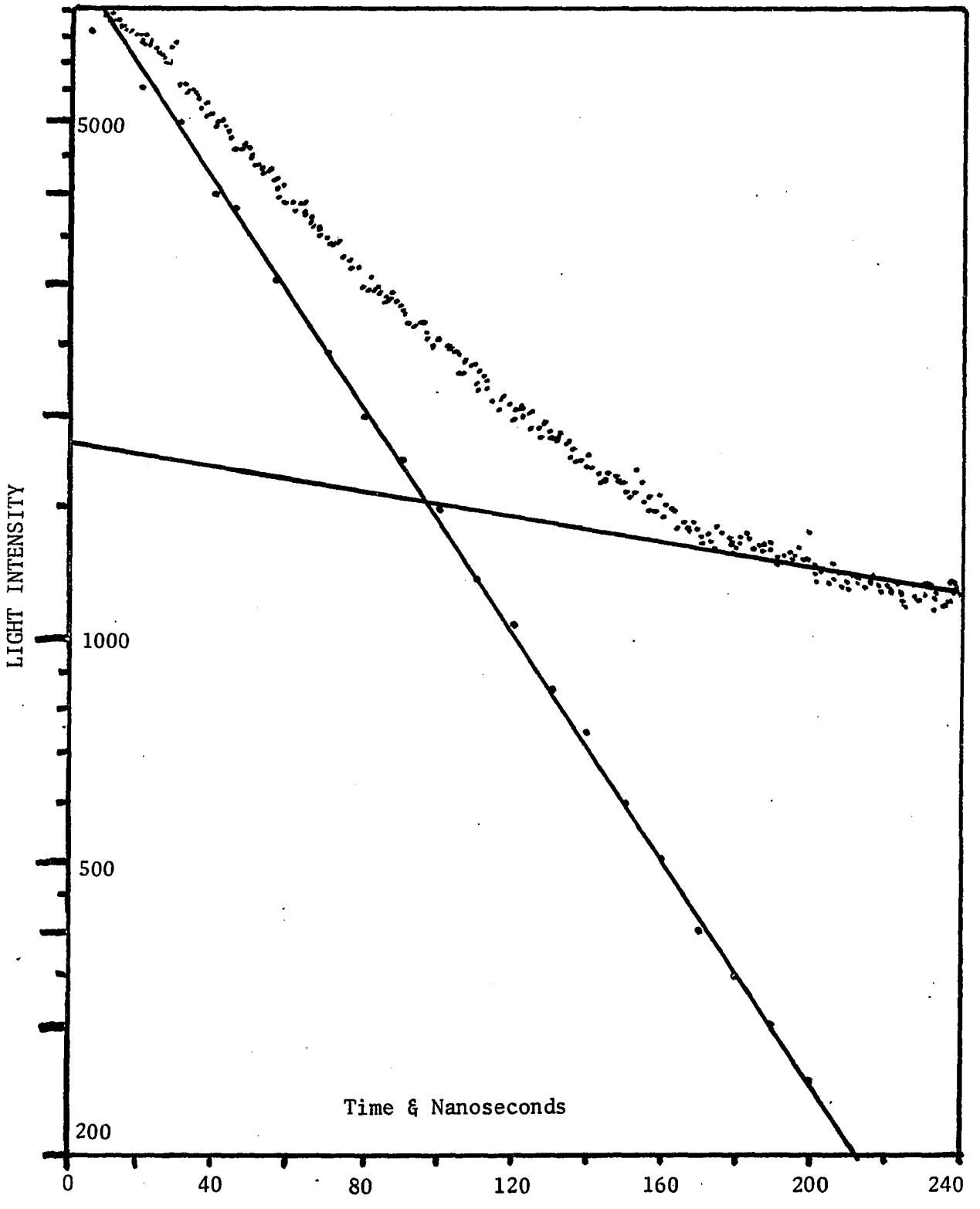

Figure 27. Graphical Data Analysis Technique.

CHAPTER IV

COMPUTER TECHNIQUES

Several computer programs have been developed for the analysis of lifetime data. This analysis problem is not unique in measurement of atomic lifetimes for it first arose in the analysis for lifetimes of various radioisotopes in nuclear physics. The graphical technique described above has been termed as the "peel off" or "stripping" technique[27] and is a valuable technique when lifetimes differ by factors of four or more.

The computer programs developed at the University of Oklahoma deal with the data in several manners. The computer program named RICH provides numerical means by which the "peel off" technique is applied and provides a background estimate. This program yields first guesses which are submitted to one of two nonlinear least squares programs. The first of these is named IBM 2EX and does an analysis on the parameters A, B, C, and D when the background K is known exactly. The second program can deal with at least three exponentials plus background by nonlinear least squares procedure. This program is LASL. It does an iterated fit to all parameters A, B, C, D, E, F, and K if necessary. We shall now describe each of these programs in detail and their use in conjunction with the online GE-430 time share computer system.

RICH

RICH is an acronym formed from the words: Regression Iterated Constant Hopeful. Its purpose is to numerically perform the peel off procedure and simultaneous provide information on the value of any background present. Mr. Richard T. Thompson is primarily responsible for its development for use on IBM 360-40 and GE 430 computers.

The algorithm used is as follows. The contents of the MCA are entered into the computer. The natural logarithm of the number of counts in each channel is calculated. Beginning with the last useful data point (a useful data point is one which follows the general trend) a least squares straight time is fitted to the last twenty points of the cascade component using a zero value for the background. The correlation coefficient (R^2) is calculated for the fitted data. The number of points is increased by twenty points and correlation coefficient recomputed using a value for the background of either 0.001, 0.01, or 0.1 of the numerical count stored in the last useful channel. The procedure is continued taking more points into account, until R^2 is maximized. Once R^2 is maximum the value of the background K is changed until R^2 is again a maximum. Now the computed least square straight line to the largest component is subtracted from the data. The data generated by the subtraction procedure are used in as input to a least squares fitting procedure with a zero background count. Again the number of points is increased gradually until R^2 is again maximized. The entire procedure is repeated until all components (two or three) present in the data are detected.

In addition the count rate and timing calibrations are calculated by least squares procedure. The count rate is the sum of the total number of counts in all channels divided by the product of the total time counted times the repetition rate of the discharge. The timing calibration is determined by imputing the number of timing cables used and their electrical time delays in nanoseconds.

In addition to a hard copy of the lifetime results a semilogarithmic plot of several parameters is printed out for inspection. The real data minus the calculated background and long lived component is plotted as A. The real data minus the short and long lived components is plotted as C. Thus A corresponds to the short component, B the long component and C the background. The plot of C is scaled differently than the plots of A and B and is a linear plot so as to show trends in the data.

An example of the output of the program RICH is shown below.

```
RUN

RICH       15:48  ACC SAT.  FEB 21,1970



G.E.COPELAND    DATE-13FEB1970    RUN # 1
 SAMPLE-TEST      WAVELENGTH=1234. A    PRESSURE= 12.0 MICRONS

 CALCULATED AT 15:48  SAT.  FEB 21,1970

PRINT REGRES. RESULTS? ,TABULATE Y? (0-NO  1-YES)
? 0,0

ENTER NO. OF PARAMETERS,FIRST POINT,LAST POINT,
 REP RATE,BREAK POINT,CONST(IF KNOWN)
? 5,1,255,10000,1

 COUNT RATE=  5.3%
 ITERATIONS NOT DISPLAYED
 EXP FIT FROM  65 TO 255LINEARITY(R2) IS 9.99811697E-01
 EXP FIT FROM   1 TO  41LINEARITY(R2) IS 9.91329588E-01
          THE UNWEIGHTED SIGMA IS   5.5606E+01
LIFETIMES (NS)       10.22647   100.65545
COEFFICIENTS      10009.83924 10093.09601     87.00376
CALIBRATION IS  1.00000 NS/CHAN  WITH STD DEV OF0.000000  NS/CHAN
PLOT?(0-NO,PLOT INCR-YES)
? 8
```

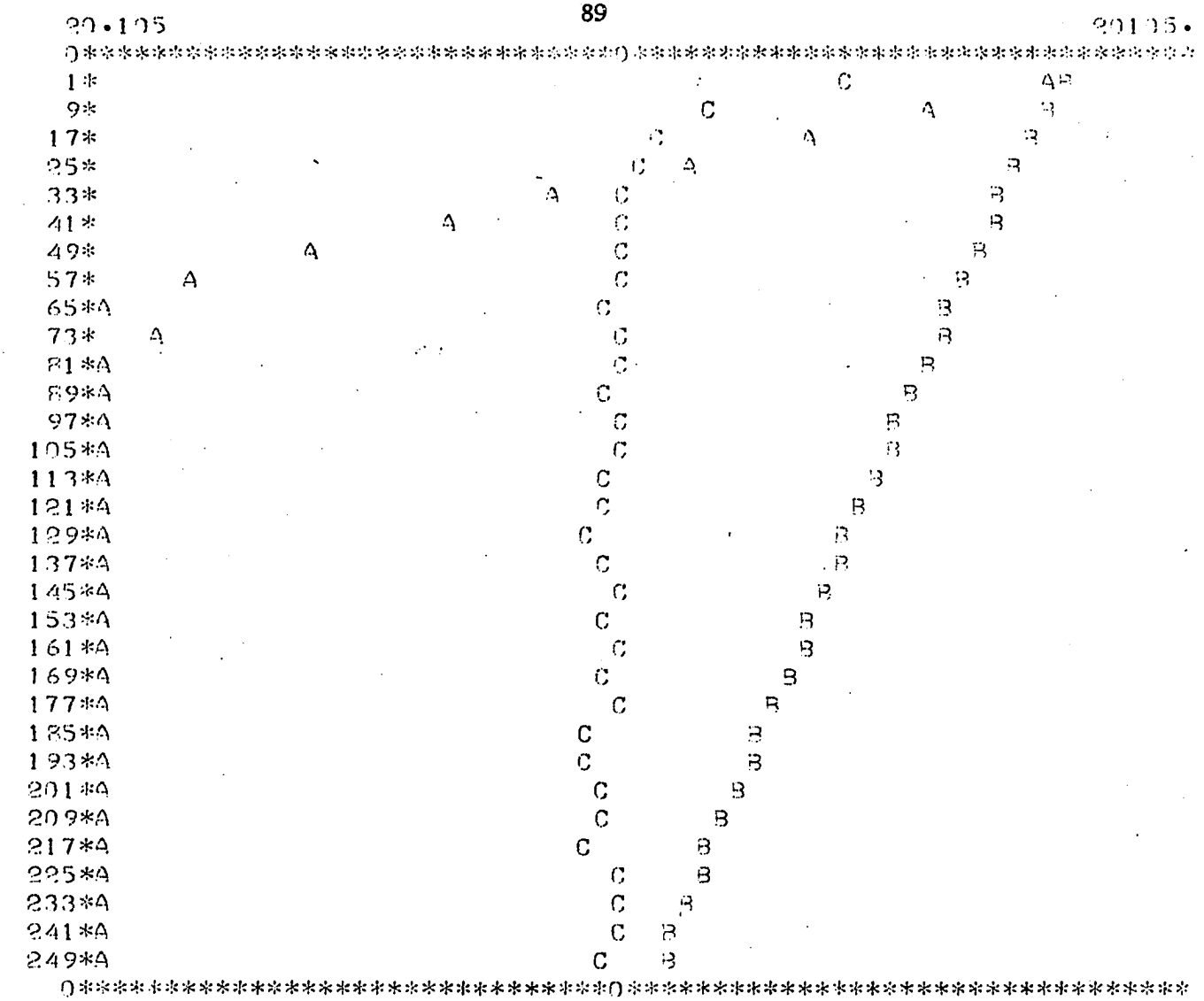


```
ENTER NØ. ØF PARAMETERS,FIRST PØINT,LAST PØINT,
 REP RATE,BREAK PØINT,CØNST(IF KNØWN)
? S

RAN:    16.5 SECS

READY
```

IBM 2EX

The program entitled IMB 2EX was obtained from the IBM Scientific Share System. It was modified for use on the GE 430 time share system by Mr. Carl Bush and the author. It does a non-linear least squares analysis on two exponentials (4 parameters) if the background is known exactly. In addition to providing iterated estimates of the parameters (A,B,C,D) it also yields estimates of the goodness of fit obtained by the program. It will provide point by point results for the abscissa (time), observed count, calculated count, ratio of observed to calculated, and difference between observed and calculated count. The differences are placed in a data file called TEST 3 which can be plotted by the program X PLOT to ascertain if there are any perodic deviations between observed and calculated values obtained by IBM 2EX..

An example output of IBM 2EX is shown on the following page.

```
READY
ØLD:IBM2EX

READY
RUNNH

 TØ SUPRESS INTERMEDIATE RESULTS SET SWIP TØ 1.0 IN 291
 G.E.CØPELAND    DATE-23JAN1970    RUN # 1
 SAMPLE-TEST      WAVELENGTH=1234. A    PRESSURE=123.4 MICRØNS
 ENTER STARTING AND ENDING PØINTS
? 1,255

ENTER TIMING CALIBRATIØN-X(NS/CHAN)
? 1

 ENTER SHØRT CØEFF.,SHØRT LIFETIME,LØNG CØEFF., LØNG LIFETIME
? 9000,9,9000,90

 ENTER NØISE LEVEL
? 90

 PRECISIØN IS     5.0E-06
CØEFFICIENTS            A              B              C              D
      INITIAL     9.00000E+03    9.00000E+00    9.00000E+03    9.00000E+01

        FINAL     1.00100E+04    1.00941E+01    9.97980E+03    1.00479E+02

   3 CYCLES
    STD. DEV.   0.6961434E+00 0.8479077E-05 0.1382448E+00 0.8525836E-07

   S.D./FINAL           0.000          0.000          0.000          0.000

 MEASURE ØF GØØDNESS ØF FIT =  3.66834E+02
ØPTIØNS AVALIABLE,(1) IS CHANGE CØNSTANT,(0) IS  STØP,
AND (-1) IS RECAP ALL RESULTS
? 100


 REPEATING CALCULATIØN USING NEW VALUE FØR CØNSTANT K ØF
? 100

      INITIAL     9.00000E+03    9.00000E+00    9.00000E+03    9.00000E+01

        FINAL     1.00007E+04    1.00143E+01    1.00016E+04    9.99776E+01

   3 CYCLES
    STD. DEV.   0.6973160E+00 0.8563541E-05 0.1376328E+00 0.8477125E-07

   S.D./FINAL           0.000          0.000          0.000          0.000

 MEASURE ØF GØØDNESS ØF FIT =  3.43375E+02
ØPTIØNS AVALIABLE,(1) IS CHANGE CØNSTANT,(0) IS  STØP,
AND (-1) IS RECAP ALL RESULTS
? -1
```

```
ENTER INCREMENT FØR READ OUT
? 8

      ABSCISSA        ØBSERVED        CALCULATED      RATIØ       DIFF        WT
    0.00000E+00     2.01050E+04     2.01024E+04     1.0001     2.6045
    8.00000E+00     1.37860E+04     1.38313E+04     0.9967    -45.2857
    1.60000E+01     1.06580E+04     1.06462E+04     1.0011     11.7261
    2.40000E+01     8.89500E+03     8.87751E+03     1.0020     17.4859
    3.20000E+01     7.78000E+03     7.77168E+03     1.0011      8.3156
    4.00000E+01     7.02200E+03     6.98792E+03     1.0049     34.0788
    4.80000E+01     6.37800E+03     6.37106E+03     1.0011      6.9450
    5.60000E+01     5.85500E+03     5.84959E+03     1.0009      5.4093
    6.40000E+01     5.39400E+03     5.38980E+03     1.0008      4.1963
    7.20000E+01     5.00600E+03     4.97508E+03     1.0062     30.9196
    8.00000E+01     4.61400E+03     4.59662E+03     1.0038     17.3842
    8.80000E+01     4.25100E+03     4.24922E+03     1.0004      1.7808
    9.60000E+01     3.95400E+03     3.92942E+03     1.0063     24.5790
    1.04000E+02     3.65200E+03     3.63461E+03     1.0048     17.3872
    1.12000E+02     3.34600E+03     3.36265E+03     0.9950    -16.6543
    1.20000E+02     3.10600E+03     3.11169E+03     0.9982     -5.6898
    1.28000E+02     2.86200E+03     2.88006E+03     0.9937    -18.0607
    1.36000E+02     2.66500E+03     2.66626E+03     0.9995     -1.2602
    1.44000E+02     2.49200E+03     2.46891E+03     1.0094     23.0917
    1.52000E+02     2.28200E+03     2.28674E+03     0.9979     -4.7361
    1.60000E+02     2.13300E+03     2.11857E+03     1.0068     14.4255
    1.68000E+02     1.96000E+03     1.96335E+03     0.9983     -3.3452
    1.76000E+02     1.83600E+03     1.82005E+03     1.0088     15.9466
    1.84000E+02     1.66900E+03     1.68778E+03     0.9889    -18.7808
    1.92000E+02     1.54700E+03     1.56568E+03     0.9881    -18.6801
    2.00000E+02     1.44200E+03     1.45297E+03     0.9925    -10.9690
    2.08000E+02     1.34700E+03     1.34893E+03     0.9986     -1.9255
    2.16000E+02     1.23700E+03     1.25288E+03     0.9873    -15.8829
    2.24000E+02     1.17000E+03     1.16422E+03     1.0050      5.7740
    2.32000E+02     1.08600E+03     1.08238E+03     1.0033      3.6132
    2.40000E+02     1.01600E+03     1.00684E+03     1.0091      9.1589
    2.48000E+02     9.26000E+02     9.37105E+02     0.9881    -11.1048
ØPTIONS AVALIABLE,(1) IS CHANGE CØNSTANT,(0) IS  STØP,
AND (-1) IS RECAP ALL RESULTS
? 0


RAN:    53.8 SECS

READY
```

```
 IBM2EX  13:53  FRI.  FEB 20,1970

      $NOM
C G.E.CUPELAND   IBM2EX  4PARAMETERS(CONSTANT MUST BE KNOWN)
      DIMENSION Y(256)
      DIMENSION TIM(8)
      DIMENSION RTY(256)
      DIMENSION BI(4)
      DIMENSION W(5,5),BA(4),RN(4),W(4),RF(4)
      DIMENSION U(10,256)
      REAL L1,L2
      CALL OPENF(1,"INPUT")
      READ(1,101) L1,L2,DA,XMO,YR,RN,SA,V,P
      READ(1,102)N
      READ(1,103)(TIM(I),I=1,NTC)
  101 FORMAT(2A6,A2,A3,A4,I2,A6,F5.0,F5.1)
  102 FORMAT(I3,I1,8I3)
  103 FORMAT(8F7.2)
  104 FORMAT(I6,9I7)
  212 MB=0
      PRINT,"TO SUPRESS INTERMEDIATE RESULTS SET SWIP=1 IN 291"
      MT=40.0
      SWIP=1.0
      N=N
      ET=0.000005
      PRINT 201,L1,L2,DA,XMO,YR,RN
      PRINT 202,SA,V,P
  201 FORMAT(1H ,2A6,3X,"DATE-",A2,A3,A4,3X,"RUN #",I2)
  202 FORMAT(1H ,"SOMPL-",A6,3X,"WAVELENGTH=",F5.0," A",
     13X,"PRESSURE=",F5.1," MICRONS")
      PRINT 1,
    1 FORMAT(1H ,"ENTER STARTING AND ENDING POINTS")
      INPUT,IN1,NN2
      PRINT,"ENTER TIMING CALIBRATION-X(NS/CHAN)"
      INPUT,CLBRTR
      NT1=IN1-1
      NT=NN2-NT1
      READ(1,104),TIME,(Y(I),I=1,NT1),(Y(J),J=1,NT)
      CALL CLOSEF(1,"INPUT")
   26 FORMAT(1H ,"PRECISION IS ",1PE10.2)
      NE=NT
  242 NA=0
  232 IP=0
C             DATA INPUT
      DO 224 I=1,NT
      AA=(I-1)*CLBRTR
      BB=Y(I)
  254 U(1,I)=AA
      U(2,I)=BB
  224 U(4,I)=U(2,I)/U(2,1)
C                   TRIAL CONSTANT
```

```
IBM2EX  13:53  FRI.  FEB 20,1970

      PRINT 2,
    2 FORMAT(1H ,"ENTER SHORT COEFF.,SHORT LIFETIME,LONG COEFF.,
     1 LONG LIFETIME")
      INPUT,BI
      BI(2)=1.0/BI(2)
      BI(4)=1.0/BI(4)
      PRINT3,
    3 FORMAT(1H ,"ENTER NOISE LEVEL")
      INPUT,CN
      PRINT 26,ET
      PRINT,"COEFFICIENTS            A            B            C
     1            D"
      GO TO236
  235 PRINT 504,
  504 FORMAT(1HO,"REPEATING CALCULATION USING NEW VALUE FOR
     1 CONSTANT K OF")
      INPUT,CN
  236 DO 230 I=1,4
  230 BA(I)=BI(I)
      BA02=1.0/BA(2)
      BA04=1.0/BA(4)
      PRINT 28,BA(1),BA02,BA(3),BA04
   28 FORMAT(5X," INITIAL ",1P4E14.6)
C     START OF MAIN LOOP
      MB=0
  312 A=BA(1)
      B=BA(2)
      C=BA(3)
      D=BA(4)
      DO 323 I=1,NT
      XB=EXP  (-B*U(1,I))
      AXB=XB*A
      XD=EXP  (-D*U(1,I))
      CXD=XD*C
      XT=AXB+CXD
      U(3,I)=XT+CN
      IF(NE-I) 323,322,322
  322 RXT=1.0/XT
C     DERIVATIVES
      U(6,I)=-XB*RXT
      U(7,I)=U(1,I)*AXB*RXT
      U(8,I)=-XD*RXT
      U(9,I)=U(1,I)*CXD*RXT
      U(10,I)=ALOG((U(2,I)-CN)*RXT)
  323 CONTINUE
C      SUMS OF DERIVATIVES
      DO 328 K=1,5
      DO 328 J=1,5
      W(J,K)=0.0
```

```
 IBM3EX  13:53  FRI.  FEB 20,1970

      DO 328 I=1,NE
      AA=ABS (U(K+5,I))
      IF(AA-1.0E-25)  328,326,326
  326 AA=ABS (U(J+5,I))
      IF(AA-1.0E-25)  328,327,327
  327 W(J,K)=W(J,K)+U(K+5,I)*U(J+5,I)
  328 CONTINUE
C     SOLVE MATRIX
  422 WW=W(5,5)
      DO 428 I=1,4
      W(5,5)=1.0/W(1,1)
      DO 423 J=1,4
  423 W(J,5)=W(J+1,1)/W(1,1)
      DO 424 J=1,3
      W(5,J)=-W(5,5)*W(1,J+1)
      DO 424 K=1,4
  424 W(K,J)=-W(K,5)*W(1,J+1)+W(K+1,J+1)
      DO 428 J=1,5
      W(J,4)=W(J,5)
  428 CONTINUE
C     TEST NEW CONSTANTS
  522 MA=1
      DO 525 J=1,4
      BN(J)=BA(J)-W(1,J)
      BB=ABS (BN(J)/BA(J)-1.0)
      IF (BB-20.0) 513,513,533
  533 PRINT 53
   53 FORMAT(12H WILD COEFS  )
      GOTO 639
  513 BA(J)=BN(J)
      IF(BB-ET) 525,523,523
  523 MA=MA+1
  525 CONTINUE
      IF(MA-1) 777,529,526
  526 MB=MB+1
      IF(MB-MT) 517,528,528
  517 CONTINUE
      IF(SWIP)312,527,312
  527 BA02=1.0/BA(2)
      BA04=1.0/BA(4)
      PRINT 57,BA(1),BA02,BA(3),BA04
   57 FORMAT(10X,1P4E14.6)
      GOTO 312
C     END OF MAIN LOOP
  528 PRINT 58,MT,MB
   58 FORMAT(18H EXIT DUE TO OVER  I5, 8H CYCLES  I5 )
      GOTO 639
  529 BA02=1.0/BA(2)
      BA04=1.0/BA(4)
```

```
 IRM2EX  13:53  FRI.  FEB 20,1970

      PRINT 59,BA(1),BA02,BA(3),BAJ4
   59 FORMAT(7X," FINAL ",1P4E14.6)
      PRINT 60,MR
   60 FORMAT(1H ,I3," CYCLES")
C    STANDARD DEVIATIONS
      ANE=NE
      SE=W(5,5)/(ANE-4.0)
      DO 539 J=1,4
      R(J)=SQRT(SE*W(J+1,J))
  539 RF(J)=R(J)/BA(J)
      PRINT 62,R,RF
   62 FORMAT(1H 2X11H STD. DEV. 4E14.7/2X12H S.D./FINAL 4F14.3
     1)
      ERSUM=0.0
      DO 531  I=1,NT
      ERS=U(2,I)-U(3,I)
  531 ERSUM=ERSUM+ERS*ERS
      OMEG=ERSUM/(NT-5)
      PRINT 77,OMEG
   77 FORMAT(1H ,"MEASURE OF GOODNESS OF FIT =",1PE13.6)
C          FINAL RESULTS
  636 CONTINUE
  686 IF(IP) 656,696,656
  696 GO TO639
  656 CONTINUE
      GO TO 639
  646 PRINT,"ENTER INCREMENT FOR READ OUT"
      INPUT,INC
      PRINT 66
   66 FORMAT(1H 4X10H ABSCISSA 4X10H OBSERVED 2X12H CALCULA
     1TED 3X6HRATIO 2X7H  DIFF 2X4H  NT)
      IP=1
      DO 628 I=1,NT,INC
  668 ED=U(2,I)-U(3,I)
      IF(U(3,I)) 627,637,627
  627 ER=U(2,I)/U(3,I)
      GO TO 648
  637 ER=0.0
  648 PRINT 68,U(1,I),U(2,I),U(3,I),ER,ED
   68 FORMAT(1H ,1P3E14.6,0P2F9.4)
      DO 888,J=1,NT,INC
  888 RTY(J)=0.0
      DO 889,J=1,NT,INC
  889 RTY(J)=RTY(J)+ABS(U(2,J)-U(3,J))
      CALL OPENF(2,"TEST3")
      WRITE(2,)(RTY(J),J=1,NT,INC)
      CALL CLOSEF(2,"TEST3")
  628 CONTINUE
  639 PRINT,"OPTIONS AVALIABLE,(1) IS CHANGE CONSTANT,(0) IS
```

```
IBMPEX  13:53  FRI.  FEB 20,1970

    1 STOP,"
      PRINT,"AND (-1) IS RECAP ALL RESULTS"
      INPUT,INST
      IF(INST)646,777,235
  777 CONTINUE
      END
```

LASL

The last of the data analysis programs is named LASL for Los-Alamos Scientific Laboratory. This program which was originally designed for use in a CDC-6400 and was modified for use in the IBM 360/40 and GE-430 systems by Mr. Richard T. Thompson. It does a non-linear least squares iterated analysis on up to three exponentials and background (7 parameters). This program is by far the most sophisticated and allows for several polynomial weighting functions if desired. It was obtained from LASL and its algorithm utilizes the Newton-Raphson technique with further modifications as described by Marquardt[28].

An example output of LASL follows.

```
ØLASL     16:08  ACC SAT.  FEB 21,1970



G.E.CØPELAND    DATE-13FEB1970    RUN # 1
 SAMPLE-TEST      WAVELENGTH=1234. A    PRESSURE= 12.0 MICRONS

 CALCULATED AT 16:08  SAT.  FEB 21,1970


ENTER NO. ØF PARAMS,FIRST PT., LAST PT., WEIGHT PØWER
,IPR=0,1,2,ØR 3 FØR INCR. ØUTPUT,IM=2 HØLD CØNST.
? 5,1,255,-.5,0

ENTER TAU(SHØRT,LØNG),CØEFF(SHØRT,LØNG),CØNSTANT
? 9,90,9000,9000,90

CALIBRATIØN IS   1.000000000E+00 NS/CHAN
WEIGHT RANGES FRØM 1.0 TØ   5.377 FØR CHAN 255
     7 ITERATIØNS, DET. ØF PART. DERIV. MATRIX =   1.30959E-03

         SUM ØF EXPØNENTIALS: Y(I)=P(1)*EXP(-X(I)/P(2))+...+P(5).


 THE WEIGHTED VARIANCE IS   7.743088E+02
 THE UNWEIGHTED SIGMA IS   1.842188E+01
AND THE UNWEIGHTED SUM ØF SQUARES ØF THE DEVS IS   8.484143E+04
     GUESS ØF  FINAL VAL ØF   S.D. ØF          EXACT LST SQRS EQNS
 K  K-TH PARAM  K-TH PARAM  K-TH PARAM     FITTED FCTN  INPUT DATA
  1   9.000E+03   1.000E+04   1.826E+01      1.998E-05   1.998E-05
  2   9.000E+00   9.977E+00   3.554E-02      5.100E-01   5.100E-01
  3   9.000E+03   1.001E+04   1.022E+01      1.784E+05   1.784E+05
  4   9.000E+01   9.976E+01   2.716E-01      4.559E+07   4.559E+07
  5   9.050E+01   1.046E+02   6.670E+00      2.276E+06   2.276E+06
ENTER PLØT INCR IF PLØT IS DESIRED.
? 8
```

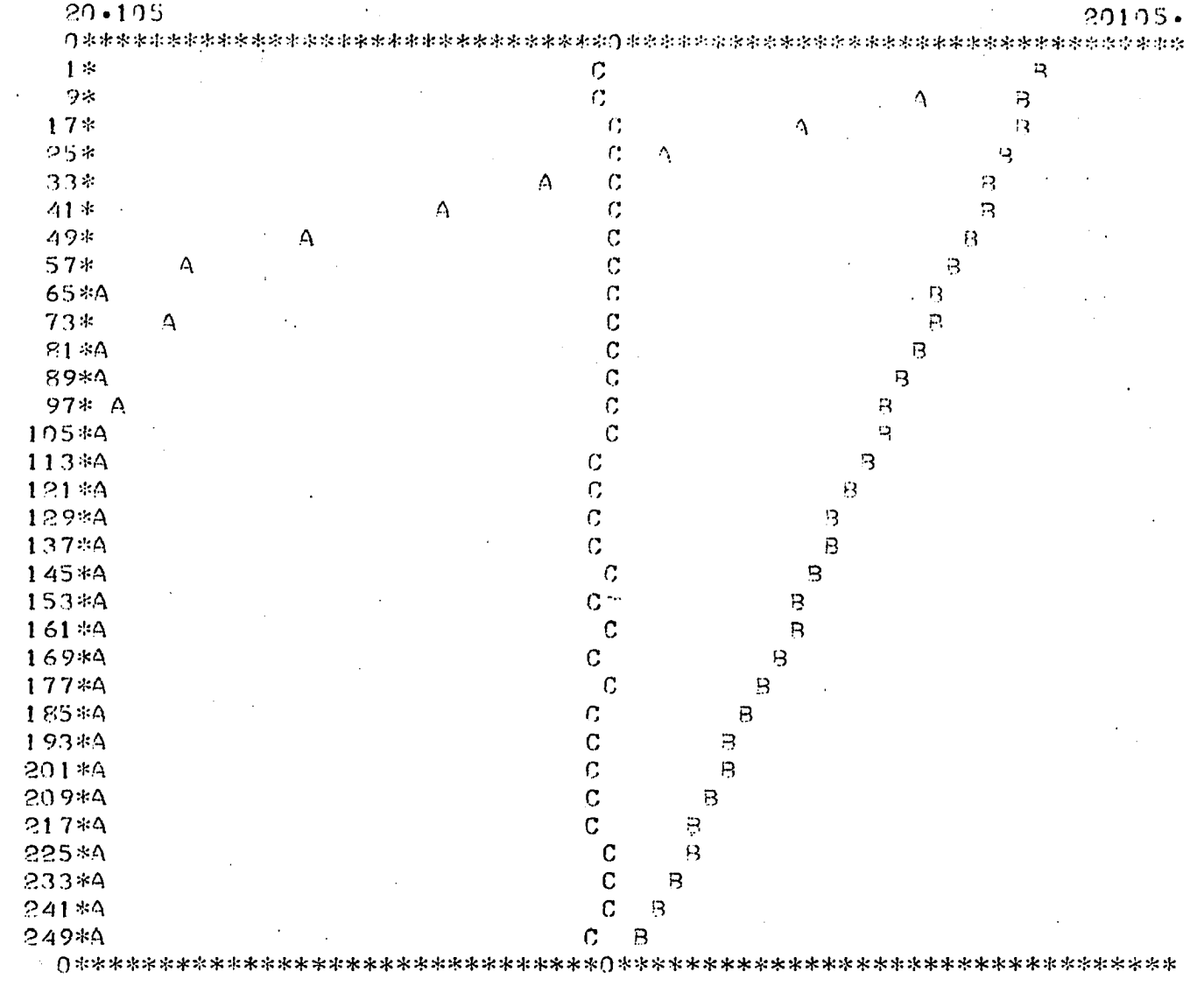


```
G.E.COPELAND    DATE-13FEB1970    RUN # 1
 SAMPLE-TEST      WAVELENGTH=1234. A    PRESSURE= 12.0 MICRONS

 CALCULATED AT 16:08  SAT.  FEB 21,1970


ENTER NO. OF PARAMS,FIRST PT.,LAST PT.,WEIGHT POWER
,IPR=0,1,2,OR 3 FOR INCR. OUTPUT,IM=2 HOLD CONST.
? S


RAN:    52.3 SECS

READY
```

Time Share Data Analysis System

The lifetime apparatus in its present configuration is designed for direct read out of the MCA on to punched paper type via a Teletype 33TBE. In addition a hard copy is obtained via the printer of the teletype. Once a data tape is obtained the following procedure is used for the analysis of the data.

The data tape is feed into the GE 430 computer via the phone lines by use of the program FILER. FILER sets up a data file called INPUT in the memory of the 430 which is used by all other programs. Next the data is plotted in a semilogarithmic manner by use of the program FPLOT. Visual inspection of the plot gives the operator information as to which data points to use for the rest of the analysis. Next the program RICH is run in which the timing calibrations and first guesses for the parameters are obtained (2 or 3 esponentials plus background). If only two exponentials are found then either IBM 2EX or LASL may be used. If three exponentials are obtained, then LASL must be used.

The time share system has drastically reduced data analysis time. Typically, graphical procedures consume eight to ten hours for analysis, whereas, the time share system utilizes only two to three minutes of computer time. In addition, the type of analysis used is much more sophisticated.

PART IV

RESULTS

CHAPTER I

THE OXYGEN MOLECULAR ION

This ionic molecule is a fifteen electron species with a permanent dipole moment since its ground state is $X^2\pi_g$. The four known excited states are $a^4\pi_u$, $A^2\pi_u$, $b^4\Sigma_g^-$, and $c^4\Sigma_u^-$. The O_2^+ molecule is formed in an electrical discharge by simultaneous excitation and ionization of the ground state of the O_2 molecule ($X^3\Sigma_g^-$). The energy level diagrams of both O_2^+ and O_2 are shown in Figs. 2 and 28. The equilibrium internuclear distance for O_2^+ $X^2\pi_g$ is 1.1227 Å and that for O_2 ($X^3\Sigma_g^-$) is 1.20739 Å. The difference in energy (between lowest vibrational states) is about 12.1 eV. Even though ionization O_2^+ may be formed (since Δr_e is small); by electron impact, excitation of some levels involves a spin flip.

There are three known excited state transitions in O_2^+. They are: the $A^2\pi_u \rightarrow X^2\pi_g$ which produces the second negative system (2-); the $b^4\Sigma_g^- \rightarrow a^4\pi_u$, which produces the first negative system (1-), and the $c^4\Sigma_u^- \rightarrow b^4\Sigma_g^-$, which produces Hopfield's emission band system.

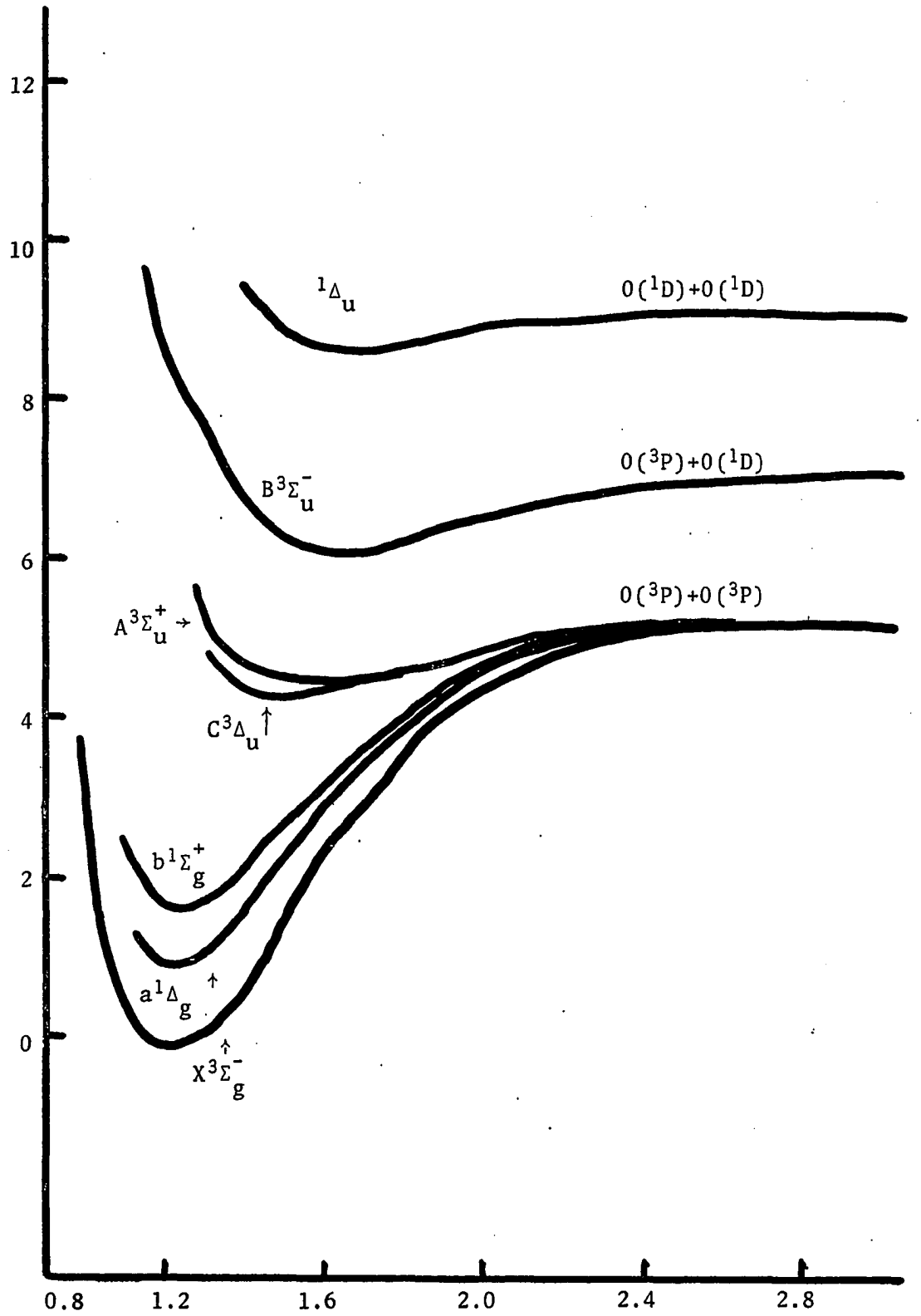

Figure 28. O_2 Energy Level Diagram.

The second negative system usually is seen at low pressure in the negative glow and is most intense in the wavelength range 4100 Å to 2300 Å. Since it is due to a $2\pi_u \rightarrow 2\pi_g$ transition the resultant bands are double headed and are separated by about 200 cm^{-1}. This system was not seen in the discharge tube used in the experiment and this is probably due to the fact that spin flip is necessary for its excitation from O_2 (electric dipole forbidden excitation).

Hopfield's system ($c^4\Sigma^- \rightarrow b^4\Sigma_g^-$), should be present since no spin flip is necessary for its production, but was not seen in the cold cathode discharge tube. It has been observed in emission with one upper vibrational level (v'=0). It lies 24.5 eV above ground state of O_2 and thus should be difficult to excite. Some evidence[29] seems to suggest that it may predissociate. The Hopfield system occurs in the wavelength range 1940 Å to 2362 Å. It should be easily excited, if traces of helium were introduced into the discharge.

The first negative band system occurs quite strongly in hollow cathode discharges at low pressures. It is due to a quartet-quartet transition ($b^4\Sigma_g^- \rightarrow a^4\pi_u$). It seems[30] that neither the $b^4\Sigma_g^-$ nor the $a^4\pi_u$ states are either purely case (a) or (b) but follow intermediate coupling. Nevin[31] has found forty (40) branches in each band of $O_2^+(1-)$. In general the bands are degraded to the violet and each band seems to be composed of 5 separate sub-bands. The wavelength range is from 4992 Å to 7891 Å, with strongest activity in the region 6856 Å to 5000 Å. The first negative system is the only known $^4\Sigma_g^- \rightarrow {}^4\pi_u$ transition in molecular physics.

Excitation cross section measurements for this state have been made by H. Nishimura[32] and J. W. McConkey[33]. Nishumura found $\sigma[0_2^+(1-)(2,1)]$ to be 8 x $10^{-19}cm^2$ at 100 eV.

Lifetime Measurements

Using the cold cathode excitation source described previously, the lifetimes of the upper eight vibrational levels v'=0,1,...7 of $b^4\Sigma_g^-$ were measured by monitoring seventeen different bands of the first negative system of the oxygen molecular ion, 0_2^+. A ½-meter Jarrell-Ash monochromator (16 Å/mm) was used as the wavelength discriminator. The spectra of the oxygen discharge was obtained from 1900 Å to 6300 Å by using the spectrohistogram technique described heretofore. The $0_2^+(1-)$ system was the only band system observed. Many lines of oxygen (OI) and the oxygen ion OII were observed. This was most fortunate since they provided convenient wavelength markers as well as interesting species for additional lifetime measurements.

Previous determinations of the lifetimes of the v'=0,1,2 levels have been made by Jeuehomme[34]. His values are quite long and of the order of 1.0μ sec. Our recent work indicates that his values are lifetimes of cascade components and not the true lifetimes of the v' levels of the $b\Sigma_g^-$ state.

The data presented here was obtained by means of the delayed coincidence method and was analyzed partially by graphical and by numeric means utilizing the program RICH.

Table 2 lists the data obtained for v'=0,1 levels of $b^4\Sigma_g^-$. The band wavelength λ, pressure, short lifetime, and long lifetime are tabulated. Table 3 continues the same listing for v'=2,3,4. Table 4 lists data for v'=5,6,7.

Table 2. $0_2^+ \ ^4b\Sigma_g^-$ v'=0,1.

(v',v'')	λ(Å)	P(μHg)	τ_S(ns)	τ_L(ns)
0,0	6026	120	94.2	267
		65	142.4	373
		85	109	249
		100	157	418
		58	196	983
1,0	5632	76	156	411
		76	144	401
		110	92.6	275
		162	119.6	249
		100	95	264
		64	118	401
		86	151	393
1,1	5973	63	169	423
		71	106	368
		88	127	343
		75	183	549

Table 3. $O_2^+ \ ^4b\Sigma_g^-$ v'=2,3,4.

(v',v'')	λ(Å)	P(μHg)	τ_S(ns)	τ_L(ns)
2,0	5296	68	125	371
		57	123	390
		105	123	325
		95	93	278
		83	152	589
2,1	5593	90	106	302
		82	123	336
		61	144	424
		78	130	368
		101	144	367
2,2	5924	115	111	298
		97	129	325
3,0	5005	80	145	369
		105	148	356
3,1	5274	90	110	288
		69	130	364
		93	116	324
		97	119	324
		96	125	343
		55	180	886
3,2	4466	78	144	413
3,3	5883	63	164	445
		105	135	330
		95	120	321
		105	130	343
		92	149	357

Table 3 (Continued)

(v',v'')	λ(Å)	P(μHg)	τ_S(ns)	τ_L(ns)
4,0	----	---	---	---
4,1	4998	84	148	331
		105	150	353
		33	144	562
4,2	5259	70	163	442
		55	119	442
4,3	5540	92	111	320
		100	136	362
4,4	5847	100	131	343

Table 4. 0_2^+ $^4b\Sigma_g^-$ v'=5,6,7.

(v',v'')	λ(A)	P(μHg)	τ_S(ns)	τ_L(ns)
5,0	----	---	---	---
5,1	----	---	---	---
5,2	4992	75	132	358
		90	166	419
5,3	5251	72	168	374
		89	---	324
		95	---	355
		90	156	369
5,4	5521	78	176	448
		101	144	371
		125	168	421
5,5	5814	---	---	---
6,4	5241	87	135	375
		75	109	299
7,5	5234	50	276	397
		60	157	460

The data obtained was found to be nearly singly exponential in several cases. We interpret the data as two exponentials, i.e.,

$$y = Ae^{-t/B} + Ce^{-t/D} + K,$$

where in these cases A/C<1. Thus separation of the two exponentials is difficult. This may indicate instrumental difficulties. If the count rate is too high (greater than 20%) serious alterations of decay curves may be obtained. However, this does not seem to be the case with these data. Since A/C<1, there are large errors in the decay constants as explained. Thus the scatter in the resultant data is large.

In Figs. (29), (30) and (31) the values of $1/\tau_v$ vs. pressure is presented for the cascade transition probabilities for the levels v' = 0,1,2. Also plotted on the same graph are values taken from Jeuehomme[34] for the "real" lifetimes. It is an easy matter to ascertain that his data must be for the cascade component. Moreover his excitation source was a clamped microwave device which had a slow (~50 nsec) cutoff, and thus he was unable to measure the short components.

Finally Table 5 lists the measured lifetimes and transition probabilities for the v' = 0,1,2,3,4,5,6,7 levels of $0_2^+(1-)b^4\Sigma_g^-$ as a function of the band measured. Since A/C is small in most cases we can only roughly estimate errors at 15 per cent.

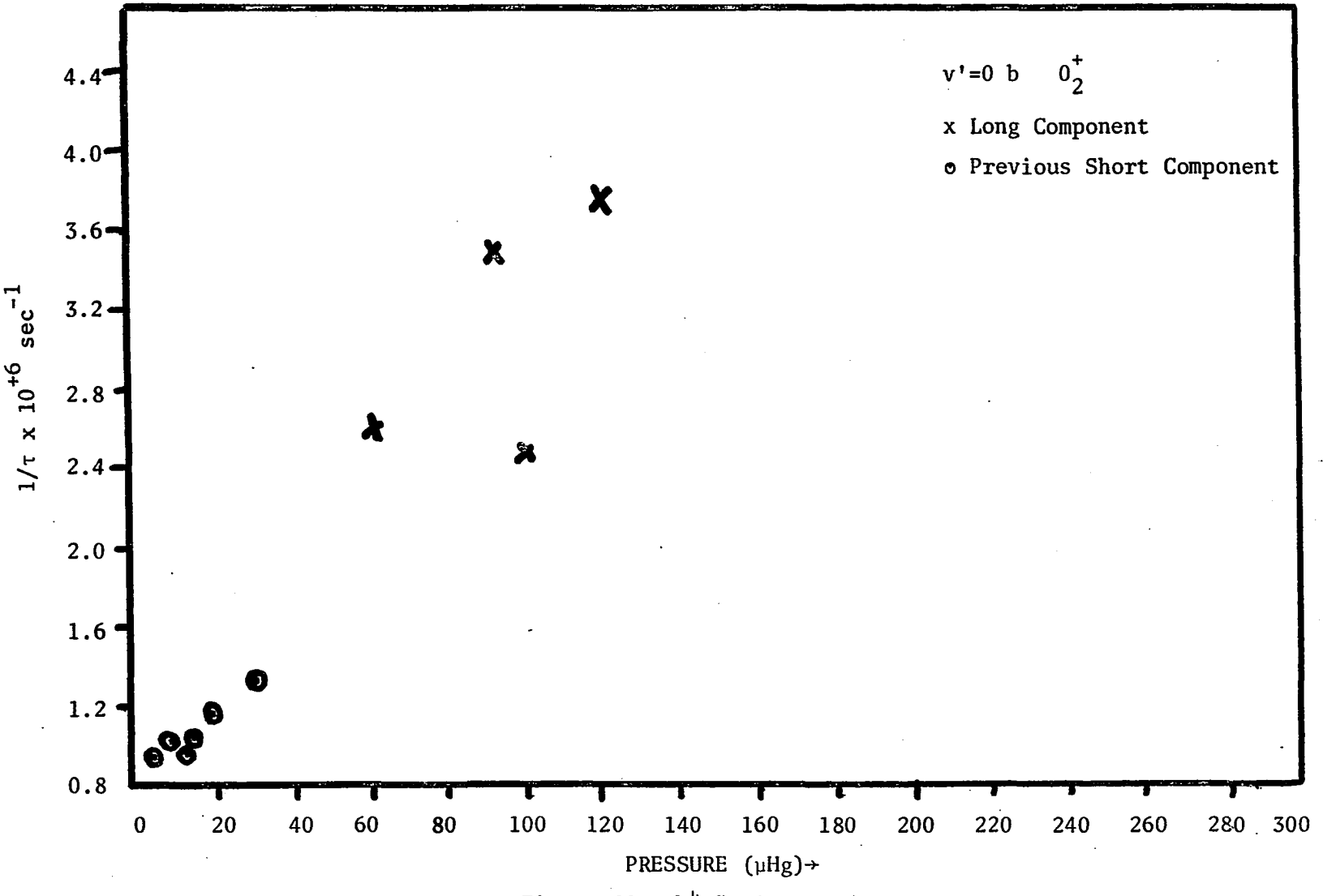

Figure 29. $b^4\Sigma_g^-$ v' = 0 $1/\tau$ versus Pressure.

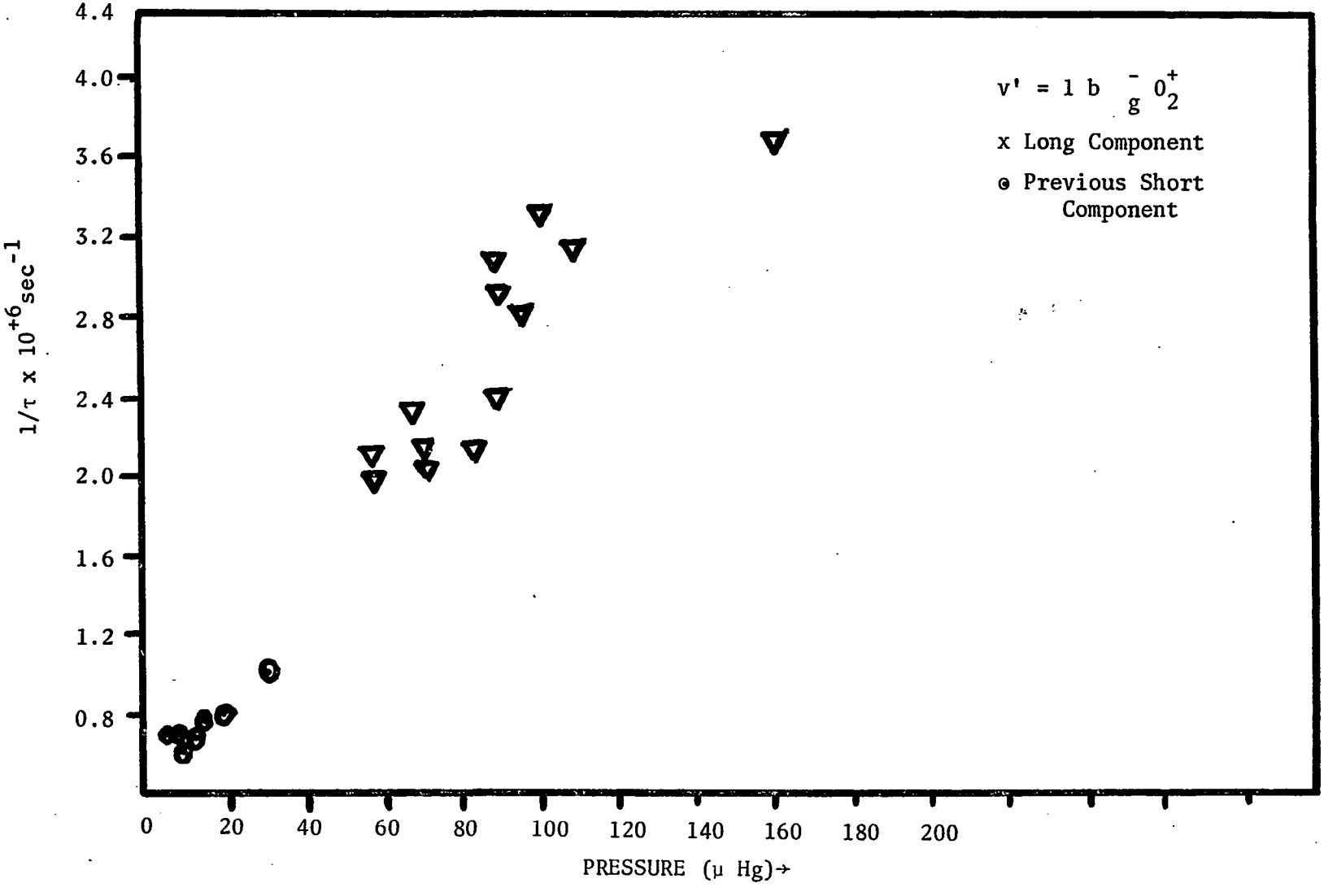

Figure 30. $b^{4}\Sigma_{g}^{-}$ v' = 1 $1/\tau$ versus Pressure.

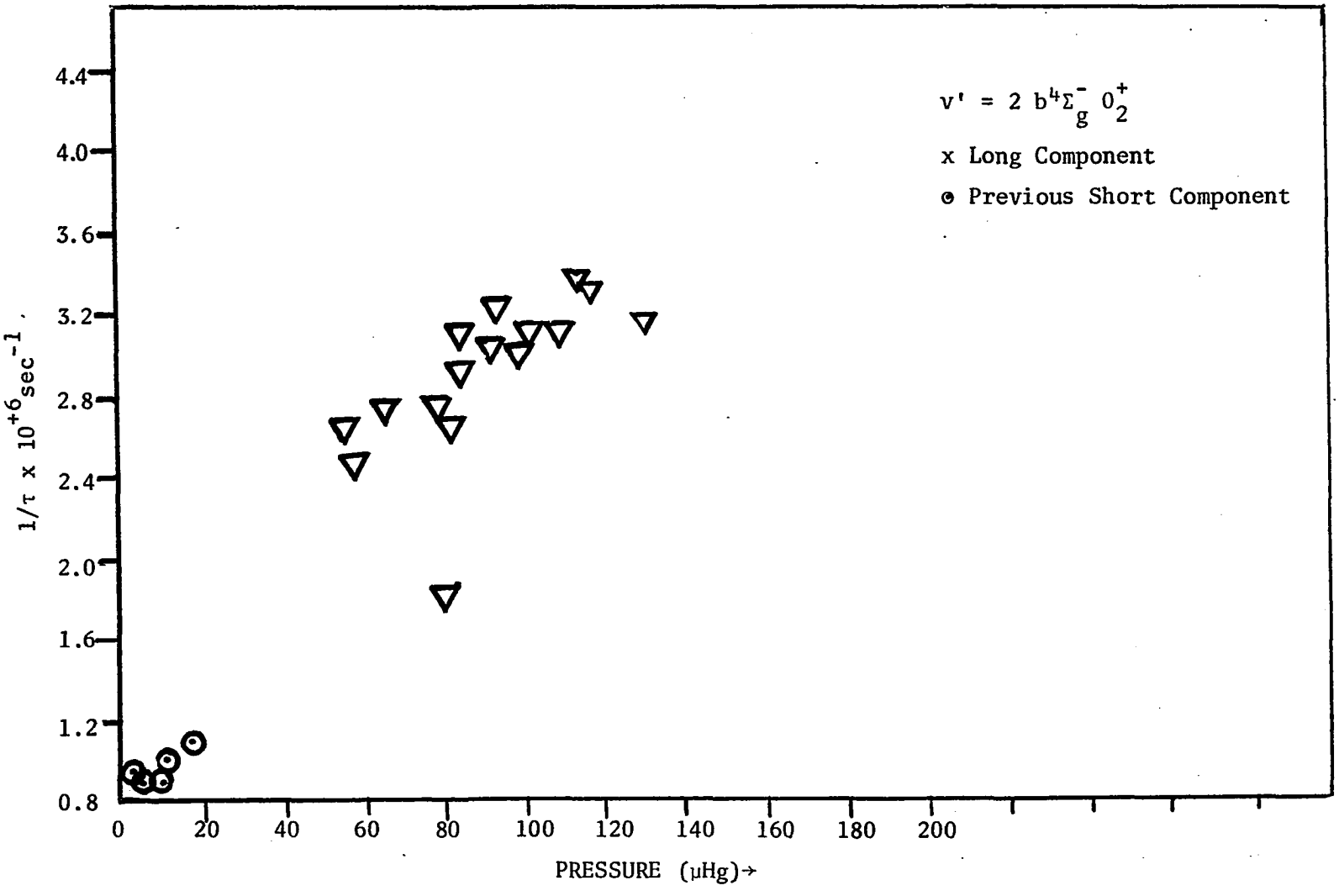

Figure 31. $b^4\Sigma_g^-$ v' = 2 $1/\tau$ versus Pressure

Table 5. $0_2^+(1-)b^4\pi_g^- \rightarrow a^4\pi_u$.

(u, ℓ)		λ(Å)	τ(short)NS.
0	0	6026	139.
1	0	5632	125.
	1	5973	146.
2	0	5296	123.
	1	5593	129.
	2	5924	120.
3	2	5566	144.
	3	5883	139.
4	1	4998	147.
	2	5259	141.
	3	5540	123.
	4	5847	131.
5	2	4992	149.
	3	5251	162.
	4	5521	163.
6	4	5241	122.
7	5	5234	157.

CHAPTER II

OXYGEN NEUTRAL AND IONIC TRANSITIONS

As has been known for some time[35], the oxygen molecule does not readily show an emission spectrum in discharges at low pressures. We wish to examine two of the excited electronic states of O_2. The first is the $A^3\Sigma_u^+$ which is the upper state of the Herzberg I system. This system is electric dipole forbidden since it involves $A^3\Sigma_u^+ \rightarrow X^3\Sigma_g^-$ transition. It has been observed in emission in afterglows at extremely low pressure and in absorption. It is not likely that a measurement of its lifetimes will be made in discharge tube, since the $+\nleftrightarrow -$ selection rule is violated.

The other interesting state of the O_2 molecule is the $B^3\Sigma_u^-$ state. The transition $B^3\Sigma_u^- \rightarrow X^3\Sigma_g^-$ produces the Schumann-Runge Bands in the wavelength range 4400 to 1700 Å. The internuclear equilibrium separation r_e of these two states are 1.6 Å ($B^3\Sigma_u^-$) and 1.20739 Å ($X^3\Sigma_g^-$). This band system is not observed at low pressure and low temperature. Due to the large separation of the minima of the potential functions ($\Delta r_e \cong 0.4$ Å), direct Franck-Condon like transitions from $v''X^3\Sigma_g^-$ to $v'B^3\Sigma_u^-$ states end up in the repulsive part of the $B^3\Sigma_u^-$ state. Thus excitations from $v'' \geq 13$ of the ground state, all produce decomposition of the O_2 molecule into its excited components $O(^3P) + O(^1D)$ according to the scheme

$$O_2(X^3\Sigma_g^-) + e^- \rightarrow O_2(B^3\Sigma^-) + e^-$$

$$O_2(B^3\Sigma_g^-) \rightarrow O(^3P) + O(^1D) \ .$$

This explains the existence of atomic spectral lines in the spectrum obtained in the low pressure cold cathode discharge. The $O(^1D)$ oxygen atom is a metastable with mean life of 100 seconds![36] Since level is so long lived, it can easily be excited to a higher level or ionized, by an additional electron impact.

Five different levels in OI were observed to emit strongly in the spectral response of the photomultiplier tube used (RCA 8575). Table 6 lists the observed data for OI. The wavelength of the transition, the pressure, and the lifetimes (short and long) are listed. Figures (32) and (33) show plots of lifetimes versus pressure for the transitions measured.

Figure (34) shows the lifetimes, transition probabilities, transition arrays, and multiplets for the 5 transitions measured. Also a partial energy level diagram is shown.

Since the $O(^1D)$ state is metastable, it can be ionized by additional electron impact, thus producing excited states of the oxygen ion (OII). Lifetimes of four multiplets were measured in OII. They were $^4P \rightarrow {}^4S^\circ$, $^4P \rightarrow {}^4P^\circ$, $^2D \rightarrow {}^2F^\circ$, and $^4P \rightarrow {}^4D^\circ$. In the $^4P \rightarrow {}^4D^\circ$ transition lifetimes of seven of the eight possible transitions were measured. This provides a test of the constancy of the dipole matrix element with multiplets in ionic oxygen.

Table 6. Lifetimes in atomic oxygen.

λ(Å)	P(μHg)	τ_S(ns)	τ_L(ns)
6157	105	45	---
	120	46	275
	130	38.2	239
5435	105	46	289
	120	46	293
	135	48.7	236
5330	68	47.5	322
	120	44.2	241
	87	49.7	---
	55	50.0	361
	95	40.0	299
	108	47.2	275
	115	40.0	225
4368	108	42.6	333
	120	43.6	292
	89	53.2	388
	135	43.0	268
	50	52.1	113
	39	54.5	130
	15	66.3	429
	39	41.5	101
	49	39.9	122
	39	41.8	224
	105	36.3	134
3947	105	54.5	277
	120	51.1	264
	140	46.4	236

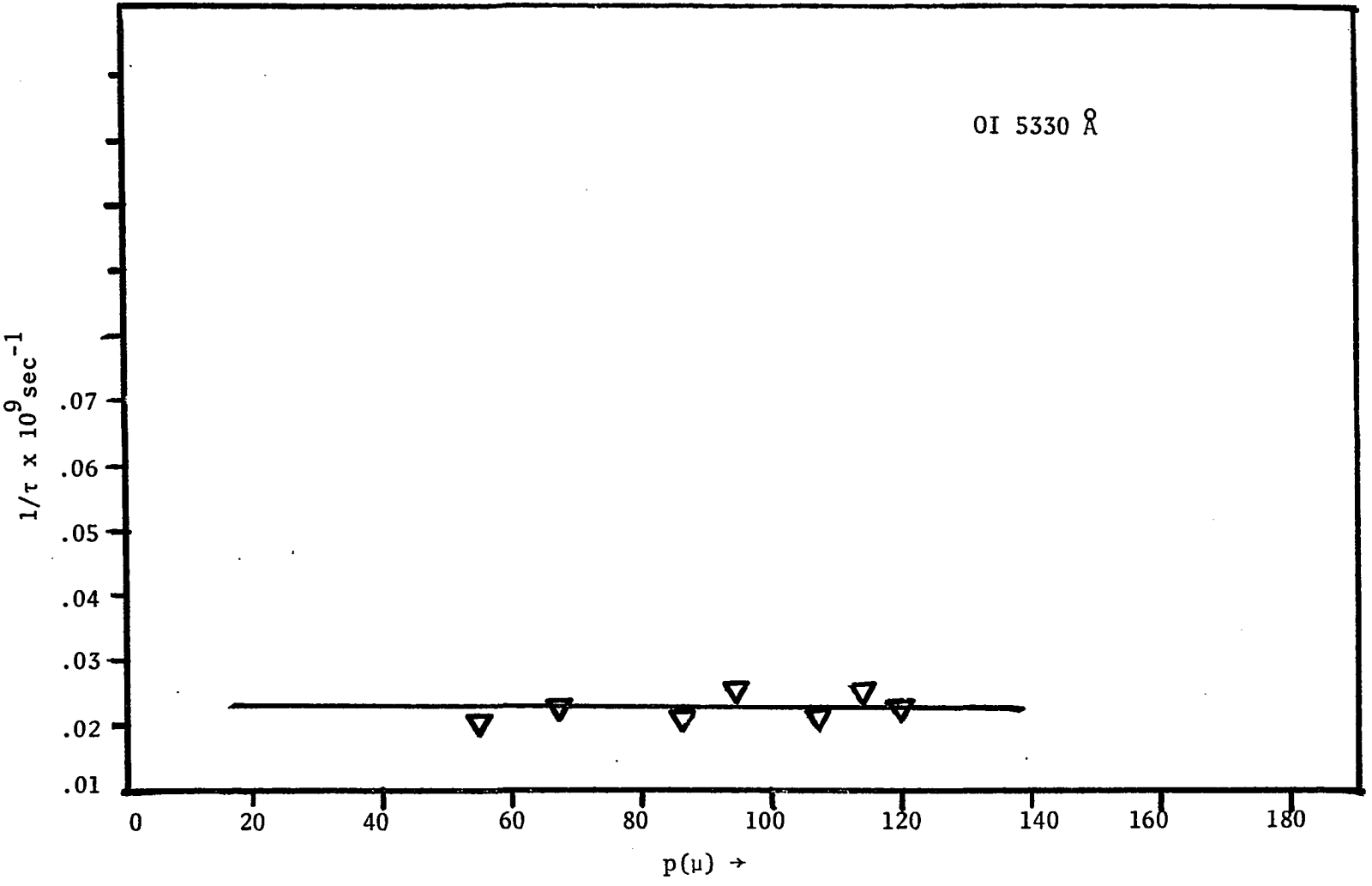

Figure 32. OI ^5P-$^5D_0$ (5330 Å) τ versus Pressure.

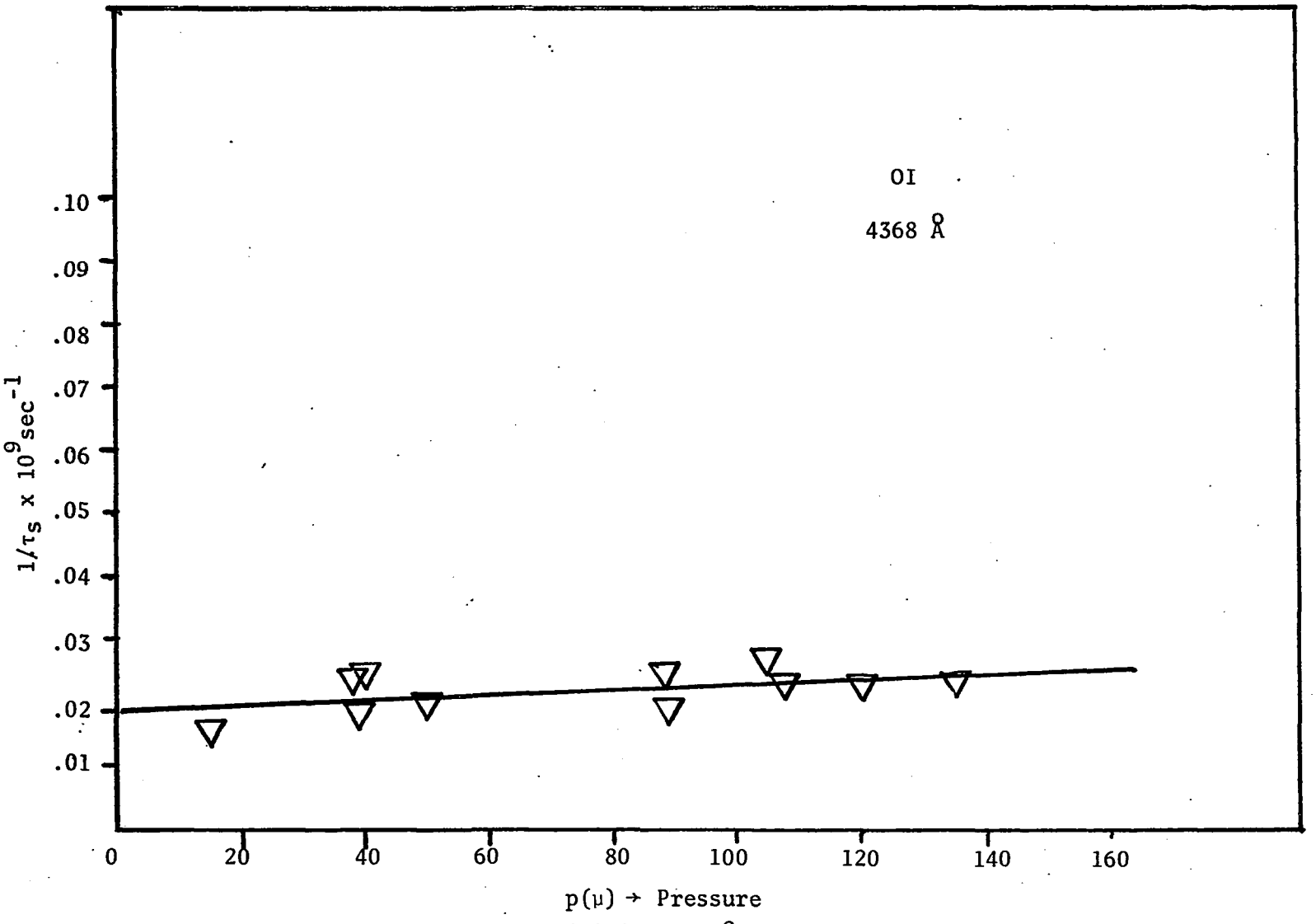

Figure 33. OI $^3S^0$-^3P(4368 Å) τ versus Pressure.

λ(Å)	Multiplet	Transition Array	(Zero Pressure) τ(NS)	ΣAx10^{8}sec^{-1}
6157	$5^5P-^5D^0$	$2p^33p-2p^34d$	43.	2.57
5435	$^5P-^5S^0$	$2p^33p-2p^36s$	47.	2.13
5330	$^5P-^5D^0$	$2p^33p-2p^35d$	46.	2.19
4368	$^3S^0-^3P$	$2p^33s-2p^34p$	47.	2.14
3947	$^5S^0-^5P$	$2p^33s-2p^34p$	51.	1.97

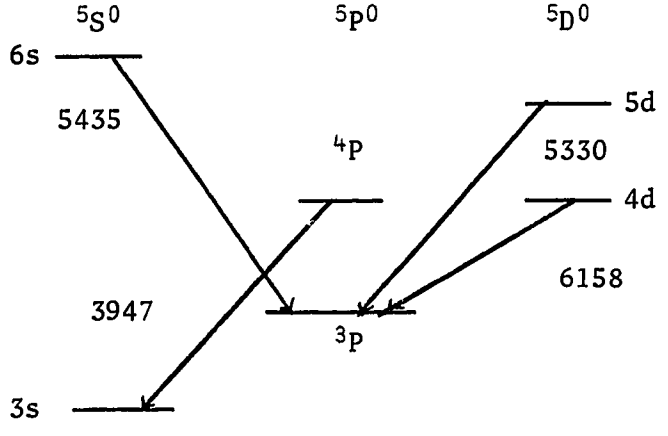

Figure 34. OI Atomic Lifetimes and Energy Level.

Table 7 lists the wavelength, pressure and lifetimes (long and short) for the components of the multiplets. Figure (35) shows the detailed transitions involved in the $^4P \rightarrow ^4D^\circ$ transition. Figure (36) shows a partial energy level diagram for OII and lists the final results for OII lifetimes.

Table 7. OII Lifetimes in Ionic Oxygen Atom

λ(A)	P(μHg)	τ_S(ns)	τ_L(ns)
3749	80	8.3	135.
4317	85	9.6	130.4
4349	85	9.9	---
	54	14.1	225.
4590	110	10.5	208.6
	70	10.2	107.2
	70	10.8	319.
4639	83	12.2	---
	88	12.7	96.9
4642	83	12.1	---
	61	11.5	57.9
	69	11.2	77.
	35	22.8	669
4650	85	12.6	---
4649	54	10.4	52.
	80	13.4	116.
4662	130	12.0	---
4661	64	14.0	175.
4674	93	14.7	188.
	93	14.1	163.
4676	47	13.9	90.8
	47	15.5	149.
	135	12.9	---

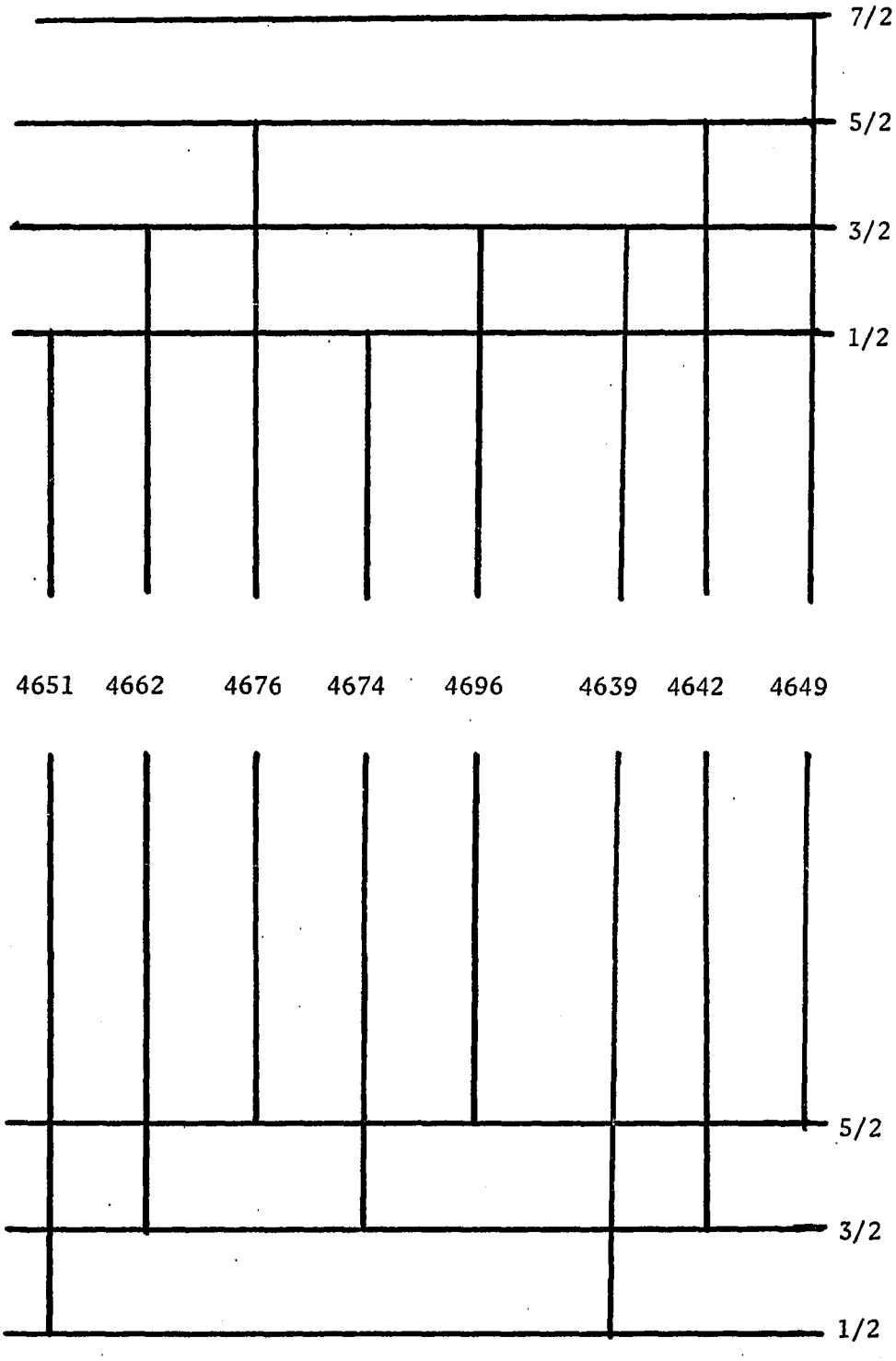

Figure 35. ^4P-$^4D^0$ OII $2p^2 3s$-$2p^2(^3P)\,^3P$ Transition.

OII

	λ	Multiplet	Transition Array	τ(NS)	$\Sigma Ax10^8 sec^{-1}$
F	3749	$^4P-^4S^0$	$2P^23s-2p^2(^3P)^3P$	8.3	1.20
E	4317	$^4P-4P^0$	$2p^23s-2p^2(^3P)^3p$	9.6	1.04
	4349			14.1	0.71
	4590	$^2D-^2F^0$	$2p^23s'-^2p^2('D)^3P'$	10.5	0.95
D	4639	$^4p-^4D^0$	$2p^23s-2p^2(^3P)^3p$	12.5	0.80
	4642			11.6	0.86
	4651			12.1	0.82
	4662			13.0	0.77
	4674			14.4	0.69
	4676			14.7	0.68
	4696			-	-
	4647			12.1	0.82

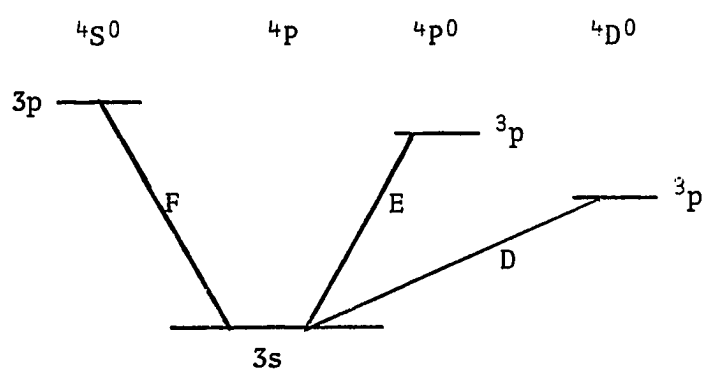

Figure 36. Lifetimes and Energy Levels in OII.

CHAPTER III

THE NITRIC OXIDE MOLECULAR TRANSITIONS

Electronic Structure

This diatomic molecule is isoelectronic to the O_2^+ molecule but differs widely in its possible structure and spectra. A complete energy level diagram is shown in Fig. (1). It will be noted that the ground state is a $^2\pi$ state which implies a permanent dipole moment. Moreover, the $X^2\pi$ state is split due to spin-orbit coupling by 233 cm^{-1}. Transitions ending at ground will be at least doubled headed when viewed with only moderately dispersing instruments.

The first excited electronic state is the $A^2\Sigma_r$ state which lies at 40055 and 40007 cm^{-1} above ground (v''=0) state. Transitions from $A^2\Sigma_r$ to $X^2\pi_r$ yielded the γ(gamma) bands in the wavelength range 1700 Å to 3300 Å. The emission spectra never show transitions from $v' \geq 3$ since a level crossing occurs at that point. In the series of experiments to be described below, emission spectra were seen only with v' = 0,1,2 in agreement with previous results[37]. The γ(gamma) bands are among the strongest impurity bands commonly seen in electrical discharges.

For this $^2\Sigma \rightarrow ^2\pi$ transitions each band has four characteristic heads. The $A^2\Sigma$ band always belongs to Hund's case (b) while the $X^2\pi$ state may be either case (a), (b) or intermediate. The $X^2\gamma$ state in NO has a large splitting and thus is case (a), so the γ bands are $^2\Sigma(b) \rightarrow ^2\pi(a)$

transition. The four characteristic heads consist of a doublet double head structure, i.e., two sub-bands which are doublets. In this experiment only the sub-bands could be resolved, not the doublet structure in each.

The next excited state of interest is the $B^2\pi$ state. It is the upper level of the β bands. The lower level of the bands is the $X^2\pi$ (ground state). The β bands are rather uniformly spread throughout the wavelength range 2000 Å to 6000 Å. This is due to the large difference of internuclear distance for the two states. According to Herzberg[38] both states are $^2\pi$ and belong to Hund's case (a), thus the selection rule $\Delta\Sigma = 0$ holds. The $^2\pi \rightarrow {}^2\pi$ bands split into two sub-bands $^2\pi_{\frac{1}{2}} \rightarrow {}^2\pi_{\frac{1}{2}}$, and $^2\pi_{3/2} \rightarrow {}^2\pi_{3/2}$. Each sub-band has six branches which form two P, two weak Q and two R branches. The next important excited levels are the $D^2\Sigma$ and $C^2\Sigma$ which connect to ground state $X^2\pi$ to form the ε(epsilon) and δ(delta) band systems. These band systems are similar and for years were thought of as being identical. They lie in the 1500 Å to 2600 Å region. The δ system is usually a strong impurity system in N_2 discharges. Both systems are $^2\Sigma \rightarrow {}^2\pi$ and have spectra similar to the γ system (Four characteristic heads - two doublet sub-bands). Several of the δ and ε bands overlap the γ bands under low dispersion.

Another interesting band system (the β' system) arises from the transition $\beta'^2\Delta_i \rightarrow X^2\pi_r$. This system is entirely in the vacuum ultraviolet and thus was not seen in this experiment. It is mentioned since the upper level ($\beta'^2\Delta_i$) is also the upper level for the strong infrared system which arises by transition to the $B^2\pi_r$ state which is the upper

level to the β bands in the visible. Measurements of the lifetimes of the $^2\Delta_i$ system can be made by looking at the infrared system instead of the vacuum ultraviolet.

The internuclear equilibrium distances r_e for these electronic states are[39] $X^2\pi$(1.1508 Å); $A^2\Sigma^+$(1.0637 Å); $B^2\pi_r$(1.385, 1.448 Å); $C^2\Sigma^+$(1.075 Å); $D^2\Sigma^+$(1.0646 Å); $E^2\Sigma^+$(1.0661 Å). Transitions are extremely favorable among the states $E^2\Sigma^+$, $D^2\Sigma^+$, $C^2\Sigma^+$, $A^2\Sigma^+$, $X^2\pi$ since their equilibrium distances are nearly euqal. Moreover, application of the Franck-Condon principle[40] indicates that in emission the bands with v'=0,1,2 will be favored over other transitions (v'≥4,5,6, etc.), even if the energy differences are small for $D^2\Sigma^+$, $C^2\Sigma^+$, $E^2\Sigma^+ \rightarrow A^2\Sigma^+$ transitions. There is great likelyhood of cascade into $A^2\Sigma^+$ due to very small change in internuclear distance r_e.

Chemical Characteristics

The nitric oxide molecule has a molecular weight of 30.01 and at atmospheric pressure melts at 100° K. It is an oderless toxic gas which can be lethal at concentrations exceeding a few ppm. Its vapor pressure at 77° K is essentially 0.100 Torr, and thus a liquid nitrogen trap can be used as a trap and cryogenic pump.

Preliminary lifetime investigations using NO obtained from Matheson Company were carried out in the inverted diode Holzberlein[41-44] excitation source (invertron). This device has a large hollow induction heated oxide coated cathode which acts as the source of electrons when the interior grid is pulsed positively. Crude spectra, taken using wide slits on a Jarrell-Ash ¼ meter monochromator, indicated molecular spectra

in the 2000 Å to 3000 Å range. However, later work indicated this molecular structure was due to CO^+ and not NO. Moreover, after short run times the cathode caoting of the invertron (barium carbonate) was found to be poisoned. This was due to the reactions

$$\left.\begin{array}{l} 2NO \rightarrow O_2 + N_2 \\ B_a + O_2 \rightarrow B_a O_2 \end{array}\right\} .$$

The first of these reactions is almost entirely complete at temperatures exceeding 1000° K, since NO has a lower dissociation energy than O_2 and N_2. Thus attempts to study NO in a heated environment had to be abandoned due to thermal decomposition alone. Substitution of another oxide cathode coating compound such as lanthanum oxide, although would cure the problem of poisoned cathodes, would not alter the tendency for NO to decompose thermally or electronically.

These results led to the development of the cold cathode discharge tube described before.

Lifetime Measurements in NO

Using the cold cathode discharge tube with flowing NO gas, the lifetimes of the v'=0,1 and 2 vibrational levels of the $A^2\Sigma^+$ electronic state have been measured. The delayed coincidence method was used and data analysis was done by the computer program RICH. In all, 17 separate bands of the γ system were monitored. The lifetimes were not found to be pressure dependent below 0.2 Torr. In addition estimates of the cascade lifetime as well as the ratio of the population coefficients A/C were obtained.

Table 8 lists the data obtained for the v'=0 ($A^2\Sigma^+$) state. In it are listed values of (B and D) from

$$y = Ae^{-t/B} + Ce^{-t/D} + K$$

and the ratio A/C, as well as, the pressure, wavelength and vibrational band. The values of the short lifetimes as a function of pressure are plotted in Fig. (37).

Table 9 shows similar data for the state v'=1 ($A^2\Sigma^+$) of NO, and the values of the short lifetimes were plotted as functions of pressure in Fig. (38). Table 10 shows similar data for the state v'=2 ($A^2\Sigma^+$) of NO and in Fig. (39) the values of the short lifetimes versus pressure are plotted.

When these values of $\tau_{v'}$ are least squares fitted to a straight line pressure graph, the lifetimes shown below result.

v'	$\langle\tau_{v'}$(NS)$\rangle$	σ(NS) Levels
0	99.9	5.5
1	104.	6.6
2	93.6	7.9
All	98.4	8.0

If one assumes that the lifetimes of the states v'=0,1,2 are independent of the quantum numbers v', then the lifetime determined by least squares analysis is 98.4 ± 8.0 NSEC.

Table 8. v'=0 State of $A^2\Sigma^+$(NO)

(v',v'')	λ(Å)	B(ns)	D(ns)	P(μHg)	A/C
0,0	2269	86.8	726	112	1.86
0,0	2262	57.4	689	121	0.32
0,0	2263	96.5	463	110	2.12
0,0	2263	68.7	707	50	3.19
0,0	2269	91.0	707	65	2.06
0,1	2370	103.3	504	165	0.52
0,1	2363	159.7	-377	51	254.
0,1	2364	1279.	(1 exp)	63	- --
0,2	2478	105.	350	97	2.13
0,2	2478	99.6	367	105	0.72
0,2	2478	101.	687	112	0.99
0,2	2471	92.7	341	48	1.19
0,2	2471	112.4	798.4	59	3.73
0,3	2595	101.9	415.7	112	1.68
0,3	2595	103.9	532	95	1.56
0,3	2587	159.9	-7201.	50	3.21
0,3	2587	165.5	-6196.	60	2.56
0,3	2587	100.0	608	101	1.37
0,4	2722	101.4	495	88	2,04
0,4	2713	103.7	598	108	2.27
0,4	2722	97.9	444	150	1.07
0,5	2849	105.7	371	87	1.70
0,5	2859	85.0	510	135	0.73
0,5	2849	107.	675	58	2.16

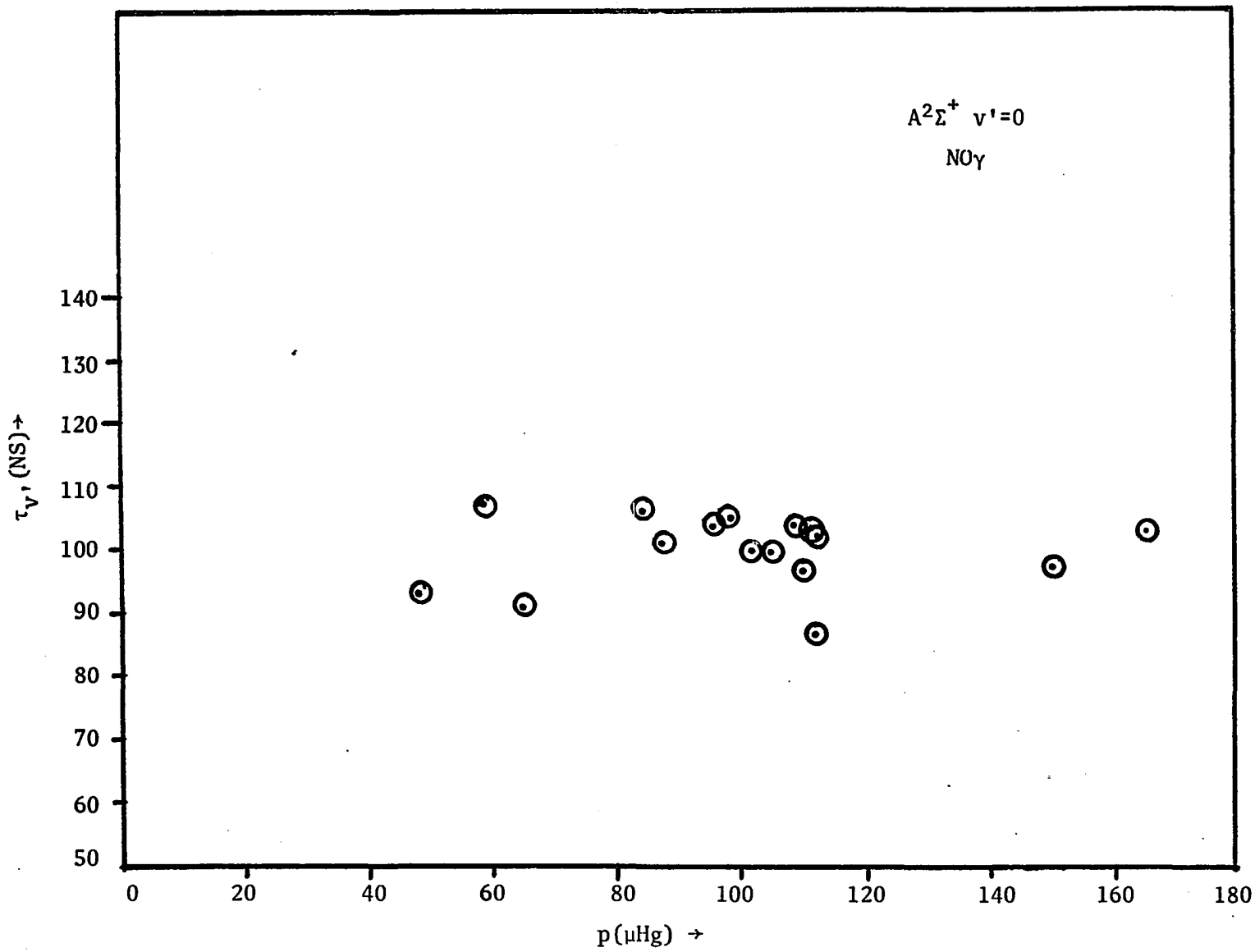

Figure 37. τ versus Pressure for v'=0.

Table 9. v'=1 State of $A^2\Sigma^+$(NO)

(v',v'')	λ(Å)	B(ns)	D(ns)	P(μHg)	A/C
1,0	2149	70.7	432	145	1.94
1,1	2239	97.9	633	145	1.04
1,3	2447	57.	853	137	0.27
1,3	2449	109.7	317	60	1.10
1,4	2559	93.8	467	137	1.29
1,4	2550	103.7	352	50	1.63
1,5	2680	110.2	275	80	0.87
1,5	2680	107.6	430	87	1.08
1,5	2671	144.7	1983	60	4.82
1,6	2810	112.8	541.5	85	1.67
1,6	2810	97.4	403.4	140	0.91

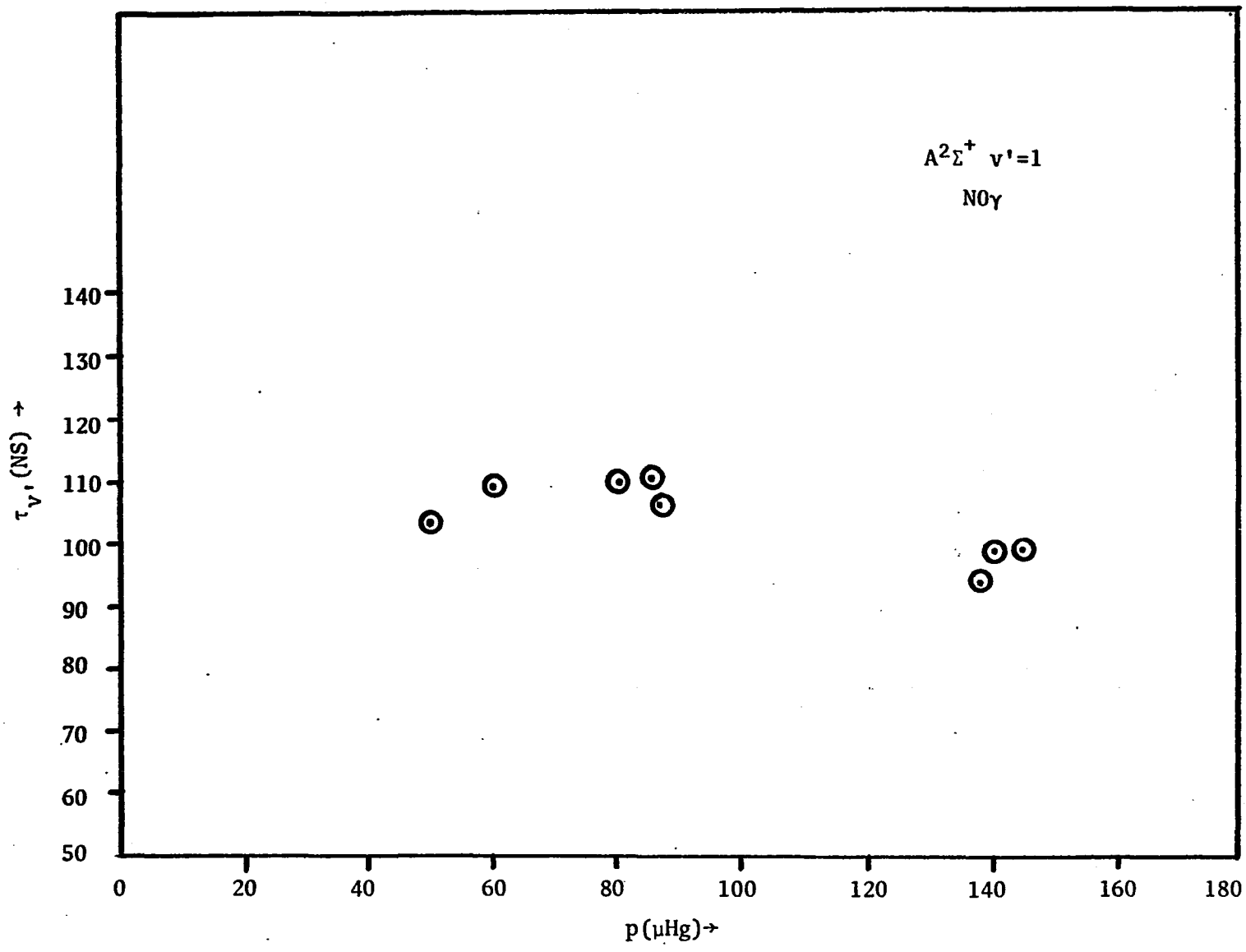

Figure 38. τ versus Pressure for v'=.

Table 10. v'=2 State of $A^2\Sigma^+$(NO)

(v',v'')	λ(Å)	B(ns)	D(ns)	P(μHg)	A/C
2,3	2316	84.8	406	94	2.63
2,3	2309	79.3	312.7	110	1.81
2,5	2524	89.4	413	100	1.41
2,5	2516	91.6	445	91	1.74
2,6	2630	106.4	362	91	2.15
2,6	2639	97.3	471.5	110	1.54
2,6	2639	87.3	365	45	1.86
2,7	2764	101.0	305	80	1.56
2,7	2764	92.1	309	125	1.86
2,7	2764	102.	325	47	1.55
2,7	2764	95.9	209.4	60	1.33
2,7	2755	118.9	689.7	108	4.57
2,8	2898	107.7	374.8	88	1.95
2,8	2898	85.2	425	125	1.74
2,8	2898	92.6	423	130	0.99
2,8	2898	90.7	565	70	2.32

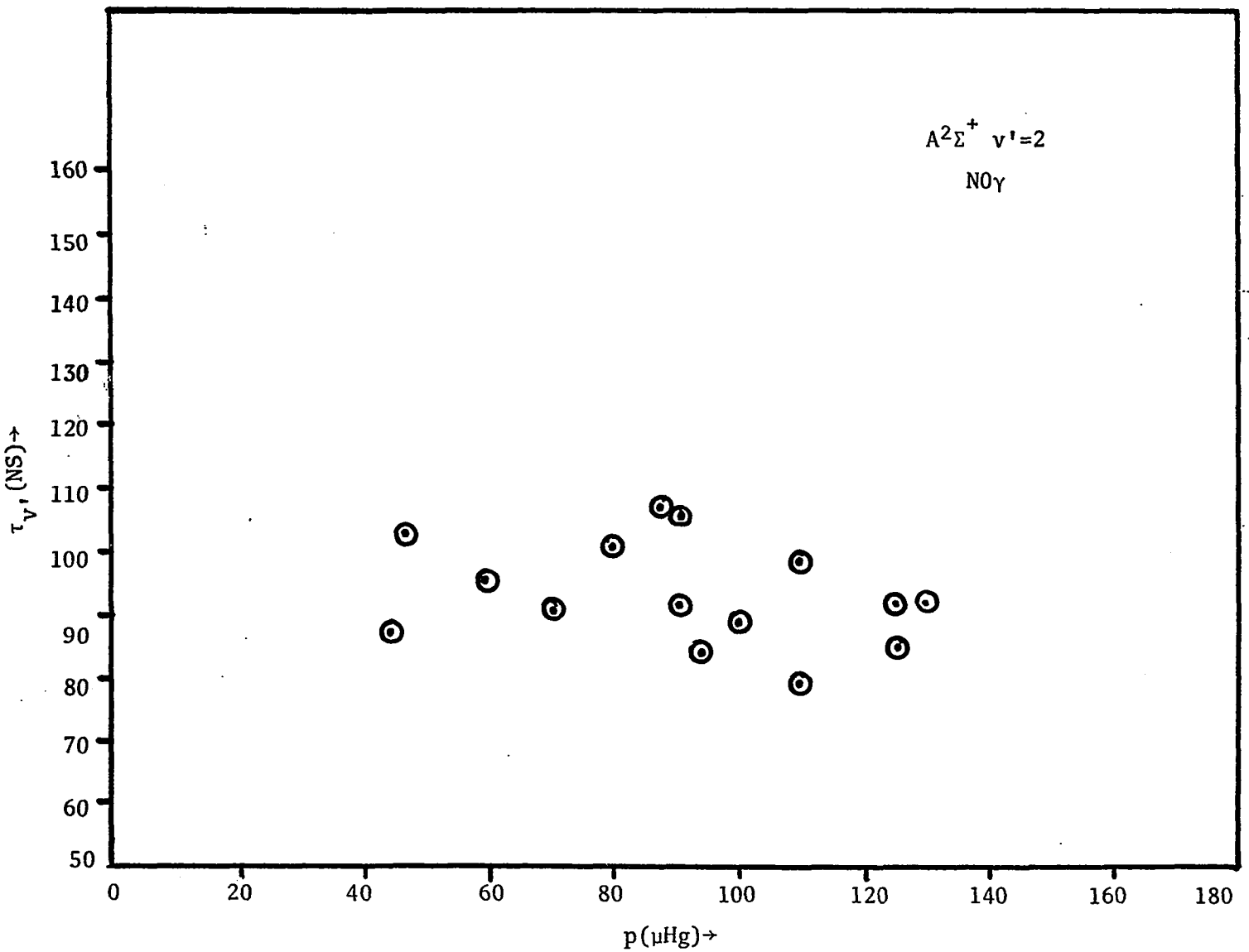

Figure 39. τ versus Pressure for v'=2.

Calculations for electronic transition moments

Let us recall that the lifetime of a state n'v' is given by

$$1/\tau_{n'v'} = \sum_{\substack{n'' \\ v''}} A^{v'v''}_{n'n''}$$

$$= \frac{64\pi^4}{3hc^3} \sum_{n''v''} \nu^3(n'v',n''v'') \frac{p'_\Sigma p'' \; \Sigma'_\Sigma \Sigma'' \left| R^{v'v''}_{n'\Sigma' \; 'n''\Sigma''p''} \right|^2}{(2-\delta_{0,\Lambda''})(2S'+1)}$$

If we assume that there is no interaction between electronic and vibrational motions, then

$$\Sigma \left| R^{v'v''}_e \right|^2 = q_{v'v''} \Sigma R^2_r(r)$$

where $\Sigma R^2_e(r)$ is the electronic transition moment. The r centroid $\bar{r}_{v'v''}$ is defined by

$$\bar{r}_{v'v''} = \frac{\langle v' | r | v'' \rangle}{\langle v' | v'' \rangle}$$

we may set $r = \bar{r}_{v'v''}$ in $R^2_e(r)$ since $\bar{r}_{v'v''}$ is a slowly varying function of r in all approximations. If we then know the Franck-Condon factors $q_{v'v''}$, the lifetimes $\tau_{n'v'}$, and the frequencies $\nu^3(n'v',n''v'')$, one can then determine the electronic transition moments.

A Fortran IV program has been written to calculate these $R_e(\bar{r})$ and is named NOFREQ. It is assumed that $R^2_e(r_{v'v''}) \neq F(v'')$ and that the $q_{v'v''}$ are given by the Morse oscillator wavefunction result of Ory[45] *et al.* The calculation uses the values of $1/\tau_{v'v''}$ the band head wavelengths, as determined by Herzberg to be

$$1/\tau_{v'v''} = \nu_{oo} + [\omega_e' - \omega_e\chi'(v'+1)]v' + [\omega_e'' - \omega_e X_e''(v''+1)]v'' \quad .$$

The constants used in the calculation are

ν_{oo}'	= 44078.3 and 44199.2 cm^{-1}	upper level $A^2\Sigma^+$
ω_e'	= 2371.3 cm^{-1}	
$\omega_e X_e'$	= 4.48 cm^{-1}	
ν_{oo}''	= 120.9 cm^{-1} or 0 cm^{-1}	lower level $^2\pi_{3/2,1/2}$
ω_e''	= 1903.68, 1904.03 cm^{-1}	
$\omega_e'' X_e''$	= 13.97 cm^{-1}	

The program first inputs the Franck-Condon factors, then using the spectroscopic constants calculates the frequencies of the band heads $\nu^3(n'v'',n''v'')$.

It can be shown that

$$\Sigma R_e^2(r) = \left(\frac{2h}{64\pi^4}\right) 1/\tau_v \frac{2}{\sum_{v''} \frac{\nu^3(v'v'')}{c^3} q_{v'v''}} \quad .$$

The calculation is straight forward and yields the results below.

v'	$\tau_{v'}$ (NS)	Transition Moment (AU)
0	99.8	0.244
1	104.1	0.231
2	93.5	0.236

In addition the electronic oscillator strength, which is wavelength dependent ($1/\lambda$) as defined by Aert Schadee[46], is calculated

$$f_{e\ell}(\lambda) = \frac{8\pi^2 m_e c}{3he^2\lambda} \frac{\Sigma R_e^2(r)}{(2-\delta_{0,\Lambda''})(2S''+1)} .$$

Values of $f_{e\ell}(\lambda)$ are not included since the calculations here have assumed that $R_e^2(r)$ was λ independent.

Using the value of the lifetime of the v' = 0 state of NO $A^2\Sigma^+$ as measured by M. Jeunehomme[47] to be 196.5 nanoseconds and the Franck-Condon factors of Ory[45], the program NOFREQ calculates the transition moment for v'=0 state as 1.74 AU. This value is about eight times the value found in the current experiment. This difference can be traced to the method utilized by Jeunehomme[48]. He measured the fluorescene decay time following excitation of NO by an intense pulsed light source of "very short duration". The excitation light was filtered by a wide-band (2200 Å to 3500 Å) Kusha filter. Decay times were determined by time averaging the signal from a gated photomultiplier.

The probable difference between Jeunehomme's and this author's results are due to the fact the former had very large band pass, thus could not distinguish various band heads. Also since a flow system was not utilized, photo decomposition of NO could have taken place. In addition no checks were made on the afterglow (relaxation time) of the exciting radiation pulse.

```
NOFREQ  14:12  FRI.  FEB 20,1970

      SNDM
C     G.E.COPELAND
      DIMENSION FR(4,22),VCO(4,22),Q(4,22),S(4),D(4)
      DIMENSION COEF(4)
      DIMENSION F(4,22),TL(4,22)
      DIMENSION TMAU(4)
      DIMENSION SSD(4),AE(4)
      PRINT,"ENTER FRANCK-CONDON FACTORS"
      INPUT,((Q(J,I),I=1,21),J=1,3)
  999 CONTINUE
      PRINT,"DO YOU WISH TO SEE INTERMEDIATE RESULTS?(1=YES;0=NO)"
      INPUT,INCD
      IF(INCD.EQ.1) GO TO 77
 1000 J=1
    1 DO 3 I=1,21
      FR(J,I)=(44199.2+(2371.3-14.46*(J))*(J-1)-(1904.03-13.97
     1*(I))*(I-1))**3
    3 CONTINUE
      IF(J-3)4,5,5
    4 J=J+1
      GO TO 1
    5 IF(INCD.EQ.1) GO TO 78
  543 A=0.0
      A=A+(3*2.6252E-27)/((64.)*(3.1415926)**4)
      DO 6 J=1,3
      DO 15 I=1,21
   15 VCO(J,I)=FR(J,I)*Q(J,I)
      SUM=0.0
      DO 16 I=1,21
   16 SUM=SUM+VCO(J,I)
      PRINT,"        V''       SUM"
      PRINT,J-1,SUM
      S(J)=SUM
    6 CONTINUE
      DO 7 J=1,3
      D(J)=2/S(J)
      COEF(J)=A*D(J)
      TJ=0.0
      PRINT,"ENTER LIFETIME OF V' STATE(IN SEC.)"
      INPUT,TJ
      AE(J)=COEF(J)/TJ
      PRINT,"        V'        MOMENT**2"
      PRINT,J-1,AE(J)
      SSD(J)=SQRT(AE(J))
      TMAU(J)=SSD(J)/2.52E-18
      PRINT,"    TRANS. MOMENT(A.U.)     V'''
    7 PRINT,TMAU(J),J-1
      B=0.0
      B=B+(8*((3.1415926)**2)*(9.1085E-28)*(2.997829E+10))/
```

```
NOV 80  14:12  FRI.  FEB 23,1979

     1((3)*(6.62252E-27)*((4.50288E-10)**2))
       J=1
     8 DO 9 I=1,21
       TL(J,I)=(44199.2+(2371.3-14.48*(J))*(J-1)-(1904.03-13.97
      1*(I))*(I-1))
     9 CONTINUE
       IF(J-3) 10,11,11
    10 J=J+1
       GO TO 8
    11 CONTINUE
       J=1
    20 DO 21 I=1,21
       F(J,I)=(B*TL(J,I)*AE(J)*Q(J,I))/4.0
    21 CONTINUE
       IF(J-3) 30,31,31
    30 J=J+1
       GO TO 20
    31 CONTINUE
       PRINT,"DO YOU WISH TO SEE ELEC.OSCILL.STRENGTHS?(YES=1;NO=0)"
       INPUT,INCT
       IF(INCT.EQ.0) CALL EXIT
       J=1
       PRINT,"        V'       V''     WAVELENGTH(A)        FEL"
    32 DO 33 I=1,21
       F(J,I)=F(J,I)/Q(J,I)
       TL(J,I)=1.0/TL(J,I)
       TL(J,I)=TL(J,I)*1.0E+08
    33 PRINT,J-1,I-1,TL(J,I),F(J,I)
       IF(J-3) 34,35,35
    34 J=J+1
       GO TO 32
    35 CALL EXIT
       GO TO 1234
    77 PRINT,"          V'     V''       (F/C)**3     Q(V',V'')"
       GO TO 1000
    78 J=1
    81 DO 79 I=1,21
    79 PRINT,J-1,I-1,FR(J,I),Q(J,I)
       IF(J-3) 80,543,543
    80 J=J+1
       GO TO 81
  1234 CALL EXIT
       END
```

```
RUN
                                        140
NØFREQ     08:48  ACC MØN.  MAR 16,1970


ENTER FRANCK-CØNDØN FACTØRS
? .16558-0,.26393-0,.23793-0,.16062-0,.90801-1,.45607-1,.21097-1,
'? .92046-2,.38510-2,.15617-2,.62187-3,.24395-3,.94939-4,.36830-4,
ØX? .14305-4,.55786-5,.21862-5,.86500-6,.34598-6,.13998-6,.56254-7,
'X? .32950-0,.10504-0,.79568-3,.72245-1,.13508-0,.13405-0,.98671-1,
'? .60824-1,.33368-1,.16886-1,.80682-2,.36991-2,.16464-2,.71762-3,
ØX? .30852-3,.13157-3,.55948-4,.23781-4,.10102-4,.42345-5,.17079-5,
ØX? .29093-0,.14680-1,.15473-0,.75294-1,.54896-3,.34387-1,.88594-1,
ØX? .10576-0,.90032-1,.62969-1,.38737-1,.21801-1,.11512-1,.58038-2,
'? .28294-2,.13462-2,.62899-3,.28933-3,.13094-3,.58273-4,.25795-4
ØX
DØ YØU WISH TØ SEE INTERMEDIATE RESULTS?(1=YES;0=NØ)
? 0

       V''       SUM
        0    6.711155661E+13
       V''       SUM
        1    7.160593449E+13
       V''       SUM
        2    7.612239458E+13
ENTER LIFETIME ØF V' STATE(IN SEC.)
? 100-9

       V'        MOMENT**2
        0    3.764756560E-37
    TRANS. MØMENT(A.U.)     V'
   2.434825876E-01          0
ENTER LIFETIME ØF V' STATE(IN SEC.)
? 100-9

       V'        MOMENT**2
        1    3.528459963E-37
    TRANS. MØMENT(A.U.)     V'
   2.357176248E-01          1
ENTER LIFETIME ØF V' STATE(IN SEC.)
? 100-9

       V'        MOMENT**2
        2    3.319110945E-37
    TRANS. MØMENT(A.U.)     V'
   2.286179594E-01          2
DØ YØU WISH TØ SEE ELEC.ØSCILL.STRENGTHS?(YES=1;NØ=0)
? 0


RAN:   04.2 SECS

READY
```

There have been several determinations of the electronic oscillator strengths $f_{v'v''}$ of the NOγ system. If $f_{v'v''}$ and Franck-Condon factors are known, the transition moment R_e can be determined. Using the $f_{v'v''}$ results of Antropov, Dronov and Sobolev[49] and of H. A. Ory[50] together with Ory's[51] Franck-Condon results, one can find R_e from

$$f_{v'v''} = \frac{8\pi^2 m_e c}{3he^2\lambda_{v'v''}} \frac{\Sigma R_e^2(\bar{r}_{v'v''})}{(2-\delta_{0,\Lambda''})(2S''+1)} q_{v'v''} \quad .$$

A computer program named FREAK has been written in Fortran IV which solves this equation for R_e. Table 11 lists the results.

Table 11. Transition Moments of NO$^+$

	v'	R_e(A.U.)
This work	0	0.244
	1	0.231
	2	0.236
Jeunehomme	0	1.68
Ory	0	0.267
	1	0.260
	2	0.249
Antropov *et al.*	0,3	0.207
	0,4	0.184
	0,1	0.161
	0,0	0.134

```
------

FREAK     SAT.  FEB 21,1970
   #01:

$NOM
C     G.E. COPELAND
DIMENSION F(3),Q(3),V(3),R(3)
PRINT,"ENTER OSCILLATOR STRENGTHS"
INPUT,F
PRINT,"ENTER FRANCK-CONDON FACTORS"
INPUT,Q
PRINT,"ENTER FREQ.(CM-1)"
INPUT,V
PRINT,"ENTER # OF STRENGTHS"
INPUT,N
PRINT,"ENTER DEGENERACY"
INPUT,G
A=3.*(6.62377E-27)*((4.8022E-10)**2)
B=8.*(9.10721E-28)*(3.141596**2)*(2.997902E+10)
C=A/B
PRINT,"          V'          RE(A.U.)"
DO 1  I=1,N
R(I)=SQRT((C*F(I)*G)/(Q(I)*V(I)))
R(I)=R(I)/(4.8022E-10*5.29167E-9)
1 PRINT,I-1,R(I)
CALL EXIT
END
```

```
RAN:    00.9 SECS

READY



RUN

FREAK      16:29   ACC SAT.   FEB 21,1970


ENTER ØSCILLATØR STRENGTHS
? 3.99-4,7.88-4,6.73-4

ENTER FRANCK-CØNDØN FACTØRS
? .16558,.32950,.29093

ENTER FREQ.(CM-1)
? 44199.2,46561.54,48914.92

ENTER # ØF STRENGTHS
? 3

ENTER DEGENERACY
? 4

          V'          RE(A.U.)
         0    2.679347703E-01
         1    2.600611647E-01
         2    2.495435659E-01

RAN:    01.4 SECS

READY
```

REFERENCES

1. A. W. Johnson, Ph.D. Dissertation, University of Oklahoma, Norman, Oklahoma (1968).
2. M. Born and R. Oppenheimer, Ann. Physik 84, 457 (1927).
3. G. Herzberg, Spectra of Diatomic Molecules (Princeton, New Jersey: D. Van Nostrand Co., Inc., 1950).
4. Mott and Marsey, The Theory of Atomic Collisions, (Oxford: Oxford Press, 1965).
5. F. E. Fajen, Ph.D. Dissertation, University of Oklahoma, Norman, Oklahoma (1968).
6. G. Herzberg, *Ibid.*
7. F. R. Gilmore, J. Q. S. R. T. 5, 369 (1965).
8. G. Herzberg, *Ibid.*
9. R. W. Nicholls and W. R. Jarmain, Proc. Phys. Soc. 69, 253 (1955).
10. P. A. Fraser, Canadian J. Phys. 32 (1954).
11. S. S. Penner, Quantitative Molecular Spectroscopy and Gas Emissivities (Reading, Mass.: Addison-Wesley Publishing Co., Inc., 1959).
12. R. Rydberg, Z. Physik 73, 376 (1932) and Z. Physik 80, 514 (1933).
13. O. Klein, Z. Physik 76, 226 (1932).
14. A.L.G. Rees, Proc. Phys. Soc. (London) 59, 998 (1947).
15. R. J. Spindler, J. Mole. Spec. Rad. Trans. 5, 165 (1965).
16. J. T. Vanderslice, E. A. Mason, E. R. Lipponcott and W. G. Maisch, J. Mol. Spectroscopy 3, 17 (1959).
17. Aert Schadee, J. Quant. Spectros. Radiat. Transfer 7, 199 (1966).

18. H. Hönl and F. London, Z. Phys. 33, 803 (1925).

19. Aert Schadee, Bull. Astr. Inst. Neth. 17, 311 (1964).

20. J. B. Tatum, Astrophy. Suppl. Series.

21. I. Kovacs, Can. J. Phys. 38, 955 (1960) and Acta. Phys. Hung. 18, 101 (1965).

22. W. Gaede, Ann. der Physik 46, 357 (1915).

23. Ernest E. Hughes, J. Chem. Physics __, 1531 (1961).

24. G. Valle, *Nuovo Cemento* 7, 174 (1950) and 9, 145 (1952).

25. J. M. Somerville, Proc. Phys. Soc. B 65, 620 (1952) and F. Llewellyn-Jones, Ionization and Breakdown in Gases (New York: John Wiley & Sons, Inc., 1957).

26. V. E. Pollizzi - Private Communication.

27. W. R. Bennett, Jr., P. J. Kindlman and G. M. Mercer, Appl. Opt. Suppl. 2, 341 (1965).

28. Donald W. Marquardt, J. Soc. Indust. Appl. Math. 11, 431 (1963).

29. Francis J. LeBlanc, J. Chem. Phys. 38, 487 (1963).

30. G. Herzberg, *Ibid.*

31. Tenevin, Phil. Trans. Roy. Soc. (London) 237, 471 (1938).

32. H. Nishimura, J. Phys. Soc. Japan 21, 1018 (1966).

33. J. W. McConkey and J. M. Woolsey (Private communication to I. D. Latimer).

34. M. Jeunehomme, J. Chem. Phys. 44, 4253 (1966).

35. R.W.B. Pearse and A. G. Gayden, The Identification of Molecular Spectra (New York: John Wiley & Sons, Inc., 1963) and L. Wallace, The Astrophysical Journal Supplement Series 7, 165 (1962).

36. E. U. Condon, Astrophys. J. 79, 217 (1934) and M. W. Fiast, Proc. Phys. Soc. ___, 114 (1948).

37. R.W.B. Pearse and A. G. Gayden, *Ibid.*

38. Gerhard Herzberg, *Ibid.*

39. Gerhard Herzberg, *Ibid.*

40. Gerhard Herzberg, *Ibid.*

41. R. G. Fowler and T. M. Holzberlein, J. Chem. Phys. 43, 1124 (1966).

42. T. M. Holzberlein, Ph.D. Dissertation, University of Oklahoma, Norman, Oklahoma (1963).

43. T. M. Holzberlein, Rev. Sci. Inst. 35, 1041 (1964).

44. R. G. Fowler, T. M. Holzberlein, C. H. Jacobson and S.J.B. Corrigan, Proc. Phys. Soc. 84, 539 (1964).

45. H. A. Ory, J. Chem. Phys. 40, 562 (1964) and H. A. Ory, A. P. Gittleman and J. P. Muddox, Astrophys. J. 139, (1964).

46. A. Schadee, J. Quant. Spectrosc. Radiat. Transfer 7, 169 (1967).

47. M. Jeunehomme, J. Chem. Phys. 45, 4433 (1966).

48. M. Jeunhomme and A.B.F. Duncan, J. Chem. Phys. 41, 1692 (1964).

49. E. T. Antropov, A. P. Dronov, and N. N. Sobolev, and Soviet Phys.-Dokl. 8, 1073 (1964).

50. H. A. Ory, J. Chem. Phys. 40, 562 (1964).

51. H. A. Ory, A. P. Gittleman and J. P. Maddox, Astrophys. J. 139, (1964).